Resource-Efficient Designs for Integrated Sensing and Communication Systems

by

Chenglong Dou

Doctor of Philosophy in Computer Science

2026

澳門大學
UNIVERSIDADE DE MACAU
UNIVERSITY OF MACAU

Faculty of Science and Technology

University of Macau

Resource-Efficient Designs for Integrated Sensing and Communication Systems

by

Chenglong Dou

SUPERVISOR: Prof. Yuan Wu

DEPARTMENT: Department of Computer and Information Science

Doctor of Philosophy in Computer Science

2026

Faculty of Science and Technology

University of Macau

Acknowledgments

It was the end of a decade, but the start of an age. The completion of this doctoral dissertation marks a significant milestone in my academic journey, a feat that would not have been possible without the guidance, support, and encouragement of many individuals. I am deeply grateful for the opportunity to express my sincere appreciation to those who have made the completion of this thesis possible.

First and foremost, I would like to express my deepest gratitude to my Ph.D. supervisor, Prof. Yuan Wu, for his invaluable guidance and unwavering support throughout my Ph.D. study. His deep academic insight, rigorous research standards, and professional dedication have fundamentally shaped my understanding of research. I am deeply indebted to him for the time and patience he has invested in my development — not only as a researcher but also as a scholar pursuing excellence — and for exemplifying that scholarship is both discipline and devotion.

I extend my heartfelt thanks to my colleagues in the laboratory, whose companionship and collaboration have made the long path of research far less solitary. Their camaraderie and constructive discussions foster a vibrant academic atmosphere. This laboratory has been the fertile soil in which my academic identity has taken root.

To my family, they are the silent bedrock upon which this achievement stands. Words often fail to capture the depth of their sacrifice and the constancy of their love. In moments when the weight of this journey threatened to crush my resolve, their unconditional belief became the anchor that held me steady. They have been a safe harbor throughout this voyage, and this glory belongs as much to them as to me.

I also acknowledge the University of Macau for providing the facilities and resources necessary for the successful completion of this thesis. It has offered a stimulating and conducive environment for academic research and personal growth, and it has been an honor to be part of this esteemed community.

Ultimately, degrees are temporary, but the gratitude I hold is immutable. I dedicate this work to all who have illuminated my path, and whose support has been my constant companion. This dissertation is a testament that while the journey was mine to walk, I never walked it alone.

Abstract

Integrated sensing and communication (ISAC) has emerged as a promising paradigm for future wireless networks, enabling spectrum-efficient dual-functional services for emerging applications that require both high-throughput data transmission and high-precision environmental sensing. However, realizing the full potential of ISAC is fundamentally constrained by resource bottlenecks across multi-dimensional domains: the rigidity of static time-slot allocation in the time domain, the saturation of orthogonal access in the frequency domain, the inequality of multi-node cooperation in the spatial domain, and the siloed operation among sensing, communications and computing in the functional domain. In this thesis, we explore four resource-efficient designs to systematically address these challenges across time, frequency, spatial, and functional domains. Specifically, we focus on the joint optimization of beamforming, scheduling, and multi-dimensional resource allocation to improve the overall system-wise resource efficiency. Firstly, we propose a channel-sharing aided ISAC scheme that overcomes the rigidity of static time-slot allocation by enabling on-demand dynamic scheduling for both sensing and communication. Secondly, we introduce a non-orthogonal multiple access (NOMA)-aided ISAC framework with sensing scheduling to unlock the spectral capacity limit. Thirdly, we present a fairness-aware cooperative sensing strategy to eliminate spatial blind spots and ensure network longevity. Lastly, we design a two-tier integrated sensing, communications, and computing (ISCC) framework to achieve the closed-loop resource optimization for energy-efficient multi-service coexistence. This thesis investigates diverse resource-efficient optimization frameworks to enhance the performance of ISAC systems, laying the foundation for a paradigm shift from simple functional coexistence to deep intelligent integration, thereby ensuring robust, scalable, and green network operations in diverse scenarios. The main works and innovations are summarized as follows.

- In our first work, we propose an energy-efficient ISAC scheme that leverages dynamic channel sharing to break the rigidity of static time-slot allocation. The proposed approach allows the base station dynamically reuses the downlink communication channels of cellular users to perform radar sensing towards mul-

tiple targets. We formulate an optimization problem aimed at maximizing the energy efficiency of the radar sensing while strictly guaranteeing the communication users' quality of service (QoS). We jointly optimize the sensing scheduling and transceiver beamforming to alleviate the co-channel interference introduced by the channel reuse. An efficient alternating optimization framework combined with Dinkelbach's method is proposed to address the non-convex fractional programming problem.

- In the second work, we address the spectral bottleneck and capacity limitations of orthogonal multiple access (OMA) in multi-user scenarios by proposing a NOMA-aided ISAC framework. The base station transmits superimposed signals to serve multiple NOMA users while simultaneously leveraging these signals as probing waveforms for multi-target sensing. We formulate an optimization problem to maximize the sensing efficiency, which is a novel metric defined as the number of successfully sensed targets per time unit, by jointly optimizing the beamforming, the NOMA transmission duration, and the sensing scheduling. We design a decomposition-based algorithm by utilizing successive convex approximation (SCA) and the penalty function method to solve the mixed-integer non-convex problem, significantly enhancing the system's connection density and concurrent sensing capability.

- In our third work, we propose a fairness-aware ISAC-enabled cooperative sensing strategy to overcome single-node blind spots and the inequality of cooperation, where distributed devices access the channel in a time-division manner, with each device performing environmental sensing and data transmission simultaneously during its assigned time slot. To address the "wooden barrel effect" in cooperative networks and prolong the network lifetime, we formulate an optimization problem aimed at maximizing the fairness-aware system-wise throughput. To tackle the non-convexity, we design a block coordinate descent (BCD)-based algorithm to decompose the problem into beamforming and time allocation subproblems. Specifically, we analyze the necessity of dedicated sensing signals and employ SCA to optimize the beamforming vectors.

Furthermore, we characterize the features of the optimal time allocation to derive a semi-analytical expression, ensuring an efficient and balanced resource allocation.

- In the final work, we design an integrated sensing and two-tier task offloading framework to address the conflict of multi-service coexistence and bridge the functional silo between sensing and computing. Specifically, we investigate a two-tier setup that facilitates NOMA-assisted task offloading for edge users while the base station performs continuous radar sensing. To counteract the resource competition between high-power sensing and latency-sensitive computing, we propose a cross-functional synergy strategy that employs tier-specific signaling to decouple mutual interference. We establish an optimization problem aimed at minimizing the total energy consumption by jointly optimizing the transmit beamforming, the two-tier dedicated sensing signals, the two-tier computation offloading strategies and the associated allocations of the communication and computing resources. Although the formulated joint optimization problem is non-convex, we identify the features of its solutions and exploit a decomposition-based framework for solving it, realizing a holistic functional closed-loop design that supports computation-intensive applications alongside ubiquitous sensing.

Declaration

I declare that the thesis here submitted is original except for the source materials explicitly acknowledged and that this thesis as a whole, or any part of this thesis has not been previously submitted for the same degree or for a different degree.

I also acknowledge that I have read and understood the Rules on Handling Student Academic Dishonesty and the Regulations of the Student Discipline of the University of Macau.

Table of Contents

List of Tables and Figures

List of Abbreviations

AP	Access Point
BCD	Block Coordinate Descent
BS	Base Station
CE	Cross-Entropy
CS	Cloudlet Server
CU	Cellular User
DoF	Degrees of Freedom
ECU	Edge Computing User
ES	Edge Server
ISAC	Integrated Sensing and Communication
ISCC	Integrated Sensing, Communications, and Computing
ISTTO	Integrated Sensing and Two-Tier Offloading
MEC	Mobile Edge Computing
MIMO	Multiple Input Multiple Output
NOMA	Non-Orthogonal Multiple Access
NU	NOMA User
OFDM	Orthogonal Frequency-Division Multiplexing
QoS	Quality of Service
REIR	Radar Estimation Information Rate
SCA	Successive Convex Approximation
SCD	Integrated Sensing and Communication Devices
SDR	Semidefinite Relaxation
SIC	Successive Interference Cancellation
ST	Sensing Target
UAV	Unmanned Aerial Vehicle

Chapter 1

Introduction

1.1 Research Background

The evolution of wireless networks towards the sixth-generation (6G) era marks a fundamental paradigm shift from "connecting things" to "perceiving the world" [1–3]. Future networks are envisioned to serve as intelligent ecosystems that integrate the physical and digital realms. To support emerging immersive applications such as autonomous driving and digital twins, the network are required to simultaneously provide ultra-reliable communication and high-precision environmental sensing [4–6]. In response to this dual demand, integrated sensing and communication (ISAC) has emerged as a key enabling technology. By unifying radar sensing and wireless communication into a single hardware platform and sharing the same radio spectrum, ISAC breaks the traditional separation of two independent systems [7–9]. This integration promises significant gains in spectral efficiency and reduced hardware costs, establishing itself as a foundational pillar of next-generation wireless infrastructure.

However, the transition from functional coexistence to deep integration introduces severe challenges regarding resource efficiency. Integrating two functions into one system implies that sensing and communication compete for the same pool of already scarce radio resources [10–12]. Radar sensing typically prioritizes high-power, short-duration pulses for accurate detection, whereas communication systems prioritize continuous transmission for high throughput. When these conflicting objectives share the same resource pool, naive resource sharing often leads to mutual interference and performance degradation [13]. Consequently, the central challenge in designing sustainable ISAC systems is how to optimally orchestrate limited resources to achieve a balance between sensing and communication.

This challenge is further exacerbated as network environments become increasingly versatile and heterogeneous. Current resource management frameworks, primarily designed for single-functional systems, struggle to cope with the multi-dimensional complexity of future services. The structural limitations of existing architectures manifest as distinct "resource bottlenecks" across four key domains:

- *Time Domain:* Traditional static time-slot allocation leads to rigid partitioning between sensing and communication functions. It fails to adapt to the varying temporal requirements, such as the bursty nature of data traffic versus the periodic nature of sensing tasks, resulting in inefficient resource utilization [14, 15].

- *Frequency Domain:* With the exponential growth of wireless devices, the electromagnetic spectrum is becoming saturated. Conventional orthogonal access schemes face a spectral capacity limit, restricting the system's ability to support dense connectivity and high-resolution sensing simultaneously [16, 17].

- *Spatial Domain:* Single-node sensing is inherently limited by physical blockage and coverage blind spots. Although cooperative strategies can mitigate this, they introduce systemic issues regarding spatial unfairness and uneven resource depletion among distributed nodes [18, 19].

- *Functional Domain:* As networks evolve to support diverse concurrent services beyond simple data transfer or environmental sensing, the functional isolation between different subsystems leads to resource silos. The lack of a unified coordination mechanism results in severe competition and inefficiency when multiple functions coexist [20, 21].

To address these challenges, this thesis is dedicated to investigating systematic resource-efficient optimization frameworks for ISAC systems. Firstly, we propose a channel-sharing aided ISAC scheme to break the rigidity of static time-slot allocation in the time domain. Secondly, we introduce a non-orthogonal multiple access (NOMA)-aided ISAC framework to unlock the spectral capacity limit in the frequency domain. Thirdly, we present a fairness-aware cooperative sensing strategy to eliminate spatial blind spots and ensure network longevity in the spatial domain. Lastly, we design a two-tier integrated sensing, communications, and computing (ISCC) framework to achieve the closed-loop resource optimization for energy-efficient multi-service coexistence. By jointly optimizing beamforming, scheduling, and multi-dimensional resource allocation, we aim to ensure robust, scalable, and sustainable network operations in diverse scenarios.

1.2 Literature Review

This section reviews the existing literature on ISAC, focusing on resource efficiency across the time, frequency, spatial, and functional domains. To systematically identify the technical limitations in current research, we categorize the related works into four subsections: resource allocation and scheduling, multiple access techniques, networked cooperative sensing, and ISCC. Each subsection analyzes the state-of-the-art strategies and highlights the specific research gaps that motivate the contributions of this thesis.

1.2.1 Resource Allocation and Scheduling in ISAC

The fundamental challenge in ISAC systems lies in the optimal management of limited radio resources to support the dual functionalities of sensing and communication. Existing research in this domain can be generally categorized into joint beamforming design and systemlevel resource scheduling. Regarding the joint beamforming design, a substantial body of literature focuses on characterizing the trade-off between sensing and communication performance. In [22], Wang *et. al.* investigated the partially-connected hybrid beamforming design for multi-user ISAC systems, aiming at minimizing the Cramér-Rao bound while satisfying the signal-to-interference-plus noise ratio constraint for individual communication user. In [23], Huang *et. al.* studied the coordinated power control among ISAC transmitters for communication and distributed radar sensing. To further optimize resource utilization, Dong *et. al.* investigated the power and bandwidth resources allocation in ISAC systems by considering the fairness of the sensing service in [24]. Similarly, in [25], He *et al.* investigated the energy-efficiency optimization of the multi-user communication in ISAC system while guaranteeing the sensing requirement. Focusing on the sensing resolution, a bandwidth allocation strategy has been proposed in [26] to optimize the weighted average range resolution for sensing while guaranteeing the sum-rate among user equipments. In [27], Liu *et. al.* proposed a single-target-multi-beams radar beam alignment scheme to obtain more accurate estimation information. In [28], He *et. al.* investigated the joint optimization of a full-duplex communication based ISAC system to improve

spectral efficiency.

Beyond the physical layer design, there have been several studies leveraging ISAC in diverse network paradigms. In [29], Huang *et. al.* investigated the trade-off between communication performance and sensing performance in unmanned aerial vehicle (UAV)-assisted ISAC systems. Extending this to ground network enhancement, Yang *et. al.* exploited ISAC UAVs for improving both communication and localization performances of the ground networks in [30]. Addressing security concerns, a secure precoding optimization scheme has been proposed in [31] for NOMA-ISAC networks. Moreover, in [32], Cui *et. al.* established a physical layer framework for digital twin based on the ISAC and proposed a dual-functional waveform augmentation strategy.

More recently, the focus has shifted towards multi-target sensing and dynamic scheduling. In [33], the spectrum allocation problem between spectrum service providers and terminals equipped with orthogonal frequency division multiplexing ISAC system is studied. Considering the temporal dynamics, Yang *et. al.* investigated the queue-aware dynamic resource scheduling for the ISAC system while taking the network stability and radar detection performance into account in [34]. For specific applications like vehicular tracking, Wang *et. al.* developed an approach for multi-vehicle tracking and identity association by using the ISAC signals in [35], which reduces the communication overhead and latency. Additionally, in [36], Liu *et. al.* proposed a joint transmitting beamforming model for ISAC systems, with the objective of maximizing the radar transmitting beamforming performance while guaranteeing the communication quality.

However, most existing works predominantly adopt a static orthogonal partitioning strategy, where sensing and communication are isolated in fixed time slots. Such rigid frameworks fail to adapt to the time-varying and asymmetric nature of service demands, where communication traffic is typically bursty while sensing tasks are periodic, leading to low resource utilization. Consequently, there is a lack of research on dynamic scheduling paradigms that can flexibly exploit the temporal degrees of freedom to coordinate these conflicting tasks. This indicates a critical requirement for a demand-responsive resource management framework to break the temporal rigidity,

which motivates the design proposed in Chapter 2.

1.2.2 Multiple Access Techniques for ISAC

ISAC has attracted wide research interests in integrated signal design and resource management owing to its potential advantages. In the context of orthogonal multiple access (OMA), Wu *et. al.* exploited the multiple input multiple output (MIMO)-orthogonal frequency division multiplexing (OFDM) data symbols carried by subcarriers for time-domain and spatial-domain signal orthogonality for ISAC in [37]. To enhance sensing accuracy, Liu *et. al.* proposed a radar beam alignment scheme in [38] for acquiring accurate estimation information in vehicle-to-everything systems by allocating multiple radar beams to the target. Furthermore, in [39], Wang *et. al.* proposed an ISAC with computation over-the-air framework to improve the spectrum efficiency and quality of service in wireless sensor networks. Leveraging artificial intelligence, Liu *et. al.* investigated the predictive ISAC beamforming in vehicular networks in [40] where the deep learning is employed to learn historical channels' features and predict the beamforming matrix for the next time slot.

To further improve spectral efficiency and connectivity, NOMA has been regarded as a key enabling technology for future B5G/6G networks. Prior to its integration with ISAC, NOMA has been extensively studied. In [41], Zhao *et. al.* investigated the security of unmanned aerial vehicle and NOMA aided networks via power allocation and beamforming. In [42], Li *et. al.* studied the secrecy performance of the simultaneously transmitting and reflecting reconfigurable intelligent surface assisted NOMA networks. In [43], Li *et. al.* proposed an adaptive multi-user association strategy for NOMA-aided visible light communication systems.

Recently, integrating NOMA with ISAC has emerged as a promising direction. In [44], Wang *et al.* studied the NOMA-empowered ISAC system to maximize the weighted sum of communication throughput and effective sensing power. From the perspective of bandwidth partition, Zhang *et. al.* investigated the NOMA assisted ISAC networks in [45], where a portion of the bandwidth is used for ISAC and the remaining bandwidth is used for wireless communication only. Furthermore, in [46], the resource allocation in NOMA-aided joint communication, sensing, and multi-tier

computing has been studied.

However, the majority of existing NOMA-ISAC frameworks implicitly assume a "sense-all" strategy, where resources are distributed to sense all potential targets simultaneously regardless of their priorities or channel conditions. In dense scenarios, such an indiscriminate approach often leads to resource fragmentation and degraded detection performance for critical targets. Consequently, there is a lack of research on joint optimization frameworks that integrate user access control with target selection mechanisms. This highlights the necessity for a spectral-efficient design that can balance the trade-off between massive connectivity and high-quality multi-target sensing through intelligent scheduling, which motivates the sensing-efficient NOMA-ISAC framework proposed in Chapter 3.

1.2.3 Networked and Cooperative ISAC

Single-node ISAC systems often face limitations in sensing coverage and resolution. Consequently, there have been several efforts on multi-target sensing and waveform design to mitigate these issues. In [47], Ma *et. al.* proposed a max-aperture radar slicing waveform to yield a large time-frequency aperture for multi-user communication and multi-target sensing. In [48], Hua *et. al.* designed the radar sensing signal in the downlink ISAC system where the base station performs multi-user communication and radar sensing simultaneously. In [49], the transceiver waveform is designed for a general scenario of multi-user multi-target ISAC systems that the communication users can be simultaneously served and detected. In [50], the authors proposed an ISAC framework established on the Markov decision process and deep reinforcement learning to enable the adaptive beamforming of autonomous vehicles for multi-target sensing.

To fundamentally address the insufficient sensing accuracy of an individual device caused by resource constraints and blockage, there have been several studies in exploring the potential of multi-device cooperative sensing. In [51], Chen *et. al.* investigated a beam sharing assisted cooperative sensing UAV networks and presented upper-bound average cooperative sensing area as the metric for cooperative sensing UAV networks. In the context of vehicular networks, Cheng *et. al.* investigated the

multi-vehicle multi-sensor cooperative tracking in vehicular communication networks in [52] with the multi-model sensing information sharing and fusion. Expanding to inference tasks, in [53], Li *et. al.* investigated the device-edge co-inference in a wireless sensing system where multiple devices collaboratively perform an inference task. In [54], Jiang *et. al.* proposed a collaborative precoding design for adjacent base stations for providing communication and wide range cooperative sensing services for vehicles. From a localization perspective, in [55], Gu *et. al.* established a general framework of self-localization and cooperative target detection and developed a hybrid coordinate descent localization algorithm for joint position estimation and cooperative target detection.

However, most existing cooperative mechanisms predominately focus on maximizing the aggregate system throughput or the total sensing area. Such sum-rate maximization strategies tend to over-exploit devices with superior channel conditions while starving those at the edge, leading to a severe "wooden barrel effect" and uneven energy depletion across the network. Therefore, a critical gap remains in investigating cooperative protocols that go beyond simple performance maximization to address the systemic resource imbalance among heterogeneous nodes, ensuring sustainable and balanced network operations. This necessitates a mechanism to balance system-wise performance with individual device fairness, motivating the fairness-aware cooperative sensing strategy proposed in Chapter 4.

1.2.4 Integrated Sensing, Communications, and Computing

As networks evolve towards intelligent ecosystems, the integration of ISAC with other emerging technologies has attracted significant attention. In [56], Liu *et al.* proposed an intelligent reflecting surface (IRS)-aided ISAC system operating in the terahertz band to maximize the system capacity. For multi-UAV scenarios, in [57], Zhang *et al.* studied an ISAC-enabled multiple unmanned aerial vehicle cooperative detection scenario. Leveraging ISAC for learning, in [58], Liu *et al.* studied a vertical federated edge learning system for collaborative objects motion recognition by exploiting the distributed ISAC. In [59], Huang *et. al.* investigated ISAC assisted mobile edge computing and leveraged IRS to improve the performances of radar sensing

and mobile edge computing. In the digital twin context, ISAC has been combined with the digital twin to address the problem of task scheduling and resource allocation in vehicular edge computing in [60].

Parallel to ISAC evolution, MEC has become a cornerstone for low-latency services. MEC has attracted a wide research interests owing to its great potential in reducing latency and energy consumption for executing computation-intensive tasks on resource-limited devices [61–63]. To further enhance MEC performance, exploiting NOMA to facilitate task offloading in MEC has been investigated in numerous studies. In [64], Sheng *et. al.* investigated the computation offloading in multi-carrier NOMA-enabled MEC under the differentiated uploading delay. Dealing with imperfect CSI, the resource allocation for the NOMA-MEC network with imperfect channel state information has been investigated in [65]. In [66], a general hybrid NOMA-MEC offloading strategy has been proposed.

Beyond relying solely on edge servers, the multi-tier MEC paradigm that allows the cooperation among edge and cloud servers enables a more efficient and flexible utilization of the computation resources across different tiers of the networks. In [67], Wang *et. al.* studied a joint edge video transcoding and client video enhancement optimization problem for adaptive bitrate streaming in multi-tier wireless computing networks. In [68], Xu *et. al.* investigated the optimization mechanism for accelerating the federated learning enabled two-tier computing based on the fully-decoupled radio access network architecture.

Recently, several efforts have been devoted to leveraging ISAC for MEC to achieve the deep integration of sensing and task offloading. In [69], Qi *et. al.* presented a framework for the general integration of three isolated functions of sensing, computing, and communication to explore their relationship. To exploit coordination gains, in [70], Zhao *et. al.* proposed a wireless scheduling architecture to exploit the coordination gains of sensing, communication, and computing. Focusing on artificial intelligence inference, In [71], Wen *et. al.* proposed a task-oriented ISCC scheme for edge artificial intelligence inference. In [72], an edge intelligence-oriented ISAC has been proposed, in which multiple base stations can offload the sensing data to the edge

server for model training.

Despite the initial explorations in ISCC, most existing works treat sensing and computing as loosely coupled add-ons, failing to address the complex interference dynamics in multi-tier architectures. Specifically, the literature lacks a closed-loop resource management framework that can effectively mitigate the inter-functionality interference while orchestrating the synergy between sensing data acquisition and subsequent computation tasks. It remains an open issue regarding how to minimize system-wide energy consumption through cross-tier coordination, which motivates the two-tier integrated sensing and task offloading framework proposed in Chapter 5.

1.3 Thesis Contributions

Motivated by the research gaps identified in the literature review, this thesis investigates four resource-efficient designs to systematically address the resource bottlenecks in ISAC systems across the time, frequency, spatial, and functional domains. We focus on the joint optimization of beamforming, scheduling, and multi-dimensional resource allocation to enhance the overall system-wise resource efficiency. The main contributions are summarized as follows:

- *Breaking Temporal Rigidity via Channel Sharing-Aided ISAC (Chapter 2):* To address the inefficiency caused by static time-slot allocation, we investigate an energy-efficient channel-sharing aided ISAC scheme. We propose a dynamic scheduling mechanism where the base station reuses the downlink channels of cellular users to perform multi-target sensing tasks. To balance the trade-off between sensing energy efficiency and communication quality, we formulate a joint optimization problem of sensing scheduling and transceiver beamforming. We solve this non-convex problem by addressing the fractional objective function via Dinkelbach's method, obtaining the beamforming solution through semidefinite relaxation (SDR) and Lagrange duality, and solving the matching-based scheduling problem using a swap-matching algorithm.

- *Unlocking Spectral Capacity via NOMA-Aided ISAC (Chapter 3):* To overcome the spectral capacity limit of orthogonal access, we investigate a NOMA-aided

ISAC framework. We design a scheme where the base station uses superimposed signals to serve multiple users while simultaneously performing sensing tasks. We formulate an optimization problem to maximize the sensing efficiency, which is a novel metric defined as the number of successfully sensed targets per time unit, by jointly optimizing the beamforming, the NOMA transmission duration, and the sensing scheduling. To tackle the mixed-integer non-convexity, we propose a decomposition-based algorithm. Specifically, the beamforming is optimized via successive convex approximation (SCA), the transmission duration is determined using a bisection-search method based on its monotonic feature, and the sensing scheduling solution is derived via a cross-entropy learning algorithm.

- *Enhancing Spatial Fairness via ISAC-Enabled Cooperative Sensing (Chapter 4):* To overcome single-node coverage blind spots and address spatial unfairness, we investigate a fairness-aware ISAC-enabled multi-device cooperative sensing strategy. In this framework, distributed devices access the channel in a time-division manner, with each device performing environmental sensing and data transmission simultaneously during its assigned time slot. We formulate an optimization problem to maximize the fairness-aware system-wise throughput while strictly guaranteeing cooperative sensing quality. We design a block coordinate descent (BCD) algorithm to decompose the problem into beamforming and time allocation subproblems. Specifically, we analyze the necessity of dedicated sensing signals and employ SCA to optimize the beamforming vectors. Furthermore, we characterize the features of the optimal time allocation to derive a semi-analytical expression, ensuring an efficient and balanced resource allocation.

- *Bridging Functional Silos via ISCC (Chapter 5):* Finally, to address the conflict of multi-service coexistence and bridge the functional silo between sensing and computing, we investigate a NOMA-assisted integrated sensing and two-tier task offloading system. We propose a framework where an access point supports edge task processing while performing continuous sensing, with ad-

ditional offloading capabilities to cloudlet servers. To counteract the resource competition between high-power sensing and latency-sensitive computing, we propose a cross-functional synergy strategy that employs tier-specific signaling to decouple mutual interference. A joint optimization problem of transmit beamforming, two-tier dedicated sensing signals, computation offloading strategies and associated allocations of the communication and computing resources is formulated, with the objective of minimizing the total energy consumption. We exploit the structural features of the problem and propose a decomposition-based algorithm to solve it, realizing a holistic functional closed-loop design that supports computation-intensive applications alongside ubiquitous sensing.

1.4 Statement of Originality

All the contributions listed in Section 1.3 are published with our own originality. The main results presented in this thesis are included in the following papers.

[1] **Chenglong Dou**, N. Huang, Y. Wu, L. Qian, and T.Q.S. Quek, "Channel Sharing aided Integrated Sensing and Communication: An Energy-Efficient Sensing Scheduling Approach," ***IEEE Transactions on Wireless Communications***, vol. 23, no. 5, pp. 4802-4814, May 2024.

[2] **Chenglong Dou**, N. Huang, Y. Wu, L. Qian, and T.Q.S. Quek, "Sensing-Efficient NOMA-aided Integrated Sensing and Communication: A Joint Sensing Scheduling and Beamforming Optimization," ***IEEE Transactions on Vehicular Technology***, vol. 72, no. 10, pp. 13591-13603, Oct. 2023.

[3] **Chenglong Dou**, N. Huang, Y. Wu, L. Qian, Z. Shi, and T.Q.S. Quek, "Integrated Sensing and Communication Enabled Multi-Device Multi-Target Cooperative Sensing: A Fairness-aware Design," ***IEEE Internet of Things Journal***, vol. 11, no. 17, pp. 29190-29201, Sept. 2024.

[4] **Chenglong Dou**, M. Dai, N. Huang, Y. Wu, L. Qian, and T.Q.S. Quek, "Integrated Sensing and Two-Tier Task Offloading via Non-orthogonal Multiple Access: An Energy-Minimization Design," ***IEEE Transactions on Wireless Communications***, vol. 23, no. 12, pp. 19157-19171, Dec. 2024.

Chapter 2

Channel Sharing Aided ISAC: An Energy-Efficient Sensing Scheduling Approach

2.1 Introduction

With the rapid development of communication and sensing technologies, integrated sensing and communication (ISAC) networks have emerged as a promising paradigm for enabling advanced wireless services that require both high-throughput transmission and accurate environment sensing [73, 74]. By utilizing the same spectrum resource for simultaneous data transmission and radar sensing, ISAC base stations can efficiently exploit valuable radio resources and enhance overall system performance. Consequently, ISAC is expected to play a vital role in future immersive services such as autonomous driving, digital twins, and augmented/virtual reality [75, 76].

Although there have been several studies investigating the coordination between sensing and communication functions without incurring severe mutual interference, the stringent spectrum resources at radio access networks still lead to a crucial bottleneck in ISAC performance [77–79]. To this end, this chapter proposes an approach to provide sensing services by actively reusing the channels of conventional cellular users, thereby effectively alleviating the scarcity of channel resources. Nevertheless, reusing cellular channels for sensing introduces a fundamental trade-off: it degrades the cellular users' quality of service (QoS), particularly in terms of throughput. This issue becomes exacerbated in multi-target sensing scenarios, where indiscriminately sensing multiple targets over a single user's channel may significantly impair that user's communication performance. Therefore, it is crucial to investigate an effective sensing scheduling mechanism, in which different sensing targets are strategically allocated to different cellular users' channels, with the objective of improving the overall sensing performance while strictly guaranteeing the QoS for cellular users.

To address these challenges, this chapter investigates an energy-efficient channel sharing aided ISAC framework, featuring a joint optimization of sensing scheduling and beamforming. The main contributions of this chapter are summarized as follows:

- We propose an energy-efficient channel sharing aided ISAC with sensing schedul-

ing, in which the ISAC base station (BS) performs sensing of multiple targets by reusing the channels of cellular users. We analyze the radar sensing echo signal when reusing the cellular user's channel, based on which we adopt the radar estimation information rate to quantify the sensing performance. We formulate a joint optimization of multi-target sensing scheduling, the BS's transmitting beamforming, and its receiving beamforming for each sensing target, with the objective of maximizing the energy efficiency for radar sensing while guaranteeing each cellular user's QoS.

- To address the non-convexity of the formulated optimization problem, we decompose it into two subproblems, including a beamforming vector optimization subproblem and a sensing scheduling optimization subproblem. For the beamforming vector optimization subproblem, we identify the property of its optimal solution and propose an efficient algorithm which is based on Dinkelbach's method and Lagrange duality to achieve the optimal beamforming (under a given sensing scheduling). For the sensing scheduling optimization subproblem under the given beamforming, we reformulate this subproblem as a matching game and solve it by using a swap matching based algorithm. We also prove the convergence of the swap matching based algorithm. We iteratively solve these two subproblems in an alternative manner to reach the solution of the original joint optimization problem.

- We demonstrate the performance advantage of our channel sharing aided ISAC in comparison with different benchmark schemes. Compared to several benchmark schemes, our algorithm can achieve better performance in terms of energy efficiency and the sum of radar estimation information rate. Moreover, compared with the solutions obtained by other existing algorithms/solvers, our proposed alternating algorithm can significantly reduce the computational time while guaranteeing the accuracy.

The remainder of this chapter is organized as follows. We illustrate the system model and problem formulation in Section 2.2. In Section 2.3, we decompose the

original optimization problem into two subproblems and propose the corresponding algorithms for solving them. Section 2.4 demonstrates the performance of our channel sharing aided ISAC and Section 2.5 summarizes this chapter.

2.2 System Model of Channel Sharing-Aided ISAC

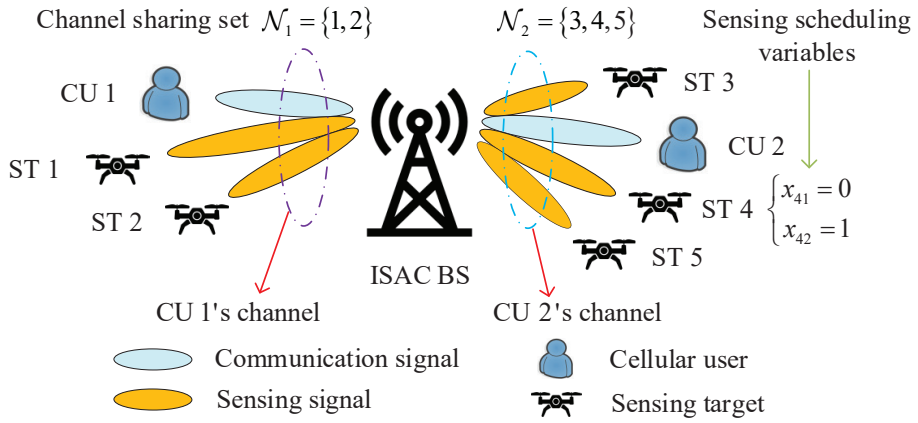

Fig. 2.1: An illustrative system model with 2 CUs and 5 STs

Figure 2.1 illustrates the channel sharing aided ISAC in one cell coverage. Specifically, there exists one ISAC BS with N_t transmit antennas and N_r receive antennas, and I single-antenna cellular users (CUs) denoted by $\mathcal{I} = \{1, 2, ..., I\}$. Each CU has a pre-assigned channel, and the channel of CU i and the channel of CU j ($\forall i, j \in \mathcal{I}, i \neq j$) are orthogonal to each other, such that there is no co-channel interference between different CUs. To enable ISAC, the BS can reuse the CUs' channels to sense N sensing targets (STs) denoted by $\mathcal{N} = \{1, 2, ..., N\}$, where each ST is allowed to be sensed over at most one CU's channel. We introduce a group of binary sensing scheduling variables $\{x_{ni}\}_{n\in\mathcal{N},i\in\mathcal{I}}$ as

$$x_{ni} = \begin{cases} 1, & \text{CU } i\text{'s channel is reused for sensing ST } n, \\ 0, & \text{otherwise.} \end{cases} \tag{2.1}$$

Moreover, we introduce set $\mathcal{N}_i = \{n | x_{ni} = 1, n \in \mathcal{N}\} \subseteq \mathcal{N}$ to denote the group of STs which are selected to be sensed over CU i's channel, with $\mathcal{N}_i \cap \mathcal{N}_j = \emptyset$ ($\forall i, j \in \mathcal{I}, i \neq j$).

2.2.1 Modeling of Data Transmission

With $\mathcal{N}_i$, the transmitted signal of the ISAC BS over CU i's channel can be expressed as

$$\mathbf{b}_i^{\text{BS}} = \mathbf{w}_i s_i + \sum_{n \in \mathcal{N}_i} \mathbf{v}_n z_n, \tag{2.2}$$

where $\mathbf{w}_i \in \mathbb{C}^{N_t \times 1}$ denotes the BS's transmitting beamforming vector for CU i and s_i with $\mathbb{E}[|s_i|^2] = 1$ denotes the information symbol for CU i. Meanwhile, in eq. (2), $\mathbf{v}_n \in \mathbb{C}^{N_t \times 1}$ denotes the BS's transmitting beamforming vector for ST n, and z_n with $\mathbb{E}[|z_n|^2] = 1$ denotes the symbol of the dedicated sensing signal for ST n. Therefore, the received signal at CU i can be expressed as

$$y_i^{\text{CU}} = \mathbf{h}_i^H \mathbf{b}_i^{\text{BS}} + n_C = \mathbf{h}_i^H \mathbf{w}_i s_i + \mathbf{h}_i^H \sum_{n \in \mathcal{N}_i} \mathbf{v}_n z_n + n_C, \tag{2.3}$$

where $\mathbf{h}_i \in \mathbb{C}^{N_t \times 1}$ denotes the channel gain between the ISAC BS and CU i, and n_C denotes the circularly symmetric complex Gaussian noise with variance σ_C^2. Correspondingly, the throughput achieved by CU i can be expressed as

$$R_i^{\text{com}} = B_i \log_2 \left(1 + \frac{|\mathbf{h}_i^H \mathbf{w}_i|^2}{\sum_{n \in \mathcal{N}_i} |\mathbf{h}_i^H \mathbf{v}_n|^2 + \sigma_C^2} \right), \tag{2.4}$$

where B_i denotes the channel bandwidth of CU i. In this work, we consider that the BS's transmitting beamforming vectors for the CUs, i.e., $\{\mathbf{w}_i\}_{i \in \mathcal{I}}$, are fixed. We aim at guaranteeing each CU's throughput requirement by properly controlling the sensing scheduling and the BS's transmitting beamforming for sensing, i.e., constraint (2.10) in our problem formulation in Section 2.2.3.

2.2.2 Modeling of Sensing

We assume that ST n's azimuth θ_n is known by the ISAC BS. As a result, the received signal at the ISAC BS over CU i's channel can be expressed as

$$\mathbf{y}_i^{\text{BS}} = \sum_{n \in \mathcal{N}_i} \alpha_{ni} \mathbf{A}(\theta_n) \mathbf{b}_i^{\text{BS}} + \mathbf{n}_S, \tag{2.5}$$

where $\mathbf{A}(\theta_n) \triangleq \mathbf{a}_r(\theta_n)\mathbf{a}_t^H(\theta_n) \in \mathbb{C}^{N_r \times N_t}$. α_{ni} is the complex channel between ST n and the ISAC BS over CU i's channel, and $\mathbf{n}_S$ is the circularly symmetric complex Gaussian noise with variance σ_S^2 of each element. The dependencies of the transmitting steering vector $\mathbf{a}_t(\theta_n)$ and the receiving steering vector $\mathbf{a}_r(\theta_n)$ on angle θ_n can be respectively expressed as

$$\mathbf{a}_t(\theta_n) = \frac{1}{\sqrt{N_t}} \left[1, e^{-j2\pi d_t \sin\theta_n}, ..., e^{-j2\pi d_t (N_t-1)\sin\theta_n}\right]^T, \tag{2.6}$$

$$\mathbf{a}_r(\theta_n) = \frac{1}{\sqrt{N_r}} \left[1, e^{-j2\pi d_r \sin\theta_n}, ..., e^{-j2\pi d_r (N_r-1)\sin\theta_n}\right]^T, \tag{2.7}$$

where d_t denotes the spacing of transmitting antenna array normalized by the wavelength, and d_r denotes the spacing of receiving antenna array normalized by the wavelength.

At the ISAC BS, different echoes from the STs can be obtained via the receiver filtering by multiplying the BS's receiving beamforming vector. Specifically, we use $\mathbf{u}_n \in \mathbb{C}^{N_r \times 1}$ to denote the BS's receiving beamforming vector for ST n. Thus, the echo from ST n over CU i's channel after the receiver filtering can be expressed as $x_{ni}\mathbf{u}_n^H \mathbf{y}_i^{\text{BS}}$. Correspondingly, the radar sensing performance for sensing ST n over CU i's channel is characterized by the radar estimation information rate (REIR) as

$$R_{ni}^{\text{rad}} = \frac{\delta}{2T}\log_2\left(1 + 2TB_i \frac{x_{ni}|\alpha_{ni}|^2 |\mathbf{u}_n^H \mathbf{A}(\theta_n)\mathbf{v}_n|^2}{\mathbf{u}_n^H \mathbf{\Gamma}_{ni} \mathbf{u}_n}\right), \tag{2.8}$$

where δ denotes the radar duty factor, and T denotes the radar pulse duration. In eq. (2.8), $\mathbf{\Gamma}_{ni}$ denotes the total interference for sensing ST n over CU i's channel, and it can be shown as

$$\begin{aligned}\mathbf{\Gamma}_{ni} = &\underbrace{\sum_{p\in\mathcal{N}_i} \alpha_{pi}^2 \mathbf{A}(\theta_p)\mathbf{w}_i\mathbf{w}_i^H\mathbf{A}^H(\theta_p)}_{\text{Interference from the communication signal}} + \underbrace{x_{ni}\alpha_{ni}^2 \mathbf{A}(\theta_n)\left(\sum_{q\in\mathcal{N}_i, q\neq n}\mathbf{v}_q\mathbf{v}_q^H\right)\mathbf{A}^H(\theta_n)}_{\text{Interference from other sensing signals on ST } n\text{'s echo}} \\ &+ \underbrace{\sum_{p\in\mathcal{N}_i, p\neq n} \alpha_{pi}^2 \mathbf{A}(\theta_p)\left(\sum_{q\in\mathcal{N}_i}\mathbf{v}_q\mathbf{v}_q^H\right)\mathbf{A}^H(\theta_p)}_{\text{Interference from other STs' echoes}} + \underbrace{\sigma_S^2\mathbf{I}}_{\text{Noise}}.\end{aligned} \tag{2.9}$$

It can be observed from eq. (2.8) that $R_{ni}^{\text{rad}} = 0$ if ST n is not sensed over CU i's channel (i.e., $x_{ni} = 0$). Thus, the total REIR of ST n can be expressed as $\sum_{i\in\mathcal{I}} R_{ni}^{\text{rad}}$.

2.2.3 Problem Formulation

In this chapter, we aim at maximizing the energy efficiency (MEE) for radar sensing which is denoted by the ratio of the total STs' REIR overall the total power consumption, while guaranteeing each CU's throughput requirement. To achieve this goal, we formulate a joint optimization of sensing scheduling variables $\{x_{ni}\}_{n\in\mathcal{N},i\in\mathcal{I}}$, the BS's transmitting beamforming vectors $\{\mathbf{v}_n\}_{n\in\mathcal{N}}$ for sensing the STs, and its receiving beamforming vectors $\{\mathbf{u}_n\}_{n\in\mathcal{N}}$ for filtering the STs' echoes as follows.

$$\text{(MEE):}\ \max \frac{\sum_{n\in\mathcal{N}}\sum_{i\in\mathcal{I}} R_{ni}^{\text{rad}}}{\mathbf{Tr}\left(\sum_{i\in\mathcal{I}} \mathbf{w}_i\mathbf{w}_i^H + \sum_{n\in\mathcal{N}} \mathbf{v}_n\mathbf{v}_n^H\right) + P^C}$$

$$\text{subject to: } R_i^{\text{com}} \geq R_i^{\text{req}}, \forall i \in \mathcal{I}, \tag{2.10}$$

$$\sum_{i\in\mathcal{I}} x_{ni} \leq 1, \forall n \in \mathcal{N}, \tag{2.11}$$

$$\sum_{n\in\mathcal{N}} x_{ni} \leq J_i^{\max}, \forall i \in \mathcal{I}, \tag{2.12}$$

$$x_{ni} \in \{0,1\}, \forall n \in \mathcal{N}, \forall i \in \mathcal{I}, \tag{2.13}$$

$$\text{variables: } \{x_{ni}\}_{n\in\mathcal{N},i\in\mathcal{I}}, \{\mathbf{v}_n\}_{n\in\mathcal{N}}, \text{ and } \{\mathbf{u}_n\}_{n\in\mathcal{N}}.$$

In the objective function, $\mathbf{Tr}\left(\sum_{i\in\mathcal{I}} \mathbf{w}_i\mathbf{w}_i^H + \sum_{n\in\mathcal{N}} \mathbf{v}_n\mathbf{v}_n^H\right)$ denotes the total transmitting power of the ISAC BS and $\mathbf{Tr}(\cdot)$ denotes the trace function. Parameter P^C denotes the circuit power consumption which is a constant. Constraint (2.10) ensures that each CU i can achieve its required throughput denoted by R_i^{req}. Constraint (2.11) ensures that at most one CU's channel is reused for sensing ST n. Constraint (2.12) indicates that at most $J_i^{\max}$ STs can be sensed over CU i's channel.

2.3 Proposed Algorithms for Solving Problem (MEE)

Problem (MEE) is a mixed binary nonlinear programming problem. The binary sensing scheduling $\{x_{ni}\}_{n\in\mathcal{N},i\in\mathcal{I}}$ and the BS's beamforming vectors $\{\mathbf{v}_n\}_{n\in\mathcal{N}}$ and $\{\mathbf{u}_n\}_{n\in\mathcal{N}}$ are tightly coupled in the objective function. Moreover, the fractional structure of the objective function leads to a non-convex optimization problem. Therefore,

it is challenging to solve Problem (MEE) directly. To address this difficulty, we propose a framework of alternating optimization to obtain the solution to Problem (MEE). The details are as follows.

2.3.1 Decomposition of Problem (MEE)

To address the difficulty due to the mixed binary and non-convexity, we decompose Problem (MEE) into two subproblems, including Problem (MEE-BVO) to optimize the continuous beamforming vectors and Problem (MEE-SSO) to optimize the binary sensing scheduling variables.

Beamforming vectors optimization (BVO) under the given sensing scheduling

Given the sensing scheduling $\{x_{ni}\}_{n\in\mathcal{N},i\in\mathcal{I}}$, Problem (MEE) turns into the following Problem (MEE-BVO).

$$\begin{aligned}\text{(MEE-BVO):}\ &\max \frac{\sum_{n\in\mathcal{N}}\sum_{i\in\mathcal{I}} R_{ni}^{\text{rad}}}{\mathbf{Tr}\left(\sum_{i\in\mathcal{I}}\mathbf{w}_i\mathbf{w}_i^H+\sum_{n\in\mathcal{N}}\mathbf{v}_n\mathbf{v}_n^H\right)+P^C}\\ &\text{subject to: constraint } (2.10),\\ &\text{variables: } \{\mathbf{v}_n\}_{n\in\mathcal{N}} \text{ and } \{\mathbf{u}_n\}_{n\in\mathcal{N}}.\end{aligned}$$

Sensing scheduling optimization (SSO) under the given beamforming vectors

Given the beamforming vectors $\{\mathbf{v}_n\}_{n\in\mathcal{N}}$ and $\{\mathbf{u}_n\}_{n\in\mathcal{N}}$, after performing some mathematical manipulations, Problem (MEE-SSO) for optimizing the sensing scheduling can be expressed as follows.

$$\begin{aligned}\text{(MEE-SSO):}\ &\max \Lambda(\{x_{ni}\}_{n\in\mathcal{N},i\in\mathcal{I}})=\sum_{n\in\mathcal{N}}\sum_{i\in\mathcal{I}} R_{ni}^{\text{rad}}\\ &\text{subject to: constraints } (2.10), (2.11), (2.12) \text{ and } (2.13),\\ &\text{variables: } \{x_{ni}\}_{n\in\mathcal{N},i\in\mathcal{I}}.\end{aligned}$$

As shown in Figure 2.2, Problem (MEE-BVO) and Problem (MEE-SSO) are executed in an alternative manner to solve the original Problem (MEE). It is different from existing algorithms which use the block coordinate descent and successive convex approximation to obtain the solution after relaxing the binary variables. In the

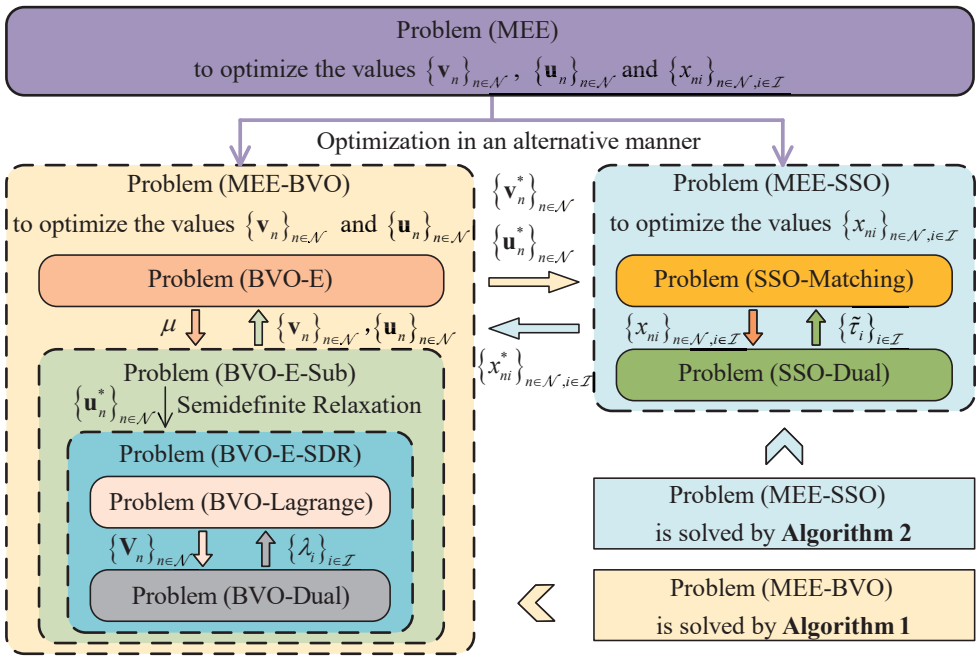

Fig. 2.2: Decomposition of Problem (MEE) into two subproblems

remainder of this section, we first perform an equivalent transformation for the fractional structure of Problem (MEE-BVO) by leveraging Dinkelbach's method. Then, we use Lagrange duality to derive the underlying structure of the optimal solutions by identifying its convexity. In particular, we formulate Problem (MEE-SSO) as a many-to-one matching problem and propose the corresponding algorithm to obtain the optimal sensing scheduling.

2.3.2 Proposed Algorithm for Solving Problem (MEE-BVO)

Problem (MEE-BVO) is a strictly non-convex problem due to its fractional structure, which is challenging to solve. To tackle with its non-convexity, we first leverage the Dinkelbach's method to deal with the objective function of Problem (MEE-BVO). For the sake of clear presentation, we define

$$f_1^{\text{obj}} \triangleq \sum_{n\in\mathcal{N}}\sum_{i\in\mathcal{I}} R_{ni}^{\text{rad}}, \tag{2.14}$$

and

$$f_2^{\text{obj}} \triangleq \mathbf{Tr}\left(\sum_{i\in\mathcal{I}} \mathbf{w}_i\mathbf{w}_i^H + \sum_{n\in\mathcal{N}} \mathbf{v}_n\mathbf{v}_n^H\right) + P^C. \tag{2.15}$$

By introducing an auxiliary variable μ as

$$\mu \leq \frac{f_1^{\text{obj}}}{f_2^{\text{obj}}}, \tag{2.16}$$

we can transform Problem (MEE-BVO) into the following equivalent form.

$$\begin{aligned}
&\text{(BVO-E): } \max\ \mu \\
&\text{subject to: constraint } (2.10), \\
&\qquad f_1^{\text{obj}} - \mu f_2^{\text{obj}} \geq 0, \qquad (2.17) \\
&\text{variables: } \mu, \{\mathbf{v}_n\}_{n\in\mathcal{N}} \text{ and } \{\mathbf{u}_n\}_{n\in\mathcal{N}}.
\end{aligned}$$

For Problem (BVO-E), we observe that for a given value of μ, the optimization problem is feasible if $f_1^{\text{obj}} - \mu f_2^{\text{obj}} \geq 0$. In particular, Problem (MEE-BVO) achieves the optimal solutions if and only if Problem (BVO-E) achieves the optimal solutions with the optimal μ^*. Moreover, $f_1^{\text{obj}} - \mu f_2^{\text{obj}}$ is strictly decreasing in μ, which indicates that the optimal value μ^* is obtained when constraint (2.17) is strictly binding. Therefore, to solve Problem (BVO-E), for a given value of μ, we solve the following subproblem

$$\begin{aligned}
&\text{(BVO-E-Sub): } \max\ \sum_{n\in\mathcal{N}}\sum_{i\in\mathcal{I}} R_{ni}^{\text{rad}} - \mu\left(\mathbf{Tr}\left(\sum_{i\in\mathcal{I}}\mathbf{w}_i\mathbf{w}_i^H + \sum_{n\in\mathcal{N}}\mathbf{v}_n\mathbf{v}_n^H\right) + P^C\right) \\
&\text{subject to: constraint } (2.10), \\
&\text{variables: } \{\mathbf{v}_n\}_{n\in\mathcal{N}} \text{ and } \{\mathbf{u}_n\}_{n\in\mathcal{N}}.
\end{aligned}$$

After solving Problem (BVO-E-Sub) and obtaining the corresponding optimal values $\{f_1^{\text{obj},*}, f_2^{\text{obj},*}\}$ of $\{f_1^{\text{obj}}, f_2^{\text{obj}}\}$ under the current value of μ (i.e., Step 12 of Algorithm 1), we can further update the value of μ as

$$\mu = \frac{f_1^{\text{obj},*}}{f_2^{\text{obj},*}}. \tag{2.18}$$

It can be proved that the convergence is guaranteed by iteratively updating μ according to eq. (2.18) since μ is non-decreasing after each iteration [80]. These iterative operations continue until $|f_1^{\text{obj},*} - \mu f_2^{\text{obj},*}|$ is no greater than a given threshold (i.e., Step 13

of Algorithm 1).

For a given value of μ, we then solve Problem (BVO-E-Sub). To solve Problem (BVO-E-Sub), we firstly identify the following feature.

Proposition 1. *In Problem (BVO-E-Sub), the optimal receiving beamforming vectors that maximize the radar sensing REIR can be given as*

$$\mathbf{u}_n^* = \max_{i \in \mathcal{I}} \left\{ \frac{x_{ni} \mathbf{\Gamma}_{ni}^{-1} \mathbf{A}(\theta_n) \mathbf{v}_n}{\mathbf{v}_n^H \mathbf{A}^H(\theta_n) \mathbf{\Gamma}_{ni}^{-1} \mathbf{A}(\theta_n) \mathbf{v}_n} \right\}. \tag{2.19}$$

Proof. According to the minimum variance distortionless response (MVDR) problem [81], for each ST n, the design of $\mathbf{u}_n$ can be expressed as

$$\max_{\mathbf{u}_n} \ \zeta_{ni}^{\text{echo}} = \frac{x_{ni} |\alpha_{ni}|^2 |\mathbf{u}_n^H \mathbf{A}(\theta_n) \mathbf{v}_n|^2}{\mathbf{u}_n^H \mathbf{\Gamma}_{ni} \mathbf{u}_n}. \tag{2.20}$$

Let $\frac{\partial \zeta_{ni}^{\text{echo}}}{\partial \mathbf{u}_n} = 0$, we can derive that

$$\mathbf{u}_n = \begin{cases} \frac{\mathbf{\Gamma}_{ni}^{-1} \mathbf{A}(\theta_n) \mathbf{v}_n}{\mathbf{v}_n^H \mathbf{A}^H(\theta_n) \mathbf{\Gamma}_{ni}^{-1} \mathbf{A}(\theta_n) \mathbf{v}_n}, & \text{when } x_{ni} = 1, \\ 0, & \text{otherwise.} \end{cases} \tag{2.21}$$

Therefore, the optimal receiving beamforming vector that maximizes the radar sensing REIR can be given as eq. (2.19). □

Substituting eq. (2.19) into eq. (2.8), the REIR for sensing ST n over CU i's channel can be calculated as

$$R_{ni}^{\text{rad}} = \frac{\delta}{2T} \log_2 \left(1 + 2TB_i x_{ni} \mathbf{v}_n^H \mathbf{\Phi}_{ni} \mathbf{v}_n\right), \tag{2.22}$$

where $\mathbf{\Phi}_{ni} = |\alpha_{ni}|^2 \mathbf{A}^H(\theta_n) \mathbf{\Gamma}_{ni}^{-1} \mathbf{A}(\theta_n)$.

For each ST n, we define $\mathbf{V}_n \triangleq \mathbf{v}_n \mathbf{v}_n^H$, with three constraints $\mathbf{V}_n \succeq 0$, $\mathbf{V}_n = \mathbf{V}_n^H$, and rank($\mathbf{V}_n$) = 1. For CU i, we define $\mathbf{H}_i \triangleq \mathbf{h}_i \mathbf{h}_i^H$ and $\mathbf{W}_i \triangleq \mathbf{w}_i \mathbf{w}_i^H$. Then, with eq. (2.4), constraint (2.10) can be rewritten as

$$\sum_{n \in \mathcal{N}_i} \mathbf{Tr}\left(\mathbf{H}_i \mathbf{V}_n\right) \leq \epsilon_i, \forall i \in \mathcal{I}, \tag{2.23}$$

where ϵ_i can be expressed as

$$\epsilon_i = \frac{\mathbf{Tr}\left(\mathbf{H}_i\mathbf{W}_i\right) - \sigma_C^2\left(2^{\frac{R_i^{\text{req}}}{B_i}} - 1\right)}{2^{\frac{R_i^{\text{req}}}{B_i}} - 1}. \tag{2.24}$$

We first address the non-convexity of $\mathbf{\Phi}_{ni}$ by using an iterative approach in which we set the values of $\{\mathbf{V}_n\}_{n\in\mathcal{N}}$ in $\mathbf{\Phi}_{ni}$ at each iteration according to the optimal values of $\{\mathbf{V}_n\}_{n\in\mathcal{N}}$ obtained in the previous iteration. Specifically, we calculate

$$\mathbf{\Phi}'_{ni} = |\alpha_{ni}|^2\mathbf{A}^H(\theta_n)\mathbf{\Gamma}_{ni}^{-1}(\{\mathbf{V}'_n\}_{n\in\mathcal{N}})\mathbf{A}(\theta_n), \tag{2.25}$$

where $\{\mathbf{V}'_n\}_{n\in\mathcal{N}}$ denotes the optimal value obtained in the previous iteration. Then, with eq. (2.25) and $\mathbf{V}_n \triangleq \mathbf{v}_n\mathbf{v}_n^H$, eq. (2.22) can be rewritten as

$$R_{ni}^{\text{rad}} = \frac{\delta}{2T}\log_2\Big(1 + 2TB_ix_{ni}\mathbf{Tr}\left(\mathbf{\Phi}'_{ni}\mathbf{V}_n\right)\Big). \tag{2.26}$$

The iterative process continues until the change in the value of eq. (2.26) is no greater than a given threshold (i.e., Step 10 of Algorithm 1). Therefore, with semidefinite relaxation (SDR), we can temporarily do not account for the constraint rank($\mathbf{V}_n$) = 1 and reformulate Problem (BVO-E-Sub) as follows.

$$\begin{aligned}\text{(BVO-E-SDR):}\ \max\ \Theta(\{\mathbf{V}_n\}_{n\in\mathcal{N}}) = &\sum_{n\in\mathcal{N}}\sum_{i\in\mathcal{I}} R_{ni}^{\text{rad}} - \\ &\mu\left(\mathbf{Tr}\left(\sum_{i\in\mathcal{I}}\mathbf{W}_i + \sum_{n\in\mathcal{N}}\mathbf{V}_n\right) + P^C\right)\end{aligned}$$

subject to: constraint (2.23),

$$\mathbf{V}_n \succeq 0, \forall n \in \mathcal{N}, \tag{2.27}$$

$$\mathbf{V}_n = \mathbf{V}_n^H, \forall n \in \mathcal{N}, \tag{2.28}$$

variables: $\{\mathbf{V}_n\}_{n\in\mathcal{N}}$.

Although Problem (BVO-E-SDR) does not include the rank-1 constraint, our Proposition 3 below guarantees that we can use the solution of Problem (BVO-E-SDR) to yield the solution that satisfies the rank-1 constraint. An important feature that enables

us to efficiently solve Problem (BVO-E-SDR) is as follows.

Proposition 2. *Problem (BVO-E-SDR) is a strictly convex optimization with respect to* $\{\mathbf{V}_n\}_{n\in\mathcal{N}}$.

Proof. We denote $O_{ni} = 2TB_i x_{ni}\mathbf{Tr}(\mathbf{\Phi}'_{ni}\mathbf{V}_n)$, which is a linear function with respect to $\{\mathbf{V}_n\}_{n\in\mathcal{N}}$. Moreover, it can be verified that $R_{ni}^{\text{rad}} = \frac{\delta}{2T}\log_2(1+O_{ni})$ is a concave function with respect to $\{O_{ni}\}_{n\in\mathcal{N},i\in\mathcal{I}}$. According to the theory of the operation that preserve convexity, R_{ni}^{rad} is a concave function with respect to $\{\mathbf{V}_n\}_{n\in\mathcal{N}}$. Moreover, in the objective function, the second term $\mu\left(\mathbf{Tr}\left(\sum_{i\in\mathcal{I}}\mathbf{W}_i+\sum_{n\in\mathcal{N}}\mathbf{V}_n\right)+P^C\right)$ is affine with respect to $\{\mathbf{V}_n\}_{n\in\mathcal{N}}$. Constraints (2.23), (2.27) and (2.28) are all affine. Therefore, Problem (BVO-E-SDR) is a strictly convex optimization with $\mathbf{V}_n$. □

With Proposition 2, we can construct a Lagrangian function by using the Lagrange duality based method [82]. The Lagrangian function of Problem (BVO-E-SDR) is shown as

$$\begin{aligned}\mathcal{L}^{\text{BVO}}(\{\mathbf{V}_n\}_{n\in\mathcal{N}},\{\lambda_i\}_{i\in\mathcal{I}}) = &\sum_{n\in\mathcal{N}}\sum_{i\in\mathcal{I}}R_{ni}^{\text{rad}} - \mu\left(\mathbf{Tr}\left(\sum_{i\in\mathcal{I}}\mathbf{W}_i+\sum_{n\in\mathcal{N}}\mathbf{V}_n\right)+P^C\right)\\ &-\sum_{i\in\mathcal{I}}\lambda_i\left(\sum_{n\in\mathcal{N}_i}\mathbf{Tr}\left(\mathbf{H}_i\mathbf{V}_n\right)-\epsilon_i\right).\end{aligned} \tag{2.29}$$

where λ_i denotes the dual variable. The Lagrange dual function can be given as

$$\text{(BVO-Lagrange): } g^{\text{SSO}}(\{\lambda_i\}_{i\in\mathcal{I}}) = \max_{\{\mathbf{V}_n\}_{n\in\mathcal{N}}}\ \mathcal{L}^{\text{BVO}}(\{\mathbf{V}_n\}_{n\in\mathcal{N}},\{\lambda_i\}_{i\in\mathcal{I}}).$$

The corresponding Lagrange dual problem can be formulated as

$$\begin{aligned}&\text{(BVO-Dual): } \min\ g^{\text{SSO}}(\{\lambda_i\}_{i\in\mathcal{I}})\\ &\text{variables: } \lambda_i\geq 0, \forall i\in\mathcal{I}.\end{aligned}$$

After the above operations, we can solve the Lagrange dual problem by firstly optimizing $\{\mathbf{V}_n\}_{n\in\mathcal{N}}$ with the given dual variables $\{\lambda_i\}_{i\in\mathcal{I}}$ via the gradient ascent method,

and then update the dual variables $\{\lambda_i\}_{i\in\mathcal{I}}$ with the optimized $\{\mathbf{V}_n\}_{n\in\mathcal{N}}$ by using the subgradient method [83]. The details are as follows.

Optimizing $\{\mathbf{V}_n\}_{n\in\mathcal{N}}$ with the given dual variables $\{\lambda_i\}_{i\in\mathcal{I}}$

The gradient of the Lagrangian function (2.29) regarding $\{\mathbf{V}_n\}_{n\in\mathcal{N}}$ can be calculated as

$$\nabla_{\mathbf{V}_n}\mathcal{L}^{\text{BVO}} = \sum_{i\in\mathcal{I}} \frac{\delta B_i x_{ni}(\mathbf{\Phi}'_{ni})^H}{(1+2TB_i x_{ni}\mathbf{Tr}\left(\mathbf{\Phi}'_{ni}\mathbf{V}_n\right))\ln 2} - \mu\mathbf{I} - \sum_{i\in\mathcal{I}} \lambda_i \mathbf{H}_i^H. \tag{2.30}$$

According to the gradient ascent method, $\mathbf{V}_n$ can be updated sequentially according to

$$\mathbf{V}_n = \mathbf{V}_n + \kappa\nabla_{\mathbf{V}_n}\mathcal{L}^{\text{BVO}}, \tag{2.31}$$

where κ denotes the updating step-size and it can be updated as

$$\kappa = \arg\max_{\kappa}\ \mathcal{L}^{\text{BVO}}(\{\mathbf{V}_n + \kappa\nabla_{\mathbf{V}_n}\mathcal{L}^{\text{BVO}}\}_{n\in\mathcal{N}}, \{\lambda_i\}_{i\in\mathcal{I}}). \tag{2.32}$$

The iterations in eq. (2.31) continue until $|\nabla_{\mathbf{V}_n}\mathcal{L}^{\text{BVO}}|$ is no greater than a given threshold (i.e., Step 7 of Algorithm 1). We denote the obtained result as $\{\mathbf{V}_n^*\}_{n\in\mathcal{N}}$.

Optimizing $\{\lambda_i\}_{i\in\mathcal{I}}$ with the optimized $\{\mathbf{V}_n^*\}_{n\in\mathcal{N}}$

With the obtained $\{\mathbf{V}_n^*\}_{n\in\mathcal{N}}$, the corresponding optimal Lagrange multipliers can be determined accordingly by solving Problem (BVO-Dual). Specifically, we exploit the subgradient method to update the dual variables $\{\lambda_i\}_{i\in\mathcal{I}}$, in which the subgradient direction can be expressed as

$$\nabla_{\lambda_i} g^{\text{SSO}} = \epsilon_i - \sum_{n\in\mathcal{N}_i} \mathbf{Tr}\left(\mathbf{H}_i\mathbf{V}_n^*\right). \tag{2.33}$$

With the subgradient method, the value of λ_i can be updated by

$$\lambda_i = \left[\lambda_i - \xi\nabla_{\lambda_i} g^{\text{SSO}}\right]^+, \tag{2.34}$$

where function $[x]^+ = \max\{0, x\}$, and ξ is a dynamic step-size that can be selected by the self-adaptive method [83]. By iteratively optimizing $\{\mathbf{V}_n\}_{n\in\mathcal{N}}$ in eq. (2.31) and updating $\{\lambda_i\}_{i\in\mathcal{I}}$ according to eq. (2.34), the optimal solution of Problem (BVO-E-SDR) can be obtained when $\Theta(\{\mathbf{V}_n^*\}_{n\in\mathcal{N}}) = g^{\text{SSO}}(\{\lambda_i^*\}_{i\in\mathcal{I}})$ (i.e., Step 9 of Algorithm 1). Recall that $\Theta(\{\mathbf{V}_n\}_{n\in\mathcal{N}})$ is the objective function of Problem (BVO-E-SDR).

In particular, SDR used to obtain Problem (BVO-E-SDR) from Problem (BVO-E-Sub) can always guarantee the existence of a solution with rank($\mathbf{V}_n$) = 1, $\forall n \in \mathcal{N}$, which is attributed to the following proposition.

Proposition 3. *There exists an optimal solution to Problem (BVO-E-SDR), denoted by* $\{\hat{\mathbf{V}}_n\}_{n\in\mathcal{N}}$*, that satisfies the following rank-1 constraint:*

$$\textit{rank}(\hat{\mathbf{V}}_n) = 1, \forall n \in \mathcal{N}. \tag{2.35}$$

Proof. Let $\tilde{\mathbf{V}}_1, ..., \tilde{\mathbf{V}}_N$ be an arbitrary global optimum to Problem (BVO-E-SDR). We construct

$$\hat{\mathbf{v}}_n = (\mathbf{C}^H\tilde{\mathbf{V}}_n\mathbf{C})^{-\frac{1}{2}}\tilde{\mathbf{V}}_n\mathbf{C}, \hat{\mathbf{V}}_n = \hat{\mathbf{v}}_n\hat{\mathbf{v}}_n^H, \forall n \in \mathcal{N}, \tag{2.36}$$

where $\mathbf{C}$ is an arbitrary $N_t \times 1$ vector. It can be observed that $\hat{\mathbf{V}}_1, ..., \hat{\mathbf{V}}_N$ are rank-1 and semidefinite. Let $\mathbf{C} = \mathbf{h}_i$, we can derive that

$$\mathbf{h}_i^H\hat{\mathbf{V}}_n\mathbf{h}_i = \mathbf{h}_i^H\hat{\mathbf{v}}_n\hat{\mathbf{v}}_n^H\mathbf{h}_i = \mathbf{h}_i^H\tilde{\mathbf{V}}_n\mathbf{h}_i, \forall n \in \mathcal{N}, \tag{2.37}$$

which is consistent with constraint (2.23). Let $\mathbf{C} = \mathbf{a}_t(\theta)$, we can derive that

$$\begin{aligned}\mathbf{a}_r(\theta)\mathbf{a}_t^H(\theta)\hat{\mathbf{V}}_n\mathbf{a}_t(\theta)\mathbf{a}_r^H(\theta) &= \mathbf{a}_r(\theta)\mathbf{a}_t^H(\theta)\hat{\mathbf{v}}_n\hat{\mathbf{v}}_n^H\mathbf{a}_t(\theta)\mathbf{a}_r^H(\theta) \\ &= \mathbf{a}_r(\theta)\mathbf{a}_t^H(\theta)\tilde{\mathbf{V}}_n\mathbf{a}_t(\theta)\mathbf{a}_r^H(\theta), \forall n \in \mathcal{N},\end{aligned} \tag{2.38}$$

which is consistent with eq. (2.26). Moreover, due to $\hat{\mathbf{V}}_n = \hat{\mathbf{v}}_n\hat{\mathbf{v}}_n^H = \tilde{\mathbf{V}}_n$, $\{\hat{\mathbf{V}}_n\}_{n\in\mathcal{N}}$ can be validated as a feasible and globally optimal solution to Problem (BVO-E-SDR), which completes the proof. □

With Proposition 3, after obtaining the solution $\{\mathbf{V}_n\}_{n\in\mathcal{N}}$ of Problem (BVO-E-SDR), we can yield the rank-1 optimal solution $\{\hat{\mathbf{V}}_n\}_{n\in\mathcal{N}}$. Furthermore, we can obtain

the corresponding value of $\{\hat{\mathbf{v}}_n\}_{n\in\mathcal{N}}$ according to eq. (2.36). The detailed algorithm for solving Problem (MEE-BVO) is shown in Algorithm 1 and explained as follows.

Step 6 to Step 9

For the given $\{x_{ni}\}_{n\in\mathcal{I},i\in\mathcal{I}}$, μ, and $\mathbf{\Phi}'_{ni}$, we iteratively update the Lagrange dual variables $\{\lambda_i\}_{i\in\mathcal{I}}$ and beamforming vectors $\{\mathbf{V}_n\}_{n\in\mathcal{N}}$ until $\Theta(\{\mathbf{V}_n^*\}_{n\in\mathcal{N}}) = g^{\text{SSO}}(\{\lambda_i^*\}_{i\in\mathcal{I}})$ to obtain the solution to Problem (BVO-E-SDR).

Step 4 to Step 10

With Step 6 to Step 9, we can perform an iterative update of $\mathbf{\Phi}'_{ni}$ based on eq. (2.25) to obtain the solution of Problem (BVO-E-Sub). The iteration continues until the change in the value of R_{ni}^{rad} given in eq. (2.26) is no greater than the threshold Δ_2.

Step 2 to Step 17

With Step 4 to Step 10, we can calculate $\{f_1^{\text{obj},*}, f_2^{\text{obj},*}\}$ according to eqs. (2.14) and (2.15), and iteratively update μ according to eq. (2.18) until $|f_1^{\text{obj},*} - \mu f_2^{\text{obj},*}|$ is no greater than the threshold Δ_1 to obtain the solution of Problem (MEE-BVO).

Algorithm 1: Solving Problem (MEE-BVO) and calculate the value of $\{\mathbf{v}_n\}_{n\in\mathcal{N}}$ and $\{\mathbf{u}_n\}_{n\in\mathcal{N}}$.

Initialization: Given $\{x_{ni}\}_{n\in\mathcal{I},i\in\mathcal{I}}$. Initialize μ satisfying $f_1^{\text{obj}} - \mu f_2^{\text{obj}} \geq 0$. Set the thresholds Δ_1, Δ_2 and Δ_3 as very small numbers.
while 1 **do**
  Initialize $\{\mathbf{V}_n\}_{n\in\mathcal{N}}$.
  repeat
    Initialize dual variables $\{\lambda_i\}_{i\in\mathcal{I}}$. Calculate $\mathbf{\Phi}'_{ni}$ using eq. (2.25).
    repeat
      Obtain the optimal $\{\mathbf{V}_n^*\}_{n\in\mathcal{N}}$ according to eqs. (2.30) and (2.31) until $|\nabla_{\mathbf{V}_n}\mathcal{L}^{\text{BVO}}| \leq \Delta_3$.
      Update dual variables $\{\lambda_i\}_{i\in\mathcal{I}}$ based on eqs. (2.33) and (2.34).
    until $\Theta(\{\mathbf{V}_n^*\}_{n\in\mathcal{N}}) = g^{\text{SSO}}(\{\lambda_i^*\}_{i\in\mathcal{I}})$
  until the change in the value of eq. (2.26) is no greater than Δ_2.
  Calculate $\{f_1^{\text{obj},*}, f_2^{\text{obj},*}\}$ according to eqs. (2.14) and (2.15).
  if $|f_1^{\text{obj},*} - \mu f_2^{\text{obj},*}| \leq \Delta_1$ **then**
    break the WHILE-LOOP.
  else
    Update μ according to eq. (2.18).
  end if
end while
Output: Calculate $\{\hat{\mathbf{v}}_n\}_{n\in\mathcal{N}}$ via eq. (2.36). Calculate $\{\mathbf{u}_n^*\}_{n\in\mathcal{N}}$ via eq. (2.19).

According to the criterion of Dinkelbach's method [80] and the Lagrangian duality [82], Algorithm 1 is guaranteed to converge.

2.3.3 Proposed Algorithm for solving Problem (MEE-SSO)

With the optimized $\{\mathbf{v}_n^*\}_{n\in\mathcal{N}}$ and $\{\mathbf{u}_n^*\}_{n\in\mathcal{N}}$, we continue to optimize the sensing scheduling $\{x_{ni}\}_{n\in\mathcal{N},i\in\mathcal{I}}$ by solving Problem (MEE-SSO). To efficiently solve this problem, we formulate the sensing scheduling problem as a two-sided many-to-one matching game problem, where each ST matches at most one CU's channel and each CU i's channel can be reused for sensing at most $J_i^{\max}$ STs, which correspond to constraints (2.11) and (2.12) before.

To facilitate the formulation of the matching game, we introduce Lagrange multipliers $\{\tau_i\}_{i\in\mathcal{I}}$ to relax constraint (2.10) as follows

$$\mathcal{L}^{\text{SSO}}(\{x_{ni}\}_{n\in\mathcal{N},i\in\mathcal{I}},\{\tau_i\}_{i\in\mathcal{I}})=\sum_{n\in\mathcal{N}}\sum_{i\in\mathcal{I}}R_{ni}^{\text{rad}}+\sum_{i\in\mathcal{I}}\tau_i\left(1-\frac{\sum_{n\in\mathcal{N}_i}|\mathbf{h}_i^H\mathbf{v}_n|^2}{\epsilon_i}\right), \tag{2.39}$$

where ϵ_i is given in eq. (2.24). We treat $\overline{\tau}_i=\frac{\tau_i}{\epsilon_i}$ as a unit price. Thus, $\overline{\tau}_i\sum_{n\in\mathcal{N}_i}|\mathbf{h}_i^H\mathbf{v}_n|^2$ can be regarded as the cost for CU i to share its channel for sensing the targets, which is proportional to the aggregate interference of sensing signals to CU i. With some further transformations, we reformulate Problem (MEE-SSO) as follows.

$$\begin{aligned}&\text{(SSO-Matching): } g^{\text{SSO}}(\{\overline{\tau}_i\}_{i\in\mathcal{I}})=\max\sum_{n\in\mathcal{N}}\sum_{i\in\mathcal{I}}R_{ni}^{\text{rad}}-\sum_{i\in\mathcal{I}}\overline{\tau}_i\sum_{n\in\mathcal{N}_i}|\mathbf{h}_i^H\mathbf{v}_n|^2\\&\quad\text{subject to: constraints }(2.11),(2.12)\text{ and }(2.13),\\&\quad\text{variables: }\{x_{ni}\}_{n\in\mathcal{N},i\in\mathcal{I}}.\end{aligned}$$

We first define $\succ_{\mathcal{I}}=\{\succ_i\}_{i\in\mathcal{I}}$ and $\succ_{\mathcal{N}}=\{\succ_n\}_{n\in\mathcal{N}}$ as the preference relation sets for the CUs and STs, respectively. Then, the many-to-one matching can be defined as a tuple $(\mathcal{I},\mathcal{N},\succ_{\mathcal{I}},\succ_{\mathcal{N}})$. Specifically, we have the following definition.

Definition 2.3.1. *For two sets $\mathcal{I}$ and $\mathcal{N}$ of disjoint matching players, a many-to-one matching strategy β is a subset of $\mathcal{I}\bigotimes\mathcal{N}$:*

1. $\beta(n) \in \mathcal{I}$ *and* $|\beta(n)| \leq 1, \forall\, n \in \mathcal{N}$,

2. $\beta(i) \in \mathcal{N}$ *and* $|\beta(i)| \leq J_i^{max}, \forall\, i \in \mathcal{I}$,

3. $n \in \beta(i)$ *if and only if* $i \in \beta(n)$,

where $\beta(n) = \{i|(n,i) \in \beta, i \in \mathcal{I}\}$ *and* $\beta(i) = \{n|(n,i) \in \beta, n \in \mathcal{N}\}$. *In addition,* $|\beta|$ *denotes the number of elements in the set* β.

Definition 2.3.1 implies that a player on one side will be matched with a group of players or an empty set on the other side, where $\beta(i)$ denotes the set of the STs that use CU i's channel and $\beta(n)$ denotes the channel used by ST n. Conditions 1) and 2) in Definition 2.3.1 ensure that constraints (2.11) and (2.12) are satisfied, respectively. Condition 3) in Definition 2.3.1 indicates the symmetry and transitivity. In particular, $\beta(n) = \{i\}$ is equivalent to $x_{ni} = 1$.

To determine the matching outcome, the utility function is designed to evaluate the preference relationship of each matching player. Given the current matching strategy β and the associated transmitting beamforming vectors $\boldsymbol{\nu}_i^{\beta} = \{x_{1i}\mathbf{v}_1^{\beta}, ..., x_{Ni}\mathbf{v}_N^{\beta}\}$ for CU i's channel, we design a utility function of ST n for CU i's channel as

$$\mathcal{U}_n(i) = R_{ni}^{\text{rad}}(\boldsymbol{\nu}_{i\backslash\{n\}}^{\beta}, \mathbf{v}_n^{\beta}) - \sum_{s\in\mathcal{N}, s\neq n} \eta_{si} \sum_{e\in\mathcal{N}_i} |\alpha_{ei}|^2 |\mathbf{u}_s^H \mathbf{A}(\theta_e)\mathbf{v}_n|^2 - \varepsilon_i, \tag{2.40}$$

where $\boldsymbol{\nu}_{i\backslash\{n\}}^{\beta}$ denotes the transmitting beamforming except ST n on the CU i's channel, and ε_i denotes the price to be paid for using CU i's channel. In particular, η_{ni} denotes the unit price of interference, and its value can be expressed as

$$\eta_{ni} = \frac{\partial R_{ni}^{\text{rad}}}{\partial E_{ni}(\{\boldsymbol{\nu}_{i\backslash\{n\}}\})} = \frac{\delta B_i}{\ln 2} \cdot \frac{x_{ni}|\alpha_{ni}|^2}{(E_{ni}(\{\boldsymbol{\nu}_{i\backslash\{n\}}\}) + 2TB_i x_{ni}|\alpha_{ni}|^2) E_{ni}(\{\boldsymbol{\nu}_{i\backslash\{n\}}\})}, \tag{2.41}$$

where $E_{ni}(\{\boldsymbol{\nu}_{i\backslash\{n\}}\}) = \mathbf{u}_n^H \boldsymbol{\Gamma}_{ni}(\{\boldsymbol{\nu}_{i\backslash\{n\}}\})\mathbf{u}_n$ is the interference from other STs received by ST n on CU i's channel. Therefore, η_{ni} denotes the unit decrease in the REIR of ST n as interference from other STs increases. Eq. (2.40) also indicates that when ST n uses CU i's channel, it achieves the corresponding REIR while incurring interference to the other STs on the same CU's channel.

Moreover, we design a utility function for CU i as

$$\mathcal{U}_i(\mathcal{N}_i) = \varepsilon_i|\mathcal{N}_i| - \overline{\tau}_i \sum_{n\in\mathcal{N}_i} |\mathbf{h}_i^H \mathbf{v}_n|^2. \tag{2.42}$$

Recall that ε_i denotes the price paid by each ST that reuses CU i's channel, and the second term in eq. (2.42) denotes the cost for CU i to share its channel. Therefore, although CU i's channel sharing leads to a degradation of its throughput, CU i can gain the benefit denoted by the first term in eq. (2.42), which thus motivates CU i to share its channels for sensing the targets.

With eqs. (2.40) and (2.42), for two different CU i and CU j ($\forall i, j \in \mathcal{I}, i \neq j$), we have $i \succ_n j \iff \mathcal{U}_n(i) > \mathcal{U}_n(j)$ and $\mathcal{N}_i \succ_i \mathcal{N}_j \iff \mathcal{U}_i(\mathcal{N}_i) > \mathcal{U}_i(\mathcal{N}_j)$. In addition, the preferences of the STs and CUs change as the game evolves, which leads to a peer effect that makes the existence of a traditional stable match no longer guaranteed [84]. To address the peer effect, we consider a concept based on the stability of two-sided swap matching with the swap operation defined as follows [85].

Definition 2.3.2. *Given a matching strategy β, for two different STs $n, n' \in \mathcal{N}$ and two different CUs $i, j \in \mathcal{I}$, a swap operation is*

$$\beta_n^{n'} = \{\beta \backslash \{(n,i),(n',j)\} \cap \{(n,j),(n',i)\}\}, \tag{2.43}$$

where $n \in \beta(i)$ and $n' \in \beta(j)$.

In the swap operation, two STs matched over different CUs' channels are swapped while keeping the matching of the remaining STs and the CUs' channels unchanged. To accomplish the swap operations, the swap-blocking pair is defined as

Definition 2.3.3. *Given a matching strategy β, a pair of STs $n, n' \in \mathcal{N}$ is swap-blocking pair if and only if*

1. $\forall b \in \{n, n', \beta(n), \beta(n')\}$, $\mathcal{U}_b(\beta_n^{n'}) \geq \mathcal{U}_b(\beta)$,
2. $\exists b \in \{n, n', \beta(n), \beta(n')\}$, $\mathcal{U}_b(\beta_n^{n'}) > \mathcal{U}_b(\beta)$.

Condition 1) in Definition 2.3.3 indicates that the utilities of all the involved matching players should not decrease after each swap operation. Condition 2) in Definition

2.3.3 indicates that the utilities of at least one of the involved matching players can be improved after the swap operation, which avoids invalid swap operations. Therefore, the swap operation between the swap-blocking pair guarantees an increase in the total utility of all involved matching players. Based on Definition 2.3.3, we have the following definition of the stability for the two-sided swap matching.

Definition 2.3.4. *The two-sided swap matching achieves stability if and only if there is no swap-blocking pair.*

After the two-sided swap matching achieves stability, we continue to solve the dual problem as follows.

$$\begin{aligned} &\text{(SSO-Dual): } \min\ g^{\text{SSO}}(\{\overline{\tau}_i\}_{i\in\mathcal{I}}) \\ &\text{variables: } \{\overline{\tau}_i \geq 0\}_{i\in\mathcal{I}}. \end{aligned}$$

We adopt a heuristic subgradient-based method, where the value of $\overline{\tau}_i$ can be updated by

$$\overline{\tau}_i = \left[\overline{\tau}_i - \varsigma\left(1 - \frac{\sum_{n\in\mathcal{N}_i}|\mathbf{h}_i^H\mathbf{v}_n|^2}{\epsilon_i}\right)\right]^+, \tag{2.44}$$

where ς is the step size. The details for solving Problem (MEE-SSO) are shown in Algorithm 2 and explained as follows.

Step 1 to Step 14

We first construct an initial matching strategy by using the deferred acceptance algorithm [86] to improve the efficiency of swap matching. Note that the initial matching strategy obtained does not guarantee the matching stability due to the peer effect.

Step 15 to Step 27

After obtaining the initial matching strategy, we perform a swap operation on the swap-blocking pair. When there is no more swap-blocking pair, we update the dual variables $\{\overline{\tau}_i\}_{i\in\mathcal{I}}$ according to eq. (2.44). This process is repeated until the value of $\left|\Lambda(\{x_{ni}^*\}_{n\in\mathcal{N},i\in\mathcal{I}}) - g^{\text{SSO}}(\{\overline{\tau}_i^*\}_{i\in\mathcal{I}})\right|$ shows a negligible variation (recall that $\Lambda(\{x_{ni}\}_{n\in\mathcal{N},i\in\mathcal{I}})$ is the objective function of Problem (MEE-SSO)).

Algorithm 2: Solving Problem (MEE-SSO) and calculate the value of $\{x_{ni}\}_{n\in\mathcal{N},i\in\mathcal{I}}$.

Each CU constructs its preference list $\mathcal{P}_i^{CU}$ and each ST constructs its preference list $\mathcal{P}_n^{ST}$. Construct a current set $\mathcal{P}^{CR}=\mathcal{N}$ of current remaining STs. Initialize $\{x_{ni}=0\}_{n\in\mathcal{N},i\in\mathcal{I}}$.
repeat
  for $\forall n\in\mathcal{P}^{CR}$ **do**
    ST n makes a request to the CU i ($i\in\mathcal{I}$) with the highest ranking in its preference list and marks $x_{ni}=1$.
  end for
  for $\forall i\in\mathcal{I}$ **do**
    if $\sum_{n\in\mathcal{N}}x_{ni}\leq J_i^{\max}$ **then**
      CU i accepts all requesting STs. Keep these STs' $x_{ni}=1$ and remove them from $\mathcal{P}^{CR}$.
    else
      CU i accepts the top $J_i^{\max}$ STs. Keep the top $J_i^{\max}$ STs' $x_{ni}=1$ and remove them from $\mathcal{P}^{CR}$. Set $x_{ni}=0$ for the other STs and add them into $\mathcal{P}^{CR}$.
    end if
    Remove i from $\mathcal{P}_n^{ST}$ of all STs that request to CU i.
  end for
until $\mathcal{P}^{CR}=\emptyset$ or $\forall\mathcal{P}_n^{ST}=\emptyset$.
Initialize β according to current $\{x_{ni}\}_{n\in\mathcal{N},i\in\mathcal{I}}$. Initialize $\{\overline{\tau}_i\}_{i\in\mathcal{I}}$.
repeat
  repeat
    For an arbitrary CU $i\in\mathcal{I}$, it selects ST $n\in\mathcal{N}_i$. For an arbitrary CU $i'\in\mathcal{I}, i'\neq i$, it selects ST $n'\in\mathcal{N}_{i'}$.
    if (n,n') is a swap-blocking pair **then**
      Update matching strategy $\beta\leftarrow\beta_n^{n'}$ according to eq. (2.43) and update the utility functions of the STs and CUs according to eqs. (2.40) and (2.42), respectively.
    else
      Keep the current matching strategy unchanged.
    end if
  until there is no swap-blocking pair in the current matching strategy.
  Update $\{\overline{\tau}_i\}_{i\in\mathcal{I}}$ according to eq. (2.44).
until the value of $\left|\Lambda(\{x_{ni}^*\}_{n\in\mathcal{N},i\in\mathcal{I}})-g^{\text{SSO}}(\{\overline{\tau}_i^*\}_{i\in\mathcal{I}})\right|$ shows a negligible variation.
Output: Calculate $\{x_{ni}\}_{n\in\mathcal{I},i\in\mathcal{I}}$ based on the current matching outcome.

In addition, we have the following proposition to illustrate the convergence of Algorithm 2.

Proposition 4. *Algorithm 2 can converge to a two-sided swap-stable matching.*

Proof. To prove Proposition 4, we first show that after each swap operation in Algorithm 2, the Lagrangian function eq. (2.39) is monotonically increasing. Specifically, for the current matching strategy β, we assume that there is a swap-blocking pair (p, p') $(\forall p, p' \in \mathcal{N}, p \neq p')$ which matches the channels of CU q and CU q' $(\forall q, q' \in \mathcal{I}, q \neq q')$, respectively. Therefore, the objective function of Problem (SSO-Matching) can be given as

$$\mathit{\Pi}(\beta) = \sum_{q\in\mathcal{I}} \sum_{p\in\beta(q)} R_{pq}^{\text{rad}} - \sum_{q\in\mathcal{I}} \tilde{\tau}_q \sum_{p\in\beta(q)} |\mathbf{h}_q \mathbf{v}_p|^2. \tag{2.45}$$

For each ST $n \in \beta(q)\backslash\{p\}$ using CU q's channel, we can express the first-order Taylor expansion of $R_{nq}^{\text{rad}}(\boldsymbol{\nu}_{q\backslash\{p,p'\}}, x_{pq}\mathbf{v}_p, x_{p'q}\mathbf{v}_{p'})$ about $(x_{pq}^{\beta}\mathbf{v}_p^{\beta}, x_{p'q}^{\beta}\mathbf{v}_{p'}^{\beta}) = (\mathbf{v}_p, \mathbf{0})$ as

$$\tilde{R}_{nq}^{\text{rad}}(\boldsymbol{\nu}_{q\backslash\{p,p'\}}, x_{pq}\mathbf{v}_p, x_{p'q}\mathbf{v}_{p'}) = R_{nq}^{\text{rad}}(\boldsymbol{\nu}_q) - \boldsymbol{\phi}_{pq}^H(x_{pq}\mathbf{v}_p - \mathbf{v}_p) - \boldsymbol{\phi}_{p'q}^H x_{pq}\mathbf{v}_{p'}, \tag{2.46}$$

where $\boldsymbol{\phi}_{pq} = \eta_{nq}\frac{\partial E_{nq}(\{\boldsymbol{\nu}_{q\backslash\{n\}}\})}{\partial \mathbf{v}_p}$. Similarly, we can express the first-order Taylor expansion of $R_{nq'}^{\text{rad}}(\boldsymbol{\nu}_{q'\backslash\{p,p'\}}, x_{pq'}\mathbf{v}_p, x_{p'q'}\mathbf{v}_{p'})$ about $(x_{pq'}^{\beta}\mathbf{v}_p^{\beta}, x_{p'q'}^{\beta}\mathbf{v}_{p'}^{\beta}) = (\mathbf{0}, \mathbf{v}_{p'})$ as

$$\tilde{R}_{nq'}^{\text{rad}}(\boldsymbol{\nu}_{q\backslash\{p,p'\}}, x_{pq'}\mathbf{v}_p, x_{p'q'}\mathbf{v}_{p'}) = R_{nq'}^{\text{rad}}(\boldsymbol{\nu}_{q'}) - \boldsymbol{\phi}_{pq'}^H x_{pq'}\mathbf{v}_p - \boldsymbol{\phi}_{p'q'}^H(x_{pq'}\mathbf{v}_{p'} - \mathbf{v}_{p'}). \tag{2.47}$$

With eqs. (2.46) and (2.47), we construct

$$\begin{aligned}\Lambda_1 &= \sum_{n\in\beta(q)} R_{nq}^{\text{rad}}(\boldsymbol{\nu}_q^{\beta}) + \sum_{n\in\beta(q')} R_{nq'}^{\text{rad}}(\boldsymbol{\nu}_{q'}^{\beta}) \\ &= \sum_{n\in\beta(q)\backslash\{p\}} \tilde{R}_{nq}^{\text{rad}}(\boldsymbol{\nu}_{q\backslash\{p,p'\}}^{\beta}, \mathbf{v}_p, \mathbf{0}) + R_{pq}^{\text{rad}}(\boldsymbol{\nu}_q^{\beta}) + \\ &\quad \sum_{n\in\beta(q')\backslash\{p'\}} \tilde{R}_{nq'}^{\text{rad}}(\boldsymbol{\nu}_{q\backslash\{p,p'\}}^{\beta}, \mathbf{0}, \mathbf{v}_{p'}) + R_{p'q'}^{\text{rad}}(\boldsymbol{\nu}_{q'}^{\beta}).\end{aligned} \tag{2.48}$$

Based on Definition 2.3.3, we have

$$\begin{aligned}\Lambda_1 < \Lambda_2 = &\sum_{n\in\beta(q)\setminus\{p\}} \tilde{R}^{\text{rad}}_{nq}(\boldsymbol{\nu}^{\beta}_{q\setminus\{p,p'\}}, \mathbf{0}, \mathbf{v}_{p'}) + R^{\text{rad}}_{p'q}(\boldsymbol{\nu}^{\beta}_{q\setminus\{p'\}}, \mathbf{v}_{p'}) \\ + &\sum_{n\in\beta(q')\setminus\{p'\}} \tilde{R}^{\text{rad}}_{nq'}(\boldsymbol{\nu}^{\beta}_{q\setminus\{p,p'\}}, \mathbf{v}_p, \mathbf{0}) + R^{\text{rad}}_{pq'}(\boldsymbol{\nu}^{\beta}_{q'\setminus\{p\}}, \mathbf{v}_p) - \boldsymbol{\phi}^H_{p'q'}\mathbf{v}_p - \boldsymbol{\phi}^H_{pq}\mathbf{v}_{p'}.\end{aligned} \tag{2.49}$$

It is obvious that $R^{\text{rad}}_{nq}(\boldsymbol{\nu}_{q\setminus\{p,p'\}}, x_{pq}\mathbf{v}_p, x_{p'q}\mathbf{v}_{p'})$ is convex with respect to $(x_{pq}\mathbf{v}_p, x_{p'q}\mathbf{v}_{p'})$. Moreover, both $\boldsymbol{\phi}^H_{p'q'}\mathbf{v}_p$ and $\boldsymbol{\phi}^H_{pq}\mathbf{v}_{p'}$ are non-negative, which yields the following equation

$$\begin{aligned}\Lambda_2 \leq \Lambda_3 = &\sum_{n\in\beta(q)\setminus\{p\}} R^{\text{rad}}_{nq}(\boldsymbol{\nu}^{\beta^{p'}_p}_{q}) + R^{\text{rad}}_{p'q}(\boldsymbol{\nu}^{\beta}_{q\setminus\{p'\}}, \mathbf{v}_{p'}) \\ &+ \sum_{n\in\beta(q')\setminus\{p'\}} R^{\text{rad}}_{nq'}(\boldsymbol{\nu}^{\beta^{p'}_p}_{q'}) + R^{\text{rad}}_{pq'}(\boldsymbol{\nu}^{\beta}_{q'\setminus\{p\}}, \mathbf{v}_p).\end{aligned} \tag{2.50}$$

After the swap operation, ST p''s REIR $R^{\text{rad}}_{p'q}(\boldsymbol{\nu}^{\beta^{p'}_p}_{q\setminus\{p'\}}, \mathbf{v}_{p'}) \geq R^{\text{rad}}_{p'q}(\boldsymbol{\nu}^{\beta}_{q\setminus\{p'\}}, \mathbf{v}_{p'})$ since ST p no longer interferes with ST p'. Therefore, we obtain

$$\begin{aligned}\Lambda_3 \leq \Lambda_4 = &\sum_{n\in\beta(q)\setminus\{p\}} R^{\text{rad}}_{nq}(\boldsymbol{\nu}^{\beta^{p'}_p}_{q}) + R^{\text{rad}}_{p'q}(\boldsymbol{\nu}^{\beta^{p'}_p}_{q\setminus\{p'\}}, \mathbf{v}_{p'}) \\ &+ \sum_{n\in\beta(q')\setminus\{p'\}} R^{\text{rad}}_{nq'}(\boldsymbol{\nu}^{\beta^{p'}_p}_{q'}) + R^{\text{rad}}_{pq'}(\boldsymbol{\nu}^{\beta^{p'}_p}_{q'\setminus\{p\}}, \mathbf{v}_p) \\ = &\sum_{n\in\beta^{p'}_p(q)} R^{\text{rad}}_{nq}(\boldsymbol{\nu}^{\beta^{p'}_p}_{q}) + \sum_{n\in\beta^{p'}_p(q')} R^{\text{rad}}_{nq'}(\boldsymbol{\nu}^{\beta^{p'}_p}_{q'}).\end{aligned} \tag{2.51}$$

With Definition 2.3.3, we also have

$$\sum_{q\in\{p,p'\}} \tilde{\tau}_q \sum_{p\in\beta(q)} |\mathbf{h}_q\mathbf{v}_p|^2 \geq \sum_{q\in\{p,p'\}} \tilde{\tau}_q \sum_{p\in\beta^{p'}_p(q)} |\mathbf{h}_q\mathbf{v}_p|^2. \tag{2.52}$$

Thus, we conclude that $\mathit{\Pi}(\beta^{p'}_p) > \mathit{\Pi}(\beta)$, which means that each swap operation increases the value of eq. (2.39). Since there is a finite number of possible matching between the STs and the CUs, Algorithm 2 will terminate after a finite number of iterations. Based on Definition 2.3.4, we conclude that the matching outcome achieves

stability, which completes the proof of Proposition 4. □

Finally, to solve the original Problem (MEE), we execute Algorithm 1 and Algorithm 2 alternately until their respective solutions keep unchanged. The overall alternative algorithm is summarized in Algorithm 3.

Algorithm 3 : The Overall Alternative Algorithm for Solving Problem (MEE).

1: **repeat**
2: Using Algorithm 1 to solve Problem (MEE-BVO) and obtain the value of $\{\mathbf{v}_n\}_{n\in\mathcal{N}}$ and $\{\mathbf{u}_n\}_{n\in\mathcal{N}}$.
3: Using Algorithm 2 to solve Problem (MEE-SSO) and obtain the value of $\{x_{ni}\}_{n\in\mathcal{N},i\in\mathcal{I}}$.
4: **until** the solutions of Algorithm 1 and Algorithm 2 keep unchanged.

2.4 Numerical Results

We present the numerical results to verify the effectiveness of our algorithms and the performance of our channel sharing aided ISAC. Specifically, we consider an ISAC BS with $N_t = 10$ transmitting antennas and $N_r = 15$ receiving antennas. We consider three scenarios including $I = 5$ CUs with $N = 10$ STs, $I = 5$ CUs with $N = 15$ STs, and $N = 8$ CUs with $I = 15$ STs. The CUs are randomly distributed within a radius of $d_i \in [50, 200]m$ from the center of the ISAC BS, and the STs are uniformly distributed within a radius of $d_n \in [200, 400]m$ to centered on the ISAC BS. We set each CU's channel bandwidth $B_i = 10MHz$, the noise power $\sigma_C^2 = \sigma_S^2 = -120dBm$, radar duty factor $\delta = 0.01$, radar pulse duration $T = 2 \times 10^{-3}s$. In addition, the channel between the ISAC BS and CUs is considered to follow the Rayleigh channel model with the path loss of $L_{Ci} = 40 + 30\log_{10} d_i$, while the channel between the ISAC BS and STs is supposed to have a line-of-sight link correlated with the path loss of $L_{Rn} = 40 + 25\log_{10} d_n$ [87]. Finally, the thresholds are set as $\Delta_1 = \Delta_2 = \Delta_3 = 10^{-5}$.

Figure 2.3 validates the convergence and effectiveness of our Algorithm 1 and Algorithm 2 under three scenarios. Specifically, Figure 2.3(a) shows that the objective value of Problem (BVO-E) can converge rapidly for all the tested scenarios. Meanwhile, the objective value of Problem (BVO-E-Sub) converges almost to zero, which is consistent with the Dinkelbach's method. In Figure 2.3(b), we perform extensive simulations and plot the cumulative distribution function of the number of swap operations for the

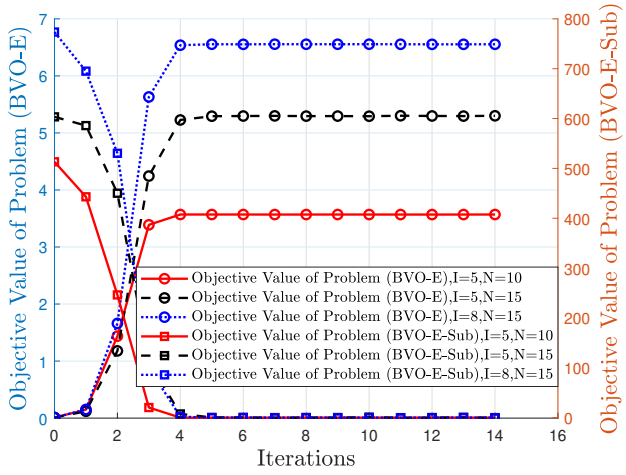

(a) Convergence of Algorithm 1

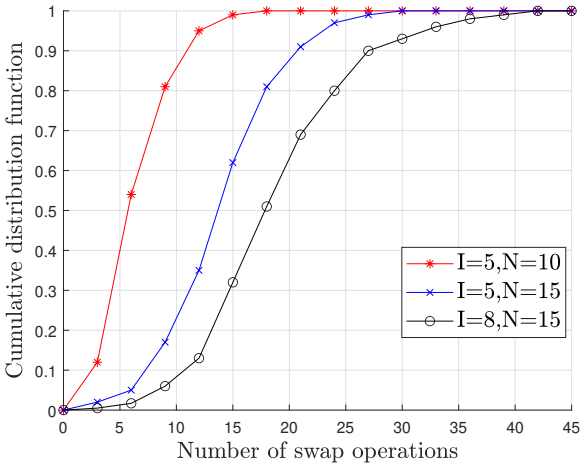

(b) Convergence of Algorithm 2

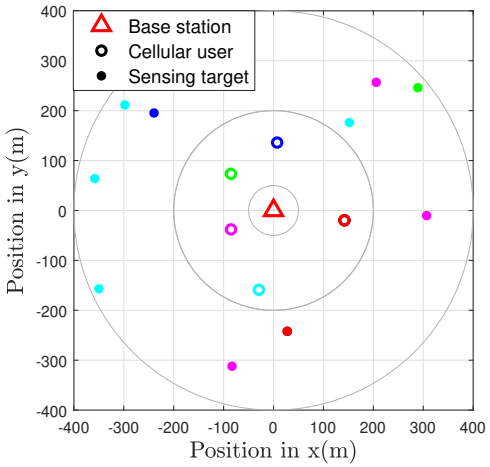

(c) Snapshot under $I = 5$, $N = 10$

Fig. 2.3: Convergence of proposed algorithms and snapshot of the final channel sharing overcomes

matching game. Figure 2.3(b) demonstrates that Algorithm 2 can converge within a small number of iterations for all three scenarios. In the scenario with $I = 8, N = 15$, 45 swap operations on average are required to ensure the convergence of Algorithm 2. Furthermore, Figure 2.3(b) also indicates that an increase in the number of the CUs or STs leads to an increase in the number of swap operations, since there will be more available swap-blocking pairs. As a concrete example, Figure 2.3(c) shows a snapshot of the optimal channel sharing solution for the scenario with $I = 5, N = 10$ by using our Algorithm 3, where the CUs and STs with the same color mean that they use the same channel.

Figure 2.4 demonstrates the performance of our proposed Algorithm 1 for solving Problem (MEE-BVO). Specifically, we use the zero-forcing (ZF) method [36] and the double-layer penalty (DLP) method [44] as the comparison benchmarks. Figure 2.4 demonstrates that our Algorithm 1 outperforms the two benchmark algorithms in terms of improving energy efficiency. Figure 2.4(a) shows that the energy efficiency increases when the number of the STs increases, which is due to the increase in the total REIR. Figure 2.4(b) shows that the energy efficiency increases as the number of the CUs increases, which is due to the reduction of mutual interference among STs. Figure 2.4(c) shows that as the maximum number of the STs which can be sensed by each CU's channel increases, the energy efficiency gradually increases until all STs are sensed by their respective most preferred CUs' channels.

Figure 2.5 demonstrates the performance of our proposed Algorithm 2 for solving Problem (MEE-SSO). We use the following two approaches as the comparison benchmarks, i.e., 1) greedy-based allocation (GBA) method based on mutual interference among STs [88] and 2) the total interference minimization allocation (TIMA) method which aims at minimizing $\sum_{n\in\mathcal{N}}\sum_{i\in\mathcal{I}} x_{ni}\mathbf{Tr}\left(\mathbf{H}_i\mathbf{V}_n\right)$ [89]. Figure 2.5 demonstrates that our Algorithm 2 outperforms the two benchmark algorithms in terms of improving the sum of REIR. Figure 2.5(a) shows that the sum of REIR increases as the number of the STs increases. Figure 2.5(b) shows that the sum of REIR increases as the number of the CUs increases. Figure 2.5(c) again demonstrates the advantage of our Algorithm 2 under different values of $J_i^{\max}$, i.e., the maximum number of the STs which can be

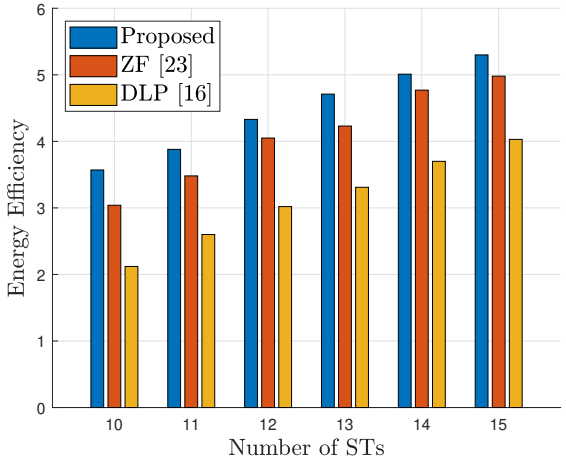

(a) With different numbers of the STs

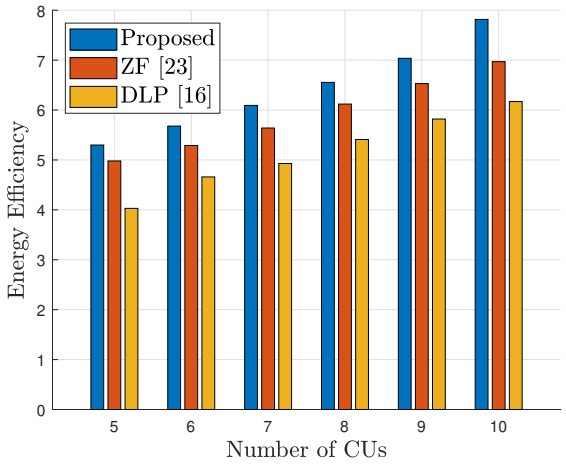

(b) With different numbers of the CUs

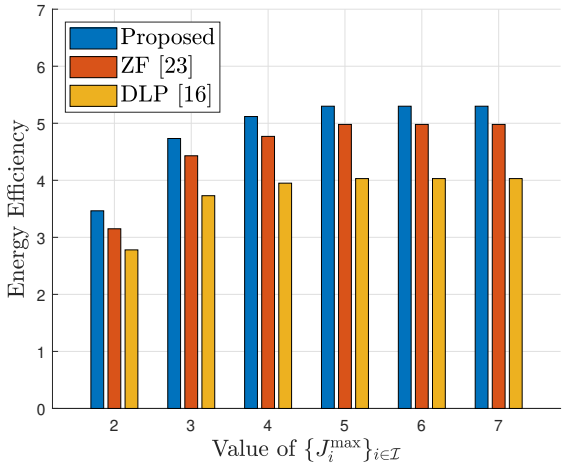

(c) With different values of $\{J_i^{\max}\}_{i\in\mathcal{I}}$

Fig. 2.4: Performance advantage of Algorithm 1

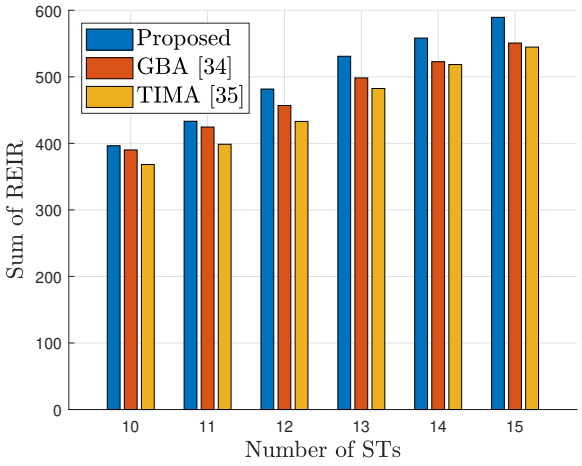

(a) With different numbers of the STs

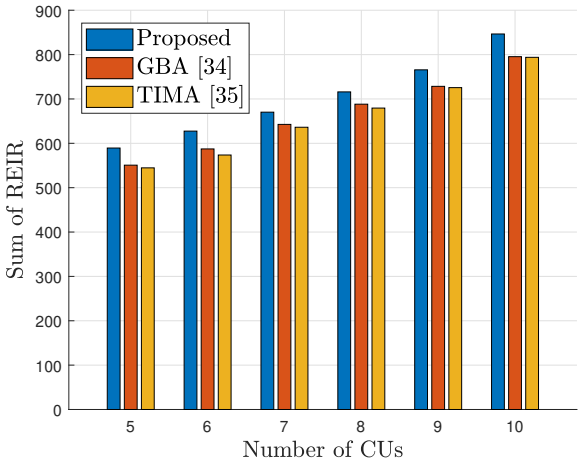

(b) With different numbers of the CUs

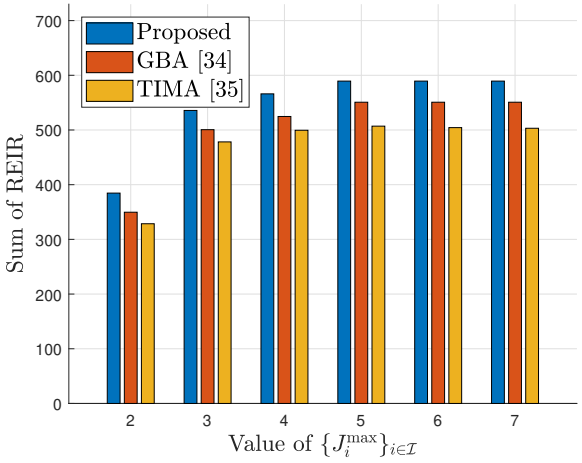

(c) With different values of $\{J_i^{\max}\}_{i\in\mathcal{I}}$

Fig. 2.5: Performance advantage of Algorithm 2

sensed by each CU's channel.

Figure 2.6 validates the accuracy and efficiency of Algorithm 3. Specifically, since our proposed alternating optimization method cannot guarantee to achieve the optimal solution of the original problem, we compare the results with the solution of LINGO [90]. In addition, we compare it with the scheme of learning which solves Problem (MEE-SSO) with the cross-entropy (CE) algorithm [91] and solves Problem (MEE-BVO) with CVX (which is a solver for convex optimizations), denoted by CE-CVX in Figure 2.6. Figures 2.6(a) and 2.6(b) show the accuracy of our Algorithm 3. Specifically, the results in Figure 2.6(a) and Figure 2.6(b) demonstrate that our algorithm can outperform the CE-CVX scheme while achieving the close-to-optimal solution compared to LINGO. For the sake of clear illustration, we also mark the average error between our proposed algorithm and the result of LINGO on the top of the two subplots, with the maximum average error no greater than 3%, which is acceptable. Furthermore, Figure 2.6(c) shows the computation efficiency of our Algorithm 3. The results show that our algorithm can significantly reduce the computation time compared to the other two benchmark schemes, i.e., LINGO and CE-CVX.

Figure 2.7 demonstrates the performance advantage of proposed channel sharing aided ISAC under the setting of $I = 8$. We use the following two schemes as the comparison benchmarks, i.e., 1) Hungarian-based orthogonal allocation scheme (HBOAS) which allocates the channels to the STs orthogonally (i.e., $\{J_i^{\max}\}_{i\in\mathcal{I}} = 1$) [92] and 2) distance-based allocation scheme (DBAS) enables the STs closest to CU i to share CU i's channel. Figure 2.7 validates that our proposed channel sharing scheme can outperform the other two benchmark schemes.

2.5 Conclusion

In this chapter, we have investigated an energy-efficient channel sharing aided ISAC with sensing scheduling. Specifically, the ISAC BS performs the multi-target sensing by reusing the CUs' channels while guaranteeing each individual CU's throughput requirement. We have proposed a joint optimization of multi-target sensing scheduling, the BS's transmitting beamforming vectors, and its receiving beamforming vectors for the STs, with the objective of maximizing the energy efficiency for radar sensing. De-

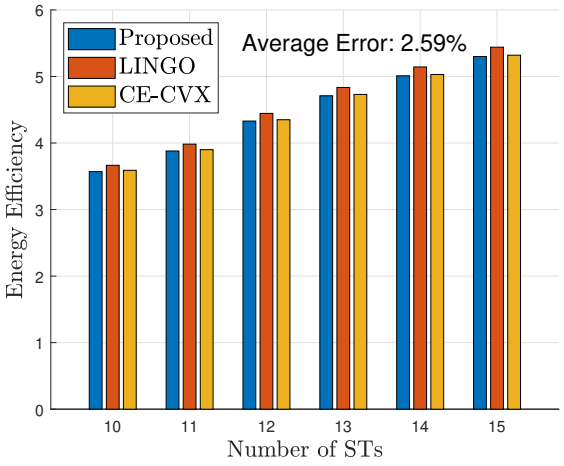

(a) Comparison of accuracy

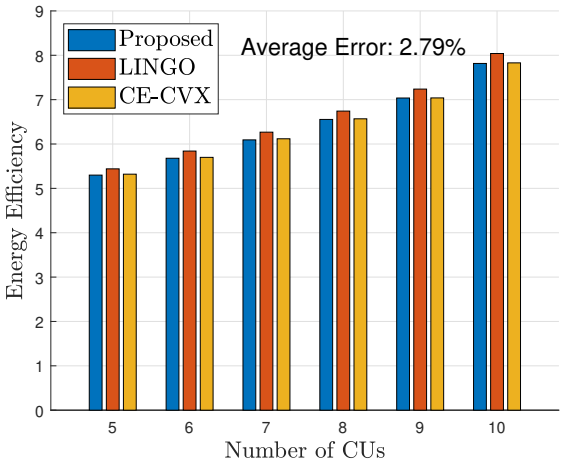

(b) Comparison of accuracy

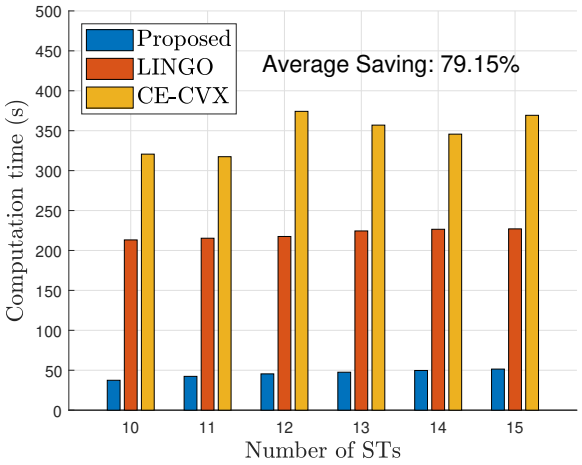

(c) Comparison of efficiency

Fig. 2.6: Accuracy and efficiency of Algorithm 3

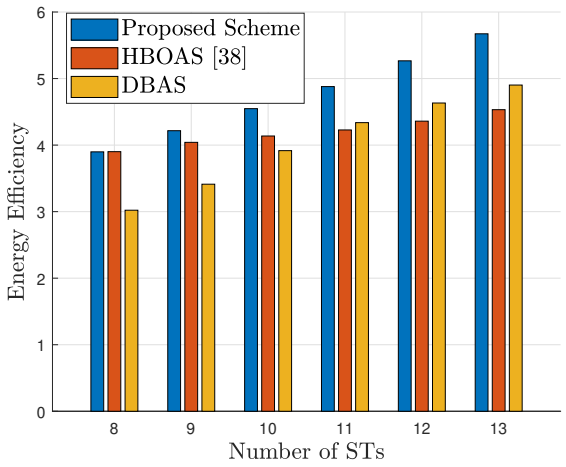

Fig. 2.7: Performance advantage of our channel sharing aided ISAC

spite that the formulated joint optimization problem is strictly non-convex, we have exploited a framework of alternating optimization and proposed the corresponding algorithms for solving the problem. Specifically, we have utilized Dinkelbach's method and Lagrange duality to obtain the beamforming vectors, and formulated the sensing scheduling problem as a matching game. Numerical results have been provided to validate the effectiveness of our algorithms and the performance advantages of the proposed channel sharing aided ISAC.

Chapter 3

Sensing-Efficient NOMA-Aided ISAC: Joint Sensing Scheduling and Beamforming Optimization

3.1 Introduction

To cope with the spectrum shortage driven by the exponential growth of wireless devices and applications, integrated sensing and communication (ISAC) system has recently raised great research interests from both academia and industry [93–95]. Unlike conventional systems that rely on separated hardware and spectrum resources, ISAC aims to exploit a unified hardware platform and shared spectrum to simultaneously perform data communication for users and transmit probing signals for sensing targets. Due to these advantages, ISAC has been envisioned to enable high-throughput transmissions while providing accurate environmental sensing for emerging scenarios such as autonomous driving, Wi-Fi sensing, and extended reality [96].

Existing literature has extensively investigated performance optimization for ISAC, covering both throughput maximization and sensing performance enhancement. For instance, [97] analyzes the fundamental limits of ISAC systems, characterizing the achievable regions for downlink and uplink communication-sensing rates. Similarly, [69] studies joint beamforming designs aiming to maximize weighted sensing and communication performance. Nevertheless, system performance inevitably degrades when an excessive number of targets are sensed simultaneously. This motivates the investigation of sensing scheduling in ISAC systems, which introduces a critical degree of freedom (DoF) to optimize the trade-off between communication and sensing.

Concurrently, given the increasing density of communication users and sensing targets, a spectrum-efficient multiple access scheme is expected to play a crucial role to the success of ISAC. Non-orthogonal multiple access (NOMA) has been regarded as a key enabler for massive connectivity in future wireless systems [98–100]. Thanks to advanced successive interference cancellation (SIC), NOMA allows multiple users to transmit simultaneously over the same spectral channel while effectively mitigating co-channel interference. Consequently, NOMA has attracted significant attention for next-generation wireless services [101–103]. In particular, recent studies have begun

to explore NOMA-assisted ISAC frameworks. For example, [104] leverages NOMA signals for radar probing to facilitate dual spectrum sharing, while [31] addresses the physical layer security of NOMA-aided ISAC. However, most existing studies overlook the scheduling of sensing targets, which is expected to play a vital role in balancing data transmission and radar sensing performance in resource-constrained environments.

To address this gap, this chapter investigates a NOMA-aided ISAC framework from the perspective of joint sensing scheduling and beamforming optimization. Specifically, we consider a scenario where an ISAC base station tracks a group of sensing targets and updates their estimation by transmitting probing signals. The main contributions of this chapter are summarized as follows:

- We propose a sensing scheduling paradigm of the NOMA-aided ISAC system, in which the ISAC base station (BS) simultaneously provides data transmissions to a group of users via NOMA (i.e., the NOMA-users, NUs) and performs multi-target sensing towards a group of sensing targets (STs). We consider that each NU should receive its required data volume with the time-interval. To measure the performance of multi-target sensing, we adopt the sensing estimation mutual information and guarantee the ISAC BS should extract a required amount of mutual information from the echoes of STs which are scheduled to be sensed. We formulate a joint optimization problem of the beamforming, the NOMA transmission duration and the sensing scheduling, with the objective of maximizing the sensing efficiency of the system (i.e., the number of the selected STs over the NOMA transmission duration).

- To tackle with the non-convexity of the formulated optimization problem, we decompose it into two problems, including a top-problem for optimizing the sensing scheduling, and a consequent bottom-problem for optimizing the beamforming and the NOMA transmission duration. For the bottom-problem, we identify the structural property of the optimal solution, and thus propose an efficient subroutine based on successive convex approximation (SCA) and penalty function for obtaining the optimal beamforming (under a given NOMA trans-

mission duration). Exploiting the optimal beamforming, we further find the optimal NOMA transmission duration in a bisection-search manner by invoking the subroutine. We finally optimize the sensing scheduling in the top-problem by adopting an algorithm based on the cross-entropy (CE) learning.

- We demonstrate the performance of NOMA-aided ISAC with optimized ST scheduling. Compared with some benchmark algorithms, our algorithm can achieve better performance in communication and sensing while consuming less computational time. We validate that the NOMA-aided ISAC scheme can provide guaranteed performance for both data transmission and radar sensing. In addition, the numerical results demonstrate the gain obtained by our sensing scheduling scheme over the scheme without accounting for the sensing scheduling.

The remainder of the chapter is organized as follows. In Section 3.2, we clarify the system model and problem formulation. In Section 3.3, we decompose the original optimization problem into a top-problem and a bottom-problem and further analyze the structural property of the optimal solution of the bottom-problem. We also propose a decomposition-based algorithm in Section 3.3. The performance of proposed algorithms are demonstrated in Section 3.4. We finally conclude this chapter in Section 3.5.

3.2 System Model of NOMA-Aided ISAC

Figure 3.1 illustrates the considered NOMA-aided ISAC system. The ISAC BS is equipped with a uniform linear array of K-antennas providing the downlink transmission to a group of NUs via NOMA. Meanwhile, the ISAC BS also performs the radar sensing towards a group of STs. There exists M single-antenna NUs denoted by $\mathcal{M} = \{1, 2, ..., M\}$ that are receiving data from the ISAC BS. For each NU $m \in \mathcal{M}$, we use D_m to denote its required amount of data to receive. Meanwhile, there exist I STs which are denoted by $\mathcal{I} = \{1, 2, ..., I\}$ to be sensed. In this work, we assume that the ISAC BS knows the existence of STs (e.g., their locations and directions). The ISAC BS performs radar sensing to the STs to estimate some specific information,

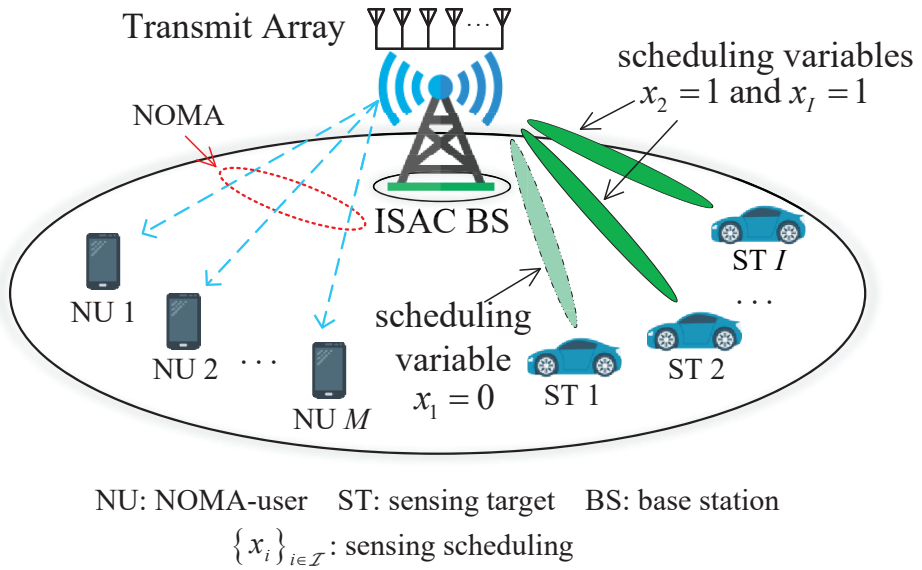

Fig. 3.1: An illustrative system model

e.g., the STs' moving velocities.

3.2.1 Communication Model

We consider that the ISAC BS exploits NOMA to serve M NUs simultaneously on the same frequency band. Specifically, the BS transmits a superimposed joint sensing and communication signal $\sum_{m\in\mathcal{M}} \mathbf{w}_m s_m$ to all NUs, where $\mathbf{w}_m \in \mathbb{C}^{K\times 1}$ are beamformers for delivering the information symbol s_m to NU m. Since the superimposed NOMA signals is utilized for sensing the selected STs, the radar sensing signal will not influence the communication links. As a result, the signal y_m received at NU m can be given as

$$y_m = \sum_{j=1}^{M} \mathbf{g}_m^H \mathbf{w}_j s_j + n_0, \forall m \in \mathcal{M}, \tag{3.1}$$

where $\mathbf{g}_m = \beta_m \widetilde{\mathbf{g}}_m$ denotes the channel gain between the ISAC BS and NU m, n_0 denotes the circularly symmetric complex Gaussian noise, β_m accounts for the large-scale channel fading gain of NU m, and $\widetilde{\mathbf{g}}_m \in \mathbb{C}^{K\times 1}$ denotes the small-scale fading channel component.

To facilitate the model of NOMA transmission, we suppose

$$\beta_1 \geq \beta_2 \geq \cdots \geq \beta_M. \tag{3.2}$$

With the above ordering and the operations of SIC [105], the symbol s_m for NU m requires to be decoded at NU n, for $n \leq m$ and $\forall m \in \mathcal{M}$, which yields the following achievable rate

$$R_{m(n)} = B \log_2 \left(1 + \frac{|\mathbf{g}_n^H \mathbf{w}_m|^2}{\sum_{j=1}^{m-1} |\mathbf{g}_n^H \mathbf{w}_j|^2 + \sigma_n^2} \right). \tag{3.3}$$

In eq. (3.3), parameter B denotes the channel bandwidth and σ_n^2 denotes the variance of the circularly symmetric complex Gaussian noise. Therefore, the overall achievable rate of NU m is

$$R_m = \min_{\forall n \leq m} \{R_{m(n)}\}, \forall m \in \mathcal{M}. \tag{3.4}$$

We use variable t to denote the NOMA transmission duration. In particular, the NOMA transmission duration should satisfy the following constraint

$$tR_m \geq D_m, \forall m \in \mathcal{M}, \tag{3.5}$$

which means that each NU m should receive its required data volume D_m.

3.2.2 Sensing Model

The superimposed signal for all NUs is employed to sense the STs. With the beamforming, the ISAC BS sends a probing signal in the direction of the selected ST and receives the echo reflected from the ST. Specifically, with the priori information of direction θ_i of ST i, the power of the probing signal in direction θ_i can be given as

$$P_i = \mathbf{a}^H(\theta_i) \left(\sum_{m \in \mathcal{M}} \mathbf{w}_m \mathbf{w}_m^H \right) \mathbf{a}(\theta_i), \forall i \in \mathcal{I}, \tag{3.6}$$

where $\mathbf{a}(\theta_i) = \left[1, e^{j\frac{2\pi}{\lambda} d \sin(\theta_i)}, \cdots, e^{j\frac{2\pi}{\lambda} d(K-1)\sin(\theta_i)}\right]^T$ is the transmit array steering vector for direction θ_i. Parameters d and λ represent the antenna spacing and carrier wavelength, respectively. $\sum_{m \in \mathcal{M}} \mathbf{w}_m \mathbf{w}_m^H$ denotes the covariance matrix of the transmitted signal, which affects the sensing quality. To further measure the quality of the received echoes, we utilize the sensing estimation mutual information for each selected

ST as the sensing quality metric. Specifically, with the NOMA transmission duration t, the sensing estimation mutual information extracted from the echoes of ST i can be given as

$$S_i = \frac{\delta}{2}\log_2\left(1+\frac{2t\alpha^2 B^3\sigma_{proc}^2\mathbf{h}_i^H P_i\mathbf{h}_i}{\sum_{j\neq i}\mathbf{h}_j^H P_j\mathbf{h}_j+\sigma_n^2}\right), \forall i\in\mathcal{I}, \tag{3.7}$$

where $\mathbf{h}_i = \mu_i\widetilde{\mathbf{h}}_i \in \mathbb{C}^{K\times 1}$ denotes the channel between the ISAC BS and ST i. Parameter α depends on the shape of the power spectral density of the probing signal, parameter δ denotes the radar's duty cycle and parameter σ_{proc}^2 denotes the variance of the range fluctuation process. Moreover, we introduce a group of binary sensing scheduling variables $\{x_i\}_{i\in\mathcal{I}}$ with $x_i = 1$ meaning that ST i is selected to be sensed during the considered NOMA transmission duration, while $x_i = 0$ meaning the opposite case.

We use the following constraint to denote that for each ST, if it is selected, the corresponding sensing estimation mutual information should be no smaller than a required level $\Gamma_i^{\min}$, i.e.,

$$S_i \geq x_i\Gamma_i^{\min}, \forall i\in\mathcal{I}. \tag{3.8}$$

When more than one ST is selected in each scheduling, the mean-squared cross-correlation Q^{ms} of probing signals can be expressed as

$$Q^{\text{ms}} = \begin{cases} \frac{2}{\left((\sum_{i\in\mathcal{I}}x_i)^2-\sum_{i\in\mathcal{I}}x_i\right)}\sum_{p=1}^{I-1}\sum_{q=p+1}^{I}x_p x_q\left|\mathbf{a}^H(\theta_p)\left(\sum_{m\in\mathcal{M}}\mathbf{w}_m\mathbf{w}_m^H\right)\mathbf{a}(\theta_q)\right|^2, & \text{when } \sum_{i\in\mathcal{I}}x_i>1, \\ 0, & \text{otherwise.} \end{cases} \tag{3.9}$$

In eq. (3.9), the summation is normalized by the total number of different pairs of probing signals, i.e., $\frac{(\sum_{i\in\mathcal{I}}x_i)^2-\sum_{i\in\mathcal{I}}x_i}{2}$. In particular, the value of Q^{ms} should be no greater than a required level ϵ to guarantee the statistical performance of the adaptive

sensing technique, i.e.,

$$Q^{\text{ms}} \leq \epsilon. \tag{3.10}$$

3.2.3 Problem Formulation

In this chapter, we aim at maximizing the sensing efficiency (SEM) which is denoted by the number of the selected STs over the NOMA duration, while satisfying the communication quality requirement of each NU and radar sensing requirement of each selected ST. To achieve this goal, we jointly optimize the beamformers $\{\mathbf{w}_m\}_{m\in\mathcal{M}}$, the NOMA transmission duration t, and the sensing scheduling $\{x_i\}_{i\in\mathcal{I}}$. Our problem formulation is detailed as follows.

$$\begin{aligned}
\text{(SEM):}\ \max\ & \frac{1}{t}\sum_{i\in\mathcal{I}} x_i \\
\text{subject to: constraints } & (3.5), (3.8) \text{ and } (3.10), \\
& x_i \in \{0,1\}, \forall i \in \mathcal{I}, && (3.11)\\
& \mathbf{Tr}\left(\sum_{m\in\mathcal{M}} \mathbf{w}_m \mathbf{w}_m^H\right) \leq P^{\text{max}}, && (3.12)\\
& 0 < t \leq T, && (3.13)\\
\text{variables: } & \{\mathbf{w}_m\}_{m\in\mathcal{M}}, \{x_i\}_{i\in\mathcal{I}}, t.
\end{aligned}$$

Constraint (3.5) ensures that each NU's communication requirement is satisfied. Constraint (3.8) ensures that the radar sensing requirement of each selected ST is guaranteed. Constraint (3.10) specifies an upper bound on the mean-square cross-correlation of the probing signals. Constraint (3.12) ensures that the BS's transmitting power cannot exceed its power capacity P^{max}. Constraint (3.13) ensures that the NOMA transmission duration cannot exceed a maximum latency denoted by T.

3.3 Layered Decomposition and Proposed Algorithm

3.3.1 Problem Reformulation

Problem (SEM) is a mixed binary and non-convex optimization problem. Specifically, the binary sensing scheduling $\{x_i\}_{i\in\mathcal{I}}$ and the NOMA transmission duration t are coupled in the objective function and constraint (3.8). Moreover, constraints (3.5) and (3.12) are both non-convex. Therefore, it is challenging to solve Problem (SEM) directly. To address this difficulty, we propose a decomposition-based approach to solve this problem. The details are as follows.

For each NU m, we firstly define $\mathbf{W}_m \triangleq \mathbf{w}_m\mathbf{w}_m^H$, with three constraints $\mathbf{W}_m \succeq 0$, $\mathbf{W}_m = \mathbf{W}_m^H$, and rank($\mathbf{W}_m$) = 1. In addition, for convenience of expression, we define

$$V_i \triangleq \mathbf{h}_i^H\mathbf{a}^H(\theta_i)\left(\sum_{m\in\mathcal{M}}\mathbf{W}_m\right)\mathbf{a}(\theta_i)\mathbf{h}_i. \tag{3.14}$$

Then, constraint (3.8) can be rewritten as

$$\frac{tV_i}{\sum\limits_{j\neq i}V_j+\sigma_n^2} \geq \rho_i, \forall i\in\mathcal{I}, \tag{3.15}$$

where

$$\rho_i = \frac{1}{2\alpha^2B^3\sigma_{proc}^2}(2^{\frac{2x_i\Gamma_i^{\min}}{\delta}}-1), \forall i\in\mathcal{I}. \tag{3.16}$$

Meanwhile, constraint (3.10) can be rewritten as

$$\frac{2}{\left((\sum\limits_{i\in\mathcal{I}}x_i)^2-\sum\limits_{i\in\mathcal{I}}x_i\right)}\sum_{p=1}^{I-1}\sum_{q=p+1}^{I}x_px_q|\mathbf{a}^H(\theta_p)\left(\sum_{m\in\mathcal{M}}\mathbf{W}_m\right)\mathbf{a}(\theta_q)|^2 \leq \epsilon, \text{ when } \sum_{i\in\mathcal{I}}x_i > 1. \tag{3.17}$$

Thus, Problem (SEM) can be equivalently transformed into

$$\text{(SEM-E): } \max \ \frac{1}{t}\sum_{i\in\mathcal{I}}x_i$$

$$\text{subject to: constraints } (3.5), (3.11), (3.13), (3.15) \text{ and } (3.17),$$

$$\mathbf{Tr}\left(\sum_{m\in\mathcal{M}}\mathbf{W}_m\right) \leq P^{\max}, \tag{3.18}$$

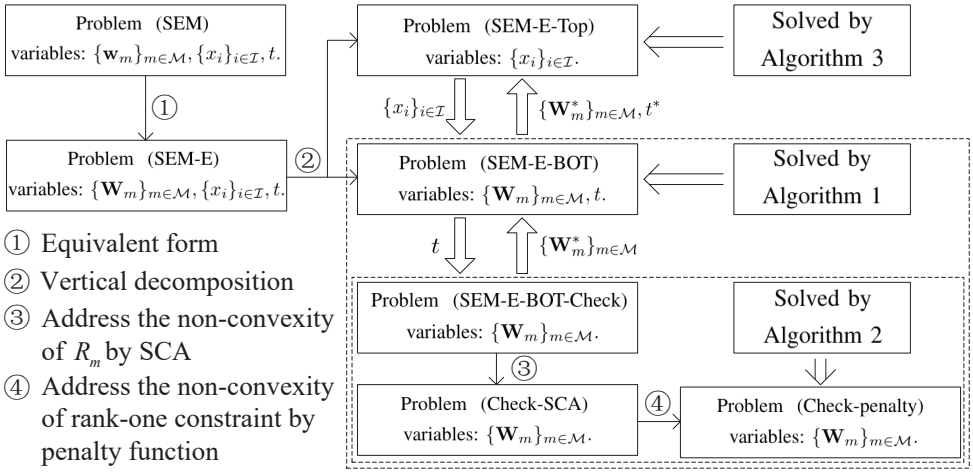

Fig. 3.2: Decomposition of Problem (SEM-E)

$$\mathbf{W}_m \succeq 0, \forall m, \tag{3.19}$$

$$\mathbf{W}_m = \mathbf{W}_m^H, \forall m, \tag{3.20}$$

$$\text{rank}(\mathbf{W}_m) = 1, \forall m, \tag{3.21}$$

variables: $\{\mathbf{W}_m\}_{m\in\mathcal{M}}, \{x_i\}_{i\in\mathcal{I}}, t.$

3.3.2 Decomposition of Problem (SEM-E)

To address the difficulty due to the mixed binary and non-convexity, we propose a vertical decomposition as follows.

Bottom-problem under given $\{x_i\}_{i\in\mathcal{I}}$

Given the sensing scheduling $\{x_i\}_{i\in\mathcal{I}}$, Problem (SEM-E) turns into the following bottom-problem.

$$\text{(SEM-E-BOT): } E^{\text{BOT}}(\{x_i\}_{i\in\mathcal{I}}) = \max \ \frac{1}{t}\sum_{i\in\mathcal{I}} x_i$$

subject to: constraints $(3.5), (3.13), (3.15), (3.17), (3.18), (3.19), (3.20)$

and (3.21),

variables: $\{\mathbf{W}_m\}_{m\in\mathcal{M}}, t.$

Top-problem of optimizing $\{x_i\}_{i\in\mathcal{I}}$

After solving Problem (SEM-E-BOT) and obtaining the value of $E^{\text{BOT}}(\{x_i\}_{i\in\mathcal{I}})$ with the given $\{x_i\}_{i\in\mathcal{I}}$, we then optimize $\{x_i\}_{i\in\mathcal{I}}$, which results in the following optimization problem.

$$\begin{aligned}&\text{(SEM-E-Top):}\ \max\ \ E^{\text{BOT}}(\{x_i\}_{i\in\mathcal{I}})\\ &\text{subject to: constraint } (3.11),\\ &\text{variables: } \{x_i\}_{i\in\mathcal{I}}.\end{aligned}$$

As shown in Figure 3.2, the above top-problem and bottom-problem work in a master-slave manner, i.e., for each $\{x_i\}_{i\in\mathcal{I}}$ given by Problem (SEM-E-Top), we invoke the subroutine for solving Problem (SEM-E-BOT) and return the result to Problem (SEM-E-Top).

3.3.3 Proposed Algorithm for Solving Problem (SEM-E-BOT)

Under a given $\{x_i\}_{i\in\mathcal{I}}$, Problem (SEM-E-BOT) can be considered as a problem of finding the minimum t that can ensure the feasible region specified by constraints (3.5), (3.15) and (3.17)-(3.21) is non-empty. To this end, we formulate an optimization problem, which is used to check whether constraints (3.5), (3.15) and (3.17)-(3.21) can form a non-empty set or not under a given t, as follows.

$$\begin{aligned}&\text{(SEM-E-BOT-Check):}\ O_{(t)}=\min\ \ \mathbf{Tr}\left(\sum_{m\in\mathcal{M}}\mathbf{W}_m\right)-P^{\max}\\ &\text{subject to: } R_m\geq\frac{D_m}{t},\forall m, &(3.22)\\ &\qquad V_i\geq\frac{\rho_i}{t}\left(\sum_{j\neq i}V_j+\sigma_n^2\right),\forall i, &(3.23)\\ &\qquad\text{constraints } (3.17),(3.19),(3.20) \text{ and } (3.21),\\ &\text{variables: } \{\mathbf{W}_m\}_{m\in\mathcal{M}}.\end{aligned}$$

Recall that constraints (3.22) and (3.23) are the equivalent form of constraints (3.5) and (3.15), respectively, when the value of t is given. Moreover, regarding constraint

(3.23), it is noticed that for each ST i, if $x_i = 0$, constraint (3.23) can always be guaranteed according to the definitions of V_i in eq. (14) and ρ_i in eq. (3.16). Specifically, if the optimal output $O_{(t)} \leq 0$, then the feasible region specified by constraints (3.5), (3.15) and (3.17)-(3.21) is non-empty, meaning that Problem (SEM-E-BOT) is feasible under the given t. Otherwise (i.e., $O_{(t)} > 0$), Problem (SEM-E-BOT) is infeasible. In addition, we identify the following feature.

Proposition 5. *The value of $O_{(t)}$ of Problem (SEM-E-BOT-Check) is non-increasing in t.*

Proof. It can be observed that the feasible region constructed by constraints (3.17), (3.19)-(3.23) increases, when t increases. Consequently, the minimum value of the objective function (i.e., $O_{(t)}$) is non-increasing in t. □

By leveraging Proposition 5, we can perform a bisection-search on $t \in (0, T]$ to solve Problem (SEM-E-BOT) and obtain the value of $E^{\text{BOT}}(\{x_i\}_{i\in\mathcal{I}})$. Specifically, if the currently given t leads $O_{(t)} \leq 0$, we reduce t. Otherwise, we increase t. Based on the above idea, we propose an efficient bisection-search based algorithm to solve Problem (SEM-E-BOT). The detail is shown in Algorithm 4.

Algorithm 4 : To solve Problem (SEM-E-BOT) and obtain $E^{\text{BOT}}(\{x_i\}_{i\in\mathcal{I}})$

1: **Initialization:** Set the convergence accuracy for the bisection-search ϑ as a very small number. Set $t^{\text{upp}} = T$ and $t^{\text{low}} = 0$.
2: **while** $|t^{\text{upp}} - t^{\text{low}}| > \vartheta$ **do**
3: Set $t^{\text{cur}} = \frac{t^{\text{upp}} + t^{\text{low}}}{2}$.
4: Given t^{cur}, use Subroutine-O to calculate $O_{(t)}$.
5: **if** $O_{(t)} \leq 0$ **then**
6: Set $t^{\text{upp}} = t^{\text{cur}}$.
7: **else**
8: Set $t^{\text{low}} = t^{\text{cur}}$.
9: **end if**
10: **end while**
11: **Output:** $E^{\text{BOT}}(\{x_i\}_{i\in\mathcal{I}}) = \frac{1}{t^{\text{cur}}} \sum_{i\in\mathcal{I}} x_i$

Notice that in Step 4 of Algorithm 4, a subroutine-O is required to calculate the value of $O_{(t)}$, the details of which are shown in the next subsection.

3.3.4 Proposed Subroutine-O for Calculating $O_{(t)}$

To solve Problem (SEM-E-BOT-Check) and obtain the value of $O_{(t)}$, there are two difficulties lie in the non-convexity of constraints (3.21) and (3.22). To propose a subroutine, we first do the following operations. With eq. (3.4), constraint (3.22) can be rewritten as

$$R_{m(n)} \geq \frac{D_m}{t}, \forall m \in \mathcal{M}, n \leq m. \tag{3.24}$$

We define $\mathbf{G}_m \triangleq \mathbf{g}_m \mathbf{g}_m^H$ and rewrite constraint (3.24) as

$$\begin{aligned} R_{m(n)} = & B \log_2 \left(\sigma_n^2 + \sum_{j=1}^{m} \mathbf{Tr} \left(\mathbf{G}_n \mathbf{W}_j \right) \right) \\ & - B \log_2 \left(\sigma_n^2 + \sum_{j=1}^{m-1} \mathbf{Tr} \left(\mathbf{G}_n \mathbf{W}_j \right) \right) \geq \frac{D_m}{t}, \forall m \in \mathcal{M}, n \leq m. \end{aligned} \tag{3.25}$$

Constraint (3.24) is non-convex due to the second term of $R_{m(n)}$. To tackle this difficulty, we adopt the operations of SCA. Specifically, we first define

$$L_{m(n)} \triangleq -B \log_2 \left(\sigma_n^2 + \sum_{j=1}^{m-1} \mathbf{Tr} \left(\mathbf{G}_n \mathbf{W}_j \right) \right), \forall m \in \mathcal{M}, n \leq m. \tag{3.26}$$

Then, we utilize the first-order Taylor expansion of $\{\mathbf{W}_m\}_{m \in \mathcal{M}}$ for any given local point $(\mathbf{W}_1^u, \cdots, \mathbf{W}_M^u)$ in the feasible domain in the u-th iteration as its lower bound, i.e.,

$$\begin{aligned} L_{m(n)} \geq L_{m(n)}^{\text{lb}} \triangleq & - B \log_2 \left(\sigma_n^2 + \sum_{j=1}^{m-1} \mathbf{Tr} \left(\mathbf{G}_n \mathbf{W}_j^u \right) \right) \\ & - B \frac{\sum_{j=1}^{m-1} \mathbf{Tr} \left(\mathbf{G}_n \left(\mathbf{W}_j - \mathbf{W}_j^u \right) \right)}{\left(\sigma_n^2 + \sum_{j=1}^{m-1} \mathbf{Tr} \left(\mathbf{G}_n \mathbf{W}_j^u \right) \right) \ln 2}, \forall m \in \mathcal{M}, n \leq m. \end{aligned} \tag{3.27}$$

Based on $L_{m(n)}^{\text{lb}}$, we define the lower bound of $R_{m(n)}$ as

$$R_{m(n)}^{\text{lb}} \triangleq B \log_2 \left(\sigma_n^2 + \sum_{j=1}^{m} \mathbf{Tr} \left(\mathbf{G}_n \mathbf{W}_j \right) \right) + L_{m(n)}^{\text{lb}} \geq \frac{D_m}{t}, \forall m \in \mathcal{M}, n \leq m. \tag{3.28}$$

By using $R_{m(n)}^{\text{lb}}$ to replace $R_{m(n)}$, we can transform constraint (3.25) into a convex one as constraint (3.28).

After the above operations, Problem (SEM-E-BOT-Check) can be rewritten as

$$\begin{aligned}&\text{(Check-SCA): } O_{(t)} = \min \ \ \mathbf{Tr}\left(\sum_{m\in\mathcal{M}} \mathbf{W}_m\right) - P^{\max}\\ &\quad \text{subject to: constraints } (3.17), (3.19), (3.20), (3.21), (3.23) \text{ and } (3.28),\\ &\quad \text{variables: } \{\mathbf{W}_m\}_{m\in\mathcal{M}}.\end{aligned}$$

With this optimization problem, the remaining difficulty comes from the non-convexity of the rank-one constraint (3.21). To tackle this issue, we adopt the penalty-based algorithm [106]. Specifically, since matrix $\mathbf{W}_m$ is positive semi-definite according to constraint (3.19), all the eigenvalues of $\mathbf{W}_m$ are non-negative, i.e., $\lambda_k(\mathbf{W}_m) \geq 0, \forall m, k = 1, 2, ..., K$, where $\lambda_k(\cdot)$ represents the k-th eigenvalue of a matrix. Due to $\mathbf{Tr}(\mathbf{W}_m) = \sum_{k=1}^{K} \lambda_k(\mathbf{W}_m)$, we first transform the rank-one constraint (3.21) into an equivalent equality constraint

$$\mathbf{Tr}(\mathbf{W}_m) - \lambda_{\max}(\mathbf{W}_m) = 0, \forall m \in \mathcal{M}, \tag{3.29}$$

where $\lambda_{\max}(\cdot)$ denotes the maximum eigenvalue of a matrix. Therefore, eq. (3.29) holds when matrix $\mathbf{W}_m$ is a rank-one matrix. On the contrary, since $\mathbf{W}_m$ is positive semi-definite, we derive that the trace of the matrix is greater than the maximum eigenvalue of the matrix, i.e., $\mathbf{Tr}(\mathbf{W}_m) - \lambda_{\max}(\mathbf{W}_m) > 0$. In order to obtain a rank-one matrix, we drop the rank-one constraint (3.21) and introduce a penalty term into the objective function, which results in the following new objective function

$$\min \ \ \mathbf{Tr}\left(\sum_{m\in\mathcal{M}} \mathbf{W}_m\right) - P^{\max} + \eta \sum_{m\in\mathcal{M}} \left(\mathbf{Tr}(\mathbf{W}_m) - \lambda_{\max}(\mathbf{W}_m)\right), \tag{3.30}$$

where $\eta > 0$ is the penalty factor. However, the second term of the penalty term makes the objective function non-convex. By further exploiting SCA, we can transform (3.30) into a convex one. Specifically, by exploiting the first-order Taylor expansion at the

feasible point $(\mathbf{W}_1^u, \cdots, \mathbf{W}_M^u)$ at the u-th iteration, the upper bound of the penalty term is given in

$$\begin{aligned} &\mathbf{Tr}\left(\mathbf{W}_m\right) - \lambda_{\max}(\mathbf{W}_m^u) - \left(\mathbf{z}_{m,\max}^u\right)^H \left(\mathbf{W}_m - \mathbf{W}_m^u\right) \mathbf{z}_{m,\max}^u \\ &\geq \mathbf{Tr}\left(\mathbf{W}_m\right) - \lambda_{\max}\left(\mathbf{W}_m\right) \geq 0, \end{aligned} \tag{3.31}$$

where $\mathbf{z}_{m,\max}$ is the unit eigenvector with respect to the maximum eigenvalue $\lambda_{\max}\left(\mathbf{W}_i\right)$. Thus, we derive the iterative optimization Problem (Check-penalty) as follows, which is Problem (Check-SCA) in the $(u+1)$-th iteration.

$$\begin{aligned} \text{(Check-penalty):}\ &\min \mathbf{Tr}\left(\sum_{m\in\mathcal{M}} \mathbf{W}_m\right) - P^{\max} \\ &+ \eta \sum_{m\in\mathcal{M}} \left(\mathbf{Tr}\left(\mathbf{W}_m\right) - \lambda_{\max}(\mathbf{W}_m^u) - \left(\mathbf{z}_{m,\max}^u\right)^H \left(\mathbf{W}_m - \mathbf{W}_m^u\right) \mathbf{z}_{m,\max}^u\right) \\ &\text{subject to: constraints } (3.17), (3.19), (3.20), (3.23) \text{ and } (3.28), \\ &\text{variables: } \{\mathbf{W}_m\}_{m\in\mathcal{M}}. \end{aligned}$$

Proposition 6. *Problem (Check-penalty) is a strictly convex optimization with* $\{\mathbf{W}_m\}$.

Proof. It can be identified that the objective function in Problem (Check-penalty) is strictly convex with $\{\mathbf{W}_m\}_{m\in\mathcal{M}}$. Constraints (3.19) and (3.20) result in a convex feasible set for $\{\mathbf{W}_m\}_{m\in\mathcal{M}}$. It can also be identified that constraints (3.17) and (3.28) are convex with $\{\mathbf{W}_m\}_{m\in\mathcal{M}}$, and constraint (3.23) is affine. Therefore, it can be concluded that Problem (Check-penalty) is a convex optimization problem with $\{\mathbf{W}_m\}_{m\in\mathcal{M}}$. □

Based on Proposition 6, Problem (Check-penalty) can be solved efficiently with several existing solvers for convex optimizations, e.g., CVX, in an iterative way. After convergence, i.e., when $\mathbf{Tr}(\mathbf{W}_m)$ is equal to $\lambda_{\max}(\mathbf{W}_m)$, we can derive that

$$\mathbf{W}_m = \lambda_{\max}\left(\mathbf{W}_m\right) \mathbf{z}_{m,\max}(\mathbf{z}_{m,\max})^H, \forall m \in \mathcal{M}. \tag{3.32}$$

Accordingly, we can calculate the optimal beamformer $\mathbf{w}_m$ according to the following

equation

$$\mathbf{w}_m^* = \sqrt{\lambda_{\max}(\mathbf{W}_m)}\mathbf{z}_{m,\max}, \forall m \in \mathcal{M}. \tag{3.33}$$

In summary, the detail of the proposed penalty-based algorithm (i.e., Subroutine-O) is shown in Algorithm 5, which is explained as follows.

Step 4 to Step 7

For the current value of penalty factor η, we can obtain the solution for the convergence of $\mathbf{W}_m$ by CVX in an iterative solution. The $\mathbf{W}_m$ converges under the value of this penalty factor η when the change of $\mathbf{W}_m$ falls below the threshold Δ.

Step 2 to Step 10

In Step 9, we check whether the value of the penalty term falls below the threshold Δ. If yes, the iteration is terminated. Otherwise, we increase the value of penalty factor to decrease the penalty term in the next iteration. In particular, we set the initial value of the next round iteration to the convergent value of the previous round iteration in Step 8, which provides a starting point to reduce the number of iterations in the next round iteration.

Step 11

When the algorithm converges, the approximate optimal beamformer $\mathbf{w}_m$ can be obtained by eq. (3.33). Meanwhile, we can obtain the value of $O_{(t)}$ which is used by Algorithm 4 to update the value of t.

3.3.5 Proposed Algorithm for Solving Problem (SEM-E-Top)

With Algorithm 4 (and its Subroutine-O), for given $\{x_i\}_{i\in\mathcal{I}}$, we can solve Problem (SEM-E-BOT) and calculate the value $E^{\text{BOT}}(\{x_i\}_{i\in\mathcal{I}})$. We thus proceed to solve Problem (SEM-E-Top), i.e., to find the optimal sensing scheduling $\{x_i\}_{i\in\mathcal{I}}$ that can maximize the sensing efficiency. The difficulty of solving Problem (SEM-E-Top) lies in that we cannot express $E^{\text{BOT}}(\{x_i\}_{i\in\mathcal{I}})$ in an analytical way. To tackle this difficulty, we adopt a CE learning based algorithm to optimize the sensing schedule variables $\{x_i\}_{i\in\mathcal{I}}$ [107]. The key of the CE learning is to update the probability of the value

Algorithm 5 : Subroutine-O to calculate the value of $O_{(t)}$ and $\mathbf{w}_m^*$.

Initialization: Set $\mathbf{w}_m^0 = \sqrt{\frac{P^{\max}}{N}}[1, 0, ..., 0]^T$. Set $\mathbf{W}_m^0 = \mathbf{w}_m^0(\mathbf{w}_m^0)^H$. Initialize a proper penalty factor η, a proper coefficient $c > 1$ and a proper maximum number of iterations $U^{\max}$. Set the convergence accuracy Δ as a very small number.
repeat
  Set iteration number $u = 0$.
  repeat
    Solve Problem (Check-penalty) with $\mathbf{W}_m^u$ by CVX, then obtain $\mathbf{W}_m^{u+1}$.
    Update $u = u + 1$.
  until $|\mathbf{W}_m^{u+1} - \mathbf{W}_m^u| < \Delta$ **or** $u > U^{\max}$
  Update $\mathbf{W}_m^0 = \mathbf{W}_m^u$.
  Increase the penalty factor with $\eta = c\eta$.
until $\sum_{m\in\mathcal{M}} |\mathbf{Tr}(\mathbf{W}_m^u) - \lambda_{\max}(\mathbf{W}_m^u)| < \Delta$
Output: Obtain $\mathbf{w}_m^*$ according to (3.33). Obtain $O_{(t)} = \mathbf{Tr}\left(\sum_{m\in\mathcal{M}} \mathbf{W}_m^*\right) - P^{\max}$.

since the sensing scheduling is a group of binary variables. Specifically, we virtually model $\{x_i\}_{i\in\mathcal{I}}$ as random variables, with each x_i following a Bernoulli distribution of parameter ω_i as follows:

$$\Phi_i(x_i) = {\omega_i}^{x_i}(1-\omega_i)^{(1-x_i)}, \forall i \in \mathcal{I}. \tag{3.34}$$

Then, we will update $\Phi_i(x_i)$ in each iteration until we reach the sensing scheduling that can maximize the sensing efficiency. The details include the following three steps [107]:

- Randomly generate a batch of samples with each sample denoting a $1 \times I$ vector. Specifically, the i-th element of each sample follows the distribution of $\Phi_i(x_i)$ in eq. (3.34).
- Select a portion of the elite samples from the batch based on the results corresponding to each sample.
- Update $\{\omega_i\}_{i\in\mathcal{I}}$ based on the CE learning criterion.

In particular, different from the conventional CE algorithm, we propose a new strategy for updating probabilities based on the memory set that accelerate the convergence of the algorithm. The details are shown in Algorithm 6 and explained as follows.

Step 3

Given the current $\{\omega_i\}_{i\in\mathcal{I}}$, we generate a batch of F samples $\{\mathbf{x}^f\}_{f=1,2,\ldots,F}$, where the superscript f is the index of the samples. Specifically, each $\mathbf{x}^f$ denotes the f-th sample $\{x_i\}_{i\in\mathcal{I}}$ with $x_i = 0$ or $x_i = 1$, which are randomly generated according to the current $\{\omega_i\}_{i\in\mathcal{I}}$.

Step 4 to Step 12

Given the sample of $\mathbf{x}^f$, we can obtain a group of samples of $\{x_i\}_{i\in\mathcal{I}}$. By invoking Algorithm 4, we can obtain the value of the sensing efficiency corresponding to each sample of $\mathbf{x}^f$, i.e., $E^{\text{BOT}}(\{x_i\}^f_{i\in\mathcal{I}})$. In particular, in Step 9, we store the generated sample values and the corresponding results in the sample memory set (SMS) and the value memory set (VMS), respectively. When the subsequent randomly generated samples already exist in the (SMS), we can directly obtain the corresponding values from the (VMS) without invoking Algorithm 4, which thus save the computational time. In Step 12, the samples of $\{\mathbf{x}^f\}_{f=1,2,\ldots,F}$ are reordered from the largest to the smallest according to the values of the obtained sensing efficiency.

Step 13 to Step 17

Based on the CE criterion, we can update $\{\omega_i\}_{i\in\mathcal{I}}$ according to the following function:

$$\omega_i^* = \arg\max_{0\le\omega_i\le 1} \mathbb{E}\left[\Phi_i(x_i)\right], \forall i \in \mathcal{I}, \tag{3.35}$$

where $\mathbb{E}[\cdot]$ represents the expectation of $\Phi_i(x_i)$ of the samples selected. By selecting the best $\hat{F}$ samples in each iteration, eq. (35) can be equivalent to the following equation:

$$\omega_i^* = \frac{1}{\hat{F}} \sum_{f=1}^{\hat{F}} x_i^f, \forall i \in \mathcal{I}. \tag{3.36}$$

In particular, to improve the convergence rate, we introduce a global optimum parameter $\omega_i^{*,\text{glo}}$. By selecting the best $\tilde{F}$ samples in the corresponding SMS based on the

Algorithm 6 : CE learning based algorithm for solving Problem (SEM-E-Top) and obtaining $\{x_i^*\}_{i\in\mathcal{I}}$.

Initialization: Initialize $\omega_i = 0.5, \forall i \in \mathcal{I}$, and set Λ as a very small positive number. Set sample memory set SMS $= \varnothing$, value memory set VMS $= \varnothing$.
while 1 **do**
  Randomly generate a batch of F binary samples $\{\mathbf{x}^f\}_{f=1,2,\ldots,F}$ of I length according to the current $\{\omega_i\}_{i\in\mathcal{I}}$. Each $\mathbf{x}^f$ denotes the f-th sample $\{x_i\}_{i\in\mathcal{I}}$ with $x_i = 0$ or 1.
  for each $\mathbf{x}^f \in \{\mathbf{x}^f\}_{f=1,2,\ldots,F}$ **do**
    if $x^f \in$ SMS **then**
      Obtain the corresponding $E^{\text{BOT}}(\{x_i\}_{i\in\mathcal{I}}^f)$ from the VMS.
    else
      For the current $\{x_i\}_{i\in\mathcal{I}}$, invoke Algorithm 4 to obtain the value of $E^{\text{BOT}}(\{x_i\}_{i\in\mathcal{I}}^f)$.
      Store current $\{x_i\}_{i\in\mathcal{I}}$ in SMS and $E^{\text{BOT}}(\{x_i\}_{i\in\mathcal{I}}^f)$ in VMS.
    end if
  end for
  Reorder the samples $\{\mathbf{x}^f\}_{f=1,2,\ldots,F}$ in the order of $E^{\text{BOT}}(\{x_i\}_{i\in\mathcal{I}}^f)$ from the largest to the smallest.
  Select $\hat{F}$ best samples from the reordered samples in order, use eq. (3.36) to calculate $\{\omega_i^*\}_{i\in\mathcal{I}}$, use eq. (3.37) to calculate $\{\omega_i^{*,\text{glo}}\}_{i\in\mathcal{I}}$ and further update $\{\omega_i^{\text{upd}}\}_{i\in\mathcal{I}}$ with eq. (3.38).
  if $\max_{i\in\mathcal{I}} |\omega_i^{\text{upd}} - \omega_i| < \Lambda$ **then**
    break
  end if
  Set $\omega_i = \omega_i^{\text{upd}}, \forall i \in \mathcal{I}$.
end while
Set $E^* = \max E^{\text{BOT}}(\{x_i\}_{i\in\mathcal{I}}^f)$, $\{x_i^*\}_{i\in\mathcal{I}} = \arg\max E^{\text{BOT}}(\{x_i\}_{i\in\mathcal{I}}^f)$.
Output: the tuple of the solutions $(E^*, \{x_i^*\}_{i\in\mathcal{I}})$.

values in the VMS, $\omega_i^{*,\text{glo}}$ can be given as

$$\omega_i^{*,\text{glo}} = \frac{1}{\tilde{F}} \sum_{f=1}^{\tilde{F}} x_i^f, \forall i \in \mathcal{I}. \tag{3.37}$$

Finally, the next iteration of $\{\omega_i\}_{i\in\mathcal{I}}$ is updated according to the following equation:

$$\omega_i^{\text{upd}} = \kappa_1\omega_i + \kappa_2\omega_i^* + \kappa_3\omega_i^{*,\text{glo}}, \forall i \in \mathcal{I}, \tag{3.38}$$

where parameters κ_1, κ_2 and κ_3 are the weight factors with $\kappa_1+\kappa_2+\kappa_3 = 1$. Algorithm 6 terminates when the change in $\{\omega_i\}_{i\in\mathcal{I}}$ falls below the threshold Λ.

These three algorithms are executed in a master-slave manner (i.e., Algorithm 6 invokes Algorithm 4 and Algorithm 4 further invokes Algorithm 5), which solves the original sensing-efficiency optimization problem.

3.4 Numerical Results

In this section, numerical results are provided to verify the effectiveness of our algorithms and to show the performance of our NOMA-aided ISAC system. Specifically, we assume that the ISAC BS is equipped with a uniform linear array of 4-antennas. The ISAC BS requires to serve $M = 3$ or 6 NUs while performing sensing towards a group of $I = 5$ STs. The NUs are randomly distributed within a radius of $d_m \in [50, 200]$ m from the center of the ISAC BS, and the STs are evenly distributed within a radius of $d_i \in [200, 300]$ m to centered on the ISAC BS. We assume that the amount of tasks required by the NUs arrives randomly between $[5, 10]$ MB, and directions $\{\theta_i\}_{i\in\mathcal{I}}$ of five STs are $\theta_1 = -60°$, $\theta_2 = -30°$, $\theta_3 = 0°$, $\theta_4 = 30°$ and $\theta_5 = 60°$. The total power capacity is $P^{\max} = 20$ dBm, the channel bandwidth is $B = 8$ MHz, and the noise power is $\sigma_n^2 = -110$ dBm. In addition, the channel between the ISAC BS and NUs is considered to follow the Rayleigh channel model with the path loss of $\sqrt{\beta_m} = 40 + 30\log_{10} d_m$, while the channel between the ISAC BS and STs is supposed to have a line-of-sight (LoS) link correlated with the path loss of $\sqrt{\mu_i} = 40 + 25\log_{10} d_i$. To characterize the channel spatial correlations of the NUs,

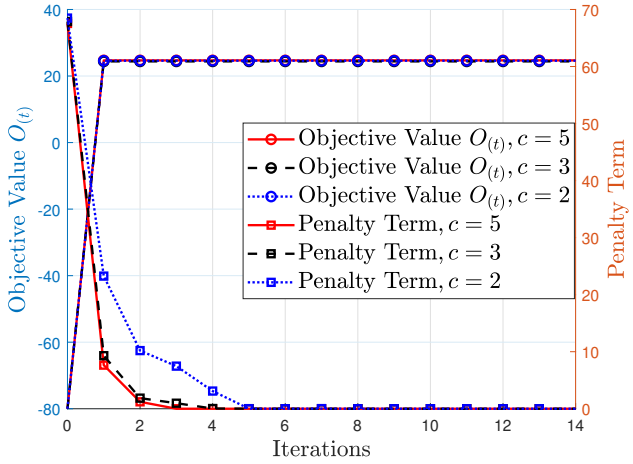

(a) t=0.8 ms

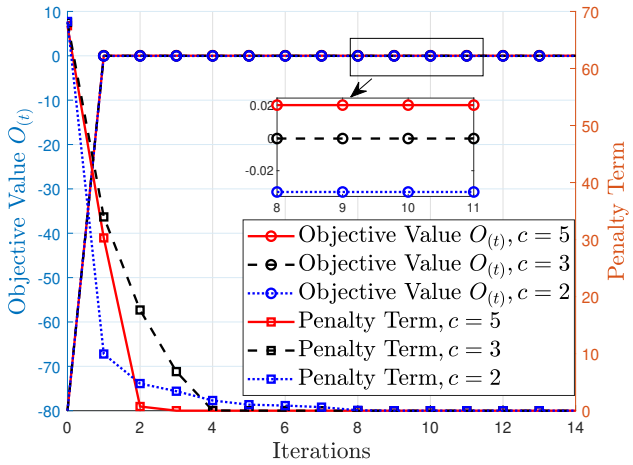

(b) t=1.07 ms

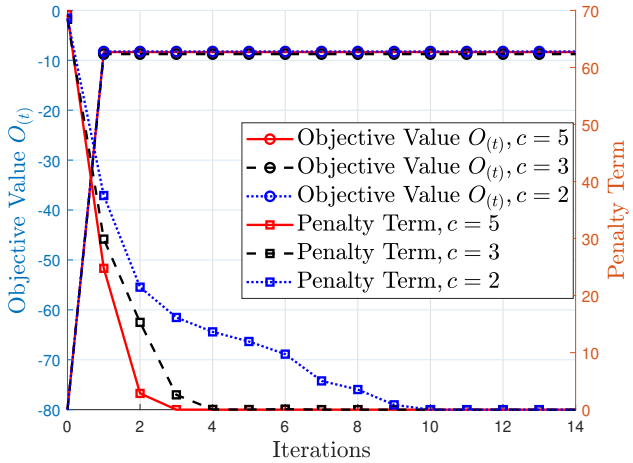

(c) t=1.2 ms

Fig. 3.3: Convergence of Algorithm 5 under $K = 4$ and $M = 3$

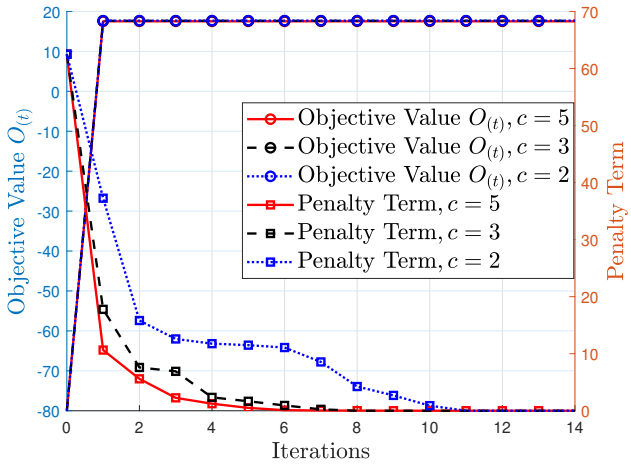

(a) t=1.5 ms

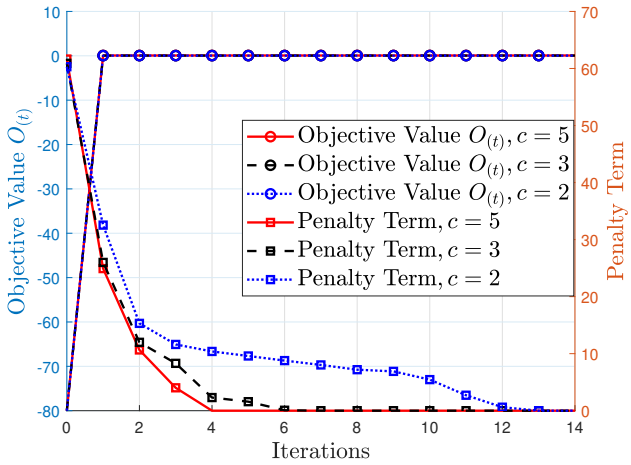

(b) t=1.82 ms

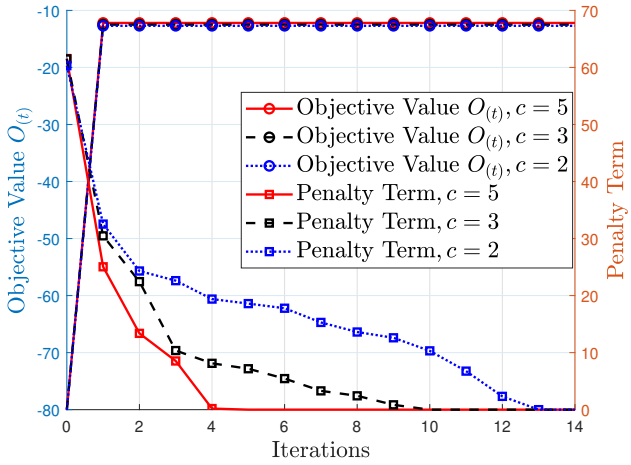

(c) t=2.0 ms

Fig. 3.4: Convergence of Algorithm 5 under $K = 4$ and $M = 6$

based on [108], we model the channel gains as

$$\mathbf{G} \triangleq \left[\frac{\mathbf{g}_1}{||\mathbf{g}_1||}, \frac{\mathbf{g}_2}{||\mathbf{g}_2||}, ..., \frac{\mathbf{g}_I}{||\mathbf{g}_I||}\right] = \tilde{\mathbf{G}}\mathbf{C}_{\mathbf{G}}^{1/2}, \tag{3.39}$$

where $\tilde{\mathbf{G}}$ denotes the normalized Rayleigh fading matrix and satisfies $\mathbb{E}\left[\tilde{\mathbf{G}}^H\tilde{\mathbf{G}}\right] = \mathbf{I}$. $\mathbf{C}_{\mathbf{G}}$ represents the covariance of $\mathbf{G}$, where the (m, n)-th factor indicates the channel relevance of NU m and NU n with the norm of $\tau^{|m-n|}$. Finally, the convergence thresholds of Algorithm 4 and Algorithm 5 are set to $\vartheta = 10^{-5}$ and $\Delta = 10^{-5}$.

Figures 3.3 and 3.4 validate the convergence and effectiveness of our Algorithm 5 under different settings. Specifically, it can be observed that for arbitrary value of the coefficient c, the objective value can converge rapidly and the penalty term can also converge almost to zero after a few iterations. It can also be seen from Figure 3.4(b) that the convergence speed increases when the value of the coefficient c increases. However, an increase in c will degrade the objective function, i.e., $O_{(t)}$ becomes larger. Such a result indicates a trade-off between the convergence speed and computation accuracy of Algorithm 5. In addition, Figures 3.3 and 3.4 show that the output of the Subroutine-O is almost zero when the value of t is optimal, which also verifies the correctness of Proposition 5 and Algorithm 4.

Figure 3.5 verifies the convergence of our Algorithm 4 under given $\{x_i\}_{i\in\mathcal{I}}$. Under two tested cases of $K = 4,\ M = 3$ and $K = 4,\ M = 6$, the top sub-figure of Figure 3.5 displays the value of $O_{(t)}$ for the output of Subroutine-O (i.e., Algorithm 5), and the bottom sub-figure displays the convergence of NOMA transmission duration t. We mark out the final convergence to the values in the two subplots with the red dashed lines. As expected, the value of t converges to the optimal value t^* when $O_{(t)}$ is close to zero. Moreover, we can observed that when t increases, the value of $O_{(t)}$ is non-increasing, which verifies the Proposition 5.

Figure 3.6 shows the convergence of Algorithm 6 and the conventional CE scheme. With the convergence values in Figure 6, we can obtain the optimal sensing scheduling, in this case, $\{x_i\} = \{0, 1, 1, 1, 0\}$, for the current setup. It can be observed that with the introduced probability update strategy, our proposed CE learning based algorithm

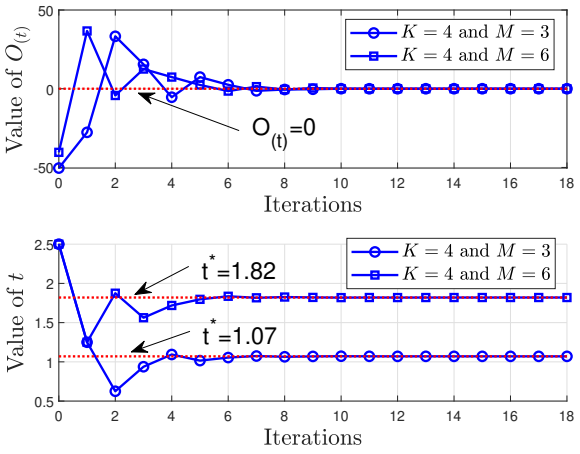

Fig. 3.5: Convergence of Algorithm 4

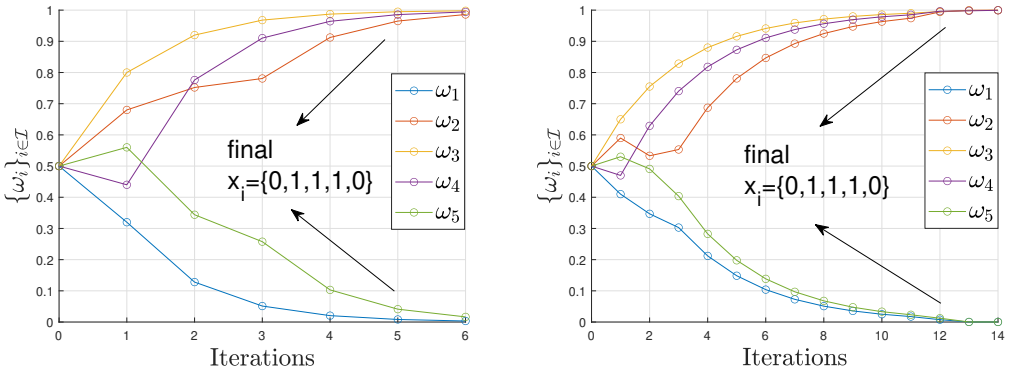

(a) Proposed CE scheme

(b) Conventional CE scheme

Fig. 3.6: Convergence of Algorithm 6 under $K = 4$ and $M = 3$

performs a less number of iterations than the conventional CE scheme.

Figure 3.7 shows the performance of our algorithm in terms of sensing efficiency, total throughput and computation time compared with some benchmark algorithms. Specifically, we set $K = 4$ and $N = 3$ and use the following two algorithms as the comparison benchmarks.

- CE-SDR algorithm. We utilize the CE learning based algorithm proposed in this chapter to solve Problem (SEM-E-Top), and utilize the method of semidefinite relaxation (SDR) and Gaussian randomization to solve Problem (SEM-E-BOT) [109].

- GA-penalty algorithm. We utilize genetic algorithm (GA) to solve Problem (SEM-E-Top) [110], and utilize penalty-based method proposed in this chap-

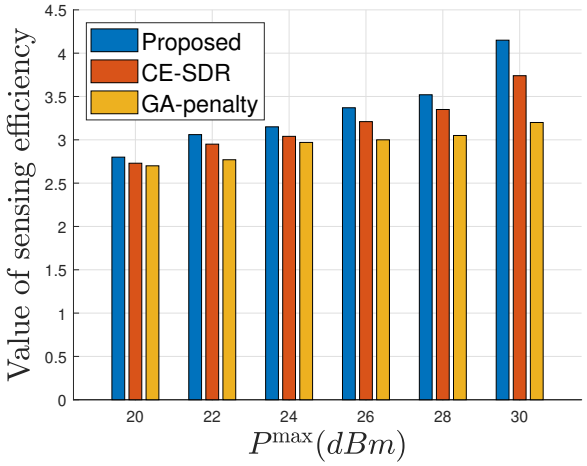

(a) Comparison of sensing efficiency

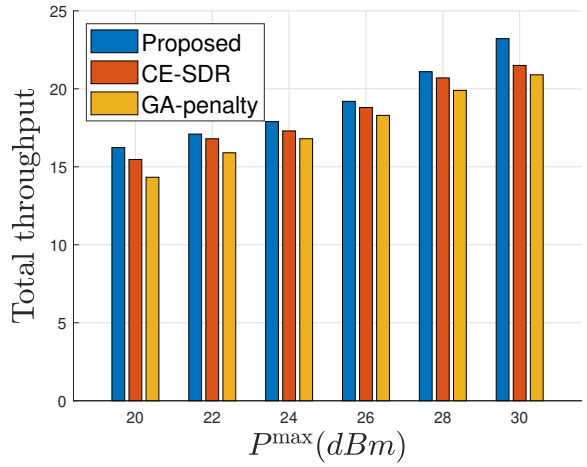

(b) Comparison of total throughput

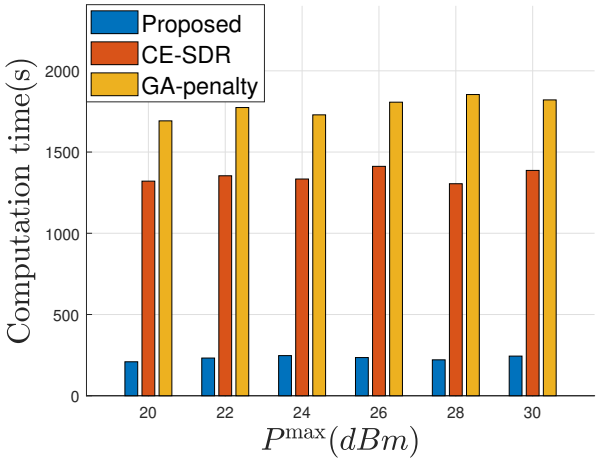

(c) Comparison of computation time

Fig. 3.7: Performance advantages of our proposed algorithm compared with benchmark algorithms

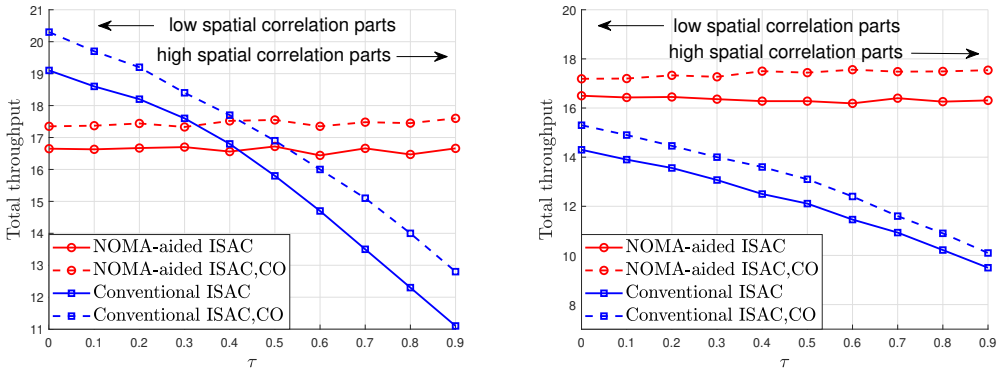

(a) $K = 4$ and $M = 3$ (b) $K = 4$ and $M = 6$

Fig. 3.8: Communication performance with different τ under t^*

ter to solve Problem (SEM-E-BOT).

Figure 3.7 shows that our algorithm outperforms the benchmark algorithms in all three aspects. In particular, the algorithm proposed in this chapter significantly outperforms the other two benchmark algorithms in terms of computation time. In addition, when the total power capacity $P^{\max}$ increases, the sensing efficiency and the total throughput increase accordingly.

Figure 3.8 demonstrates the communication performance, i.e., total throughput, with different spatial correlation under t^*. Each point in Figure 3.8 represents the average result of 200 random channel realizations. We compare the achievable communication capability of our NOMA-aided ISAC with the conventional ISAC and use the communication-only (CO) scheme as an upper bound for the communication performance. Specifically, the achievable rate at communication user $\forall m \in \mathcal{M}$ in the conventional ISAC can be expressed as

$$R_{m,\text{con}} = B \log_2 \left(1 + \frac{|\mathbf{g}_m^H \mathbf{w}_m|^2}{\sum\limits_{n \in \mathcal{M}, n \neq m} |\mathbf{g}_m^H \mathbf{w}_n|^2 + \sigma_n^2} \right). \tag{3.40}$$

It can be observed that the achievable communication performance of NOMA-aided ISAC is almost independent of the channel spatial correlation, while the achievable communication performance of conventional ISAC degrades severely as the channel spatial correlation increases.

We consider in Figure 3.8(a) the case of the number of antennas $K = 4$ and the

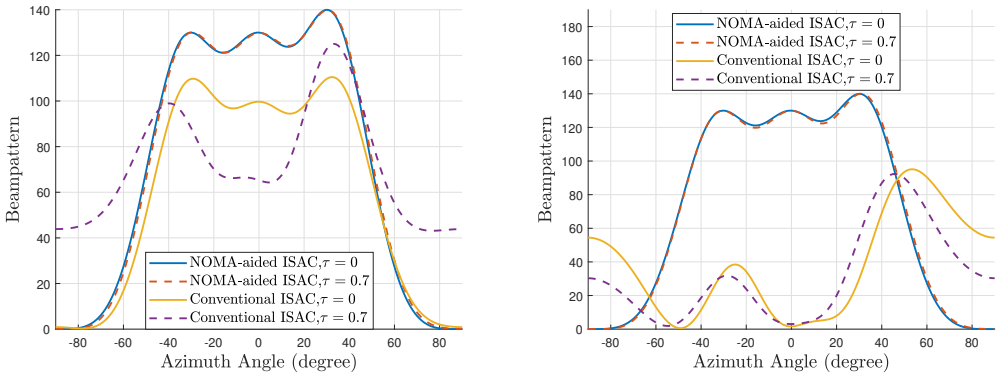

(a) $K = 4$ and $M = 3$ (b) $K = 4$ and $M = 6$

Fig. 3.9: Transmit beampattern

number of NUs $M = 3$. As can be observed from Figure 3.8(a) that the NOMA-aided ISAC achieves better communication performance at high channel spatial correlation. This is because under high channel spatial correlation, the spatial DoFs are restricted, while NOMA can provide additional DoFs to ensure the communication capability. In Figure 3.8(b), we consider the case of $K = 4$ and $M = 6$, in which it is not possible to assign one spatial DoF to each NU, in spite of not performing sensing. As we can see from Figure 3.8(b), there is a significant loss in the communication performance achieved because conventional ISAC cannot mitigate inter-user interference well and require sacrificing a portion of communication resources to guarantee the sensing performance. The NOMA-aided ISAC outperforms the conventional ISAC in terms of the communication capability, regardless of the strength of channel spatial correlation. This is because the NOMA-aided ISAC can still provide additional DoF by mitigating inter-user interference through SIC. In addition, the NOMA-aided ISAC is closer to the upper limit of achievable communication performance in the communication-only scheme than conventional ISAC.

Figure 3.9 compares the transmit beampatterns of NOMA-aided ISAC and conventional ISAC with different channel spatial correlations. As can be observed from Figure 3.9(a) that at low spatial correlation, both schemes are capable of realizing the dominant peak of the transmitted beampattern in the direction of interest, and at high spatial correlation, the power gain of the conventional ISAC in the above direction is significantly reduced. When the number of NUs increases, in Figure 3.9(b), the

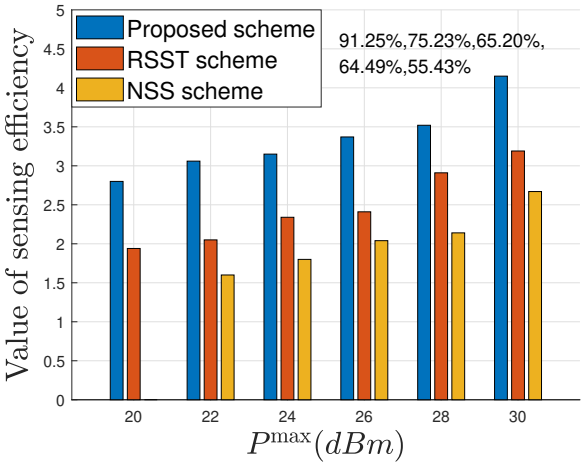

(a) Comparison of sensing efficiency

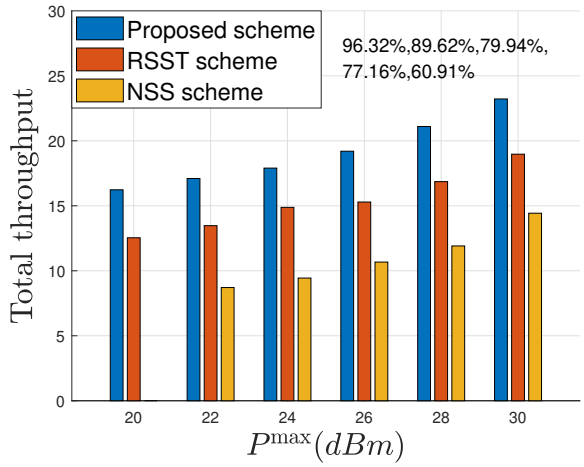

(b) Comparison of total throughput

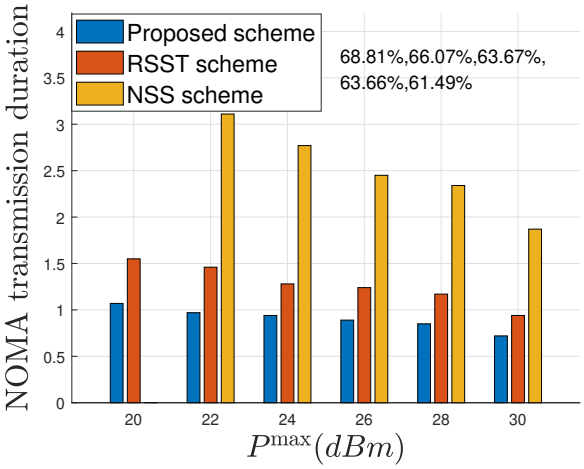

(c) Comparison of NOMA transmission duration

Fig. 3.10: Performance advantages of our proposed algorithm compared with benchmark schemes

NOMA-aided ISAC can still achieve dominant peaks, while the conventional ISAC has major damage to power leakage in undesirable directions.

Figure 3.10 shows the advantages of the proposed sensing scheduling scheme in comparison with the random selection of sensing targets (RSST) scheme and the no-sensing scheduling (NSS) scheme. Figure 3.10 shows that the sensing scheduling scheme proposed in this chapter outperforms the other two schemes in terms of both communication and sensing performance. In particular, the gain obtained by our sensing scheduling scheme over the scheme without accounting for the sensing scheduling (i.e., NSS scheme) is marked at the top of three subplots. Moreover, it can be observed from the first set of data in each of the subplots of Figure 3.10 that when sensing scheduling is not considered, sensing may even fail to execute (i.e., failing to reach the sensing requirements for any of the STs). This further illustrates the importance of sensing scheduling.

3.5 Conclusion

In this chapter, we have investigated the NOMA-aided ISAC system. Specifically, we have utilized the superimposed NOMA signal for the NUs to perform multi-target sensing while satisfying the quality of service for both communication and sensing. We have proposed a joint optimization of the beamforming, the NOMA transmission duration and the sensing scheduling, with the objective of maximizing the sensing efficiency in ISAC system. Despite the formulated joint optimization problem is strictly non-convex, we have exploited the vertical layered structure of the problem and proposed a decomposition-based algorithm that employs the techniques of the penalty function and SCA and the CE learning. Numerical results have been provided to validate the effectiveness of our algorithms and the performance benefits of the proposed NOMA-aided ISAC sensing scheduling scheme.

Chapter 4

ISAC-Enabled Multi-device Multi-target Cooperative Sensing: A Fairness-Aware Design

4.1 Introduction

With the deep convergence of the Internet of Things (IoT), artificial intelligence and communication networks, future 6G wireless networks are evolving rapidly to deliver comprehensive and immersive services [111–113]. The emergence of immersive services in 6G networks, such as autonomous driving, extended reality and digital twins, imposes stringent demands for both ultra-reliable low-latency transmission and high-precision localization [114]. Integrated sensing and communication (ISAC), which enables simultaneous data transmission and sensing information collection via integrated signals over the same spectrum, has been recognized as a spectrum-efficient paradigm to address the conflict between these growing demands and limited wireless resources, and thus attracts wide research interests [115–119]. Due to the great potential of ISAC in improving the spectrum efficiency and resource utilization, it has been expected to serve as an enabling technology in numerous future application scenarios, such as intelligent transportation and intelligent manufacturing.

Existing literature has explored deploying ISAC on wireless devices to acquire accurate environmental information, leveraging their wide distribution and proximity to targets [120–123]. Nevertheless, the performance of ISAC in single-device systems is fundamentally constrained by stringent hardware resources and limited sensing apertures, particularly in multi-target scenarios. Furthermore, managing the mutual interference between communication and multi-target sensing poses significant challenges for resource allocation within a single device. To overcome these limitations, leveraging multi-device cooperative sensing has emerged as a promising solution. By exploiting the spatial diversity of distributed devices, cooperative sensing allows multiple nodes to jointly accomplish sensing tasks, thereby alleviating the resource bottlenecks faced by individual devices. Moreover, sensing from diverse spatial locations yields more comprehensive environmental reconstruction and mitigates performance degradation caused by potential shadowing or blockage. In this context, this chapter

considers a framework where devices perform cooperative sensing in a time-division manner, allowing each device to execute ISAC functions without inter-device interference. However, time-division access introduces a critical fairness concern. In cooperative networks, allocating time resources to maximize system-wise performance often leads to the over-exploitation of devices with superior channel conditions, while others are starved. Designing fairness-aware mechanisms is therefore crucial to achieving balanced performance and prolonging network lifetime, yet efficiently utilizing heterogeneous resources across different devices remains a challenge. Additionally, achieving a flexible trade-off between data transmission and high-precision sensing in multi-target scenarios with diverse requirements remains an open issue.

To address these challenges, this chapter proposes a fairness-aware ISAC-enabled multi-device cooperative sensing framework. We investigate a joint optimization of time allocation and transceiver beamforming, aiming to balance system-wise throughput with individual device fairness. The main contributions of this chapter are summarized as follows.

- We propose a fairness-aware ISAC-enabled multi-device cooperative sensing system in which the devices engage in cooperative sensing towards multiple targets in a time-division manner. Within the allocated time, each device senses the targets and transmits data to the base station simultaneously via ISAC. We formulate a joint optimization of the beamforming for both sensing and transmission as well as the time allocation for different devices, aiming at maximizing the total throughput of the devices while guaranteeing the multi-target sensing quality, the cooperative sensing requirement and the fairness in data transmission.

- To tackle the non-convexity of the problem, we decompose it into a subproblem for beamforming optimization and a subproblem for time allocation via the block coordinate descent. For the beamforming optimization subproblem, we first analyze the necessity of the additional dedicated sensing signal. Then, we present a convex surrogate problem for the non-convex subproblem by designing surrogate functions, and obtain the solution of the beamforming via the

successive convex approximation method. For the time allocation subproblem, we analyze the feature of the optimal time allocation for different devices while providing the semi-analytical expression.

- We present the simulation results to verify the effectiveness of our proposed algorithm. Compared with several benchmark algorithms, our algorithm achieves a superior performance. Moreover, simulation results validate the performance advantages of our fairness-aware ISAC-enabled cooperative sensing scheme. Compared with several benchmark schemes, our fairness-aware ISAC-enabled cooperative sensing scheme outperforms other benchmark schemes in both throughput and cooperative sensing accuracy.

The remainder of the chapter is organized as follows. Section 4.2 illustrates the system model and problem formulation. In Section 4.3, show the problem decomposition and identify the solution features of the decomposed subproblems. We further propose an efficient algorithm for solving the formulated problem in Section 4.3. Section 4.4 demonstrates the performance of our fairness-aware ISAC-enabled multi-device cooperative sensing and Section 4.5 conclude this chapter.

Notations: The trace of matrix $\mathbf{I}$ is denoted by $\mathbf{Tr}(\mathbf{I})$. The transpose of matrix $\mathbf{I}$ is denoted by $\mathbf{I}^T$. The conjugate transpose of matrix $\mathbf{I}$ is denoted by $\mathbf{I}^H$. The conjugate of matrix $\mathbf{I}$ is denoted by $\mathbf{I}^\dagger$. $\mathrm{Re}\{\cdot\}$ denotes the real part of a complex value. $||\cdot||_F^2$ denotes the square of Frobenius-norm.

4.2 System Model of ISAC-Enabled Cooperative Sensing

Figure 4.1 illustrates the system model of our ISAC-enabled multi-device cooperative sensing. There exists a group of integrated sensing and communication devices (SCDs) with N_t transmit antennas and N_r receive antennas denoted by $\mathcal{K} = \{1, 2, ..., K\}$. All SCDs perform cooperative sensing of a group of given targets which are denoted by $\mathcal{M} = \{1, 2, ..., M\}$ in a time-division multiple-access manner, with each SCD sensing the targets as well as transmitting data to the base station (BS) simultaneously within its allocated time. We model the cooperative sensing as a K-phase process, where we allocate time t_k to SCD k at Phase k.

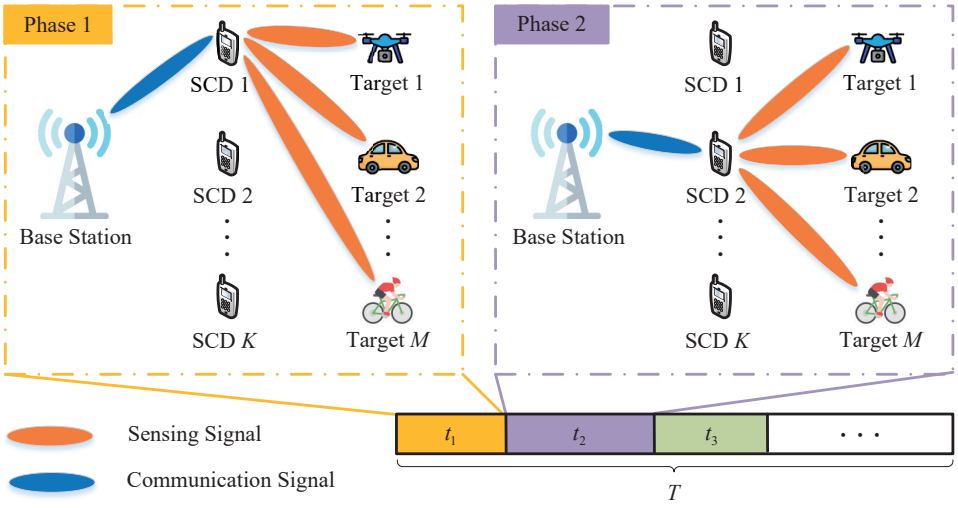

Fig. 4.1: An illustrative system model

4.2.1 Modeling of Phase k

In Phase k, the integrated signal of SCD k for delivering its data to the BS and sensing the targets can be expressed as

$$\mathbf{x}_k = \mathbf{u}_k z_k + \mathbf{v}_k, \tag{4.1}$$

where $\mathbf{u}_k \in \mathbb{C}^{N_t \times 1}$ denotes the SCD k's transmit beamforming vector for the BS, and z_k denotes the data symbol of SCD k. Vector $\mathbf{v}_k$ denotes the dedicated sensing signal of SCD k. The received signal at the BS within Phase k is given by

$$y_k^{\text{BS}} = \mathbf{g}_k^H \mathbf{u}_k z_k + \mathbf{g}_k^H \mathbf{v}_k + n_0, \tag{4.2}$$

where $\mathbf{g}_k \in \mathbb{C}^{N_t \times 1}$ denotes the channel gain between the BS and SCD k, and n_0 denotes the noise at the BS with variance σ_0^2.

We next model the sensing channel for SCD k regarding the targets. Assume that both the transmit and receive uniform linear arrays are half-wavelength antenna spacing. Then, the transmit steering vector and the receive steering vector on direction θ are respectively given by

$$\mathbf{a}_t(\theta) = \frac{1}{\sqrt{N_t}} \left[1, e^{j\pi \sin\theta}, ..., e^{j\pi(N_t-1)\sin\theta}\right]^T, \tag{4.3}$$

$$\mathbf{a}_r(\theta) = \frac{1}{\sqrt{N_r}} \left[1, e^{j\pi \sin\theta}, ..., e^{j\pi(N_r-1)\sin\theta}\right]^T. \tag{4.4}$$

The received signal at SCD k within Phase k consists of three parts, including the sensing echoes from the desired targets with the direction of $\{\theta_{km}\}_{m\in\mathcal{M}}$, the clutter interference from J undesired clutters under the direction $\{\theta_{kj}\}_{j\in\mathcal{J}}$, and the self-interference and noise. We consider that the SCDs have prior knowledge of the targets and clutters. Therefore, we express the received signal at SCD k within Phase k as

$$\begin{aligned}\mathbf{y}_k^{\text{ID}} = &\underbrace{\sum_{m\in\mathcal{M}} \beta_{km}\mathbf{a}_r(\theta_{km})\mathbf{a}_t^H(\theta_{km})\mathbf{x}_k}_{\text{sensing echoes from } M \text{ desired targets}} + \\ &\underbrace{\sum_{j\in\mathcal{J}} \beta_{kj}\mathbf{a}_r(\theta_{kj})\mathbf{a}_t^H(\theta_{kj})\mathbf{x}_k}_{\text{clutter interference from } J \text{ undesired targets}} + \underbrace{\mathbf{H}_k^{\text{SI}}\mathbf{x}_k + \mathbf{n}_k}_{\text{self-interference and noise}},\end{aligned} \tag{4.5}$$

where β_{km} is the complex amplitude of target m regarding SCD k. The value of β_{km} is mainly determined by the path loss and the radar cross-section. Vector $\mathbf{H}_k^{\text{SI}} \in \mathbb{C}^{N_r\times N_t}$ denotes the residual self-interference channel at SCD k, and $\mathbf{n}_k$ denotes the noise with variance σ_k^2. In the following context, we define $\mathbf{A}_{km} \triangleq \beta_{km}\mathbf{a}_r(\theta_{km})\mathbf{a}_t^H(\theta_{km})$, and $\mathbf{A}_k^{\text{ITF}} \triangleq \sum_{j\in\mathcal{J}} \beta_{kj}\mathbf{a}_r(\theta_{kj})\mathbf{a}_t^H(\theta_{kj}) + \mathbf{H}_k^{\text{SI}}$.

Based on eq. (4.2), the achievable data transmission rate R_k from SCD k to the BS is expressed as

$$R_k = B\log_2\left(1 + \frac{|\mathbf{g}_k^H\mathbf{u}_k|^2}{|\mathbf{g}_k^H\mathbf{v}_k|^2 + \sigma_0^2}\right), \tag{4.6}$$

where B denotes the channel bandwidth. The covariance of SCD k's transmitted signal is given by

$$\mathbf{W}_k = \mathbb{E}(\mathbf{x}_k\mathbf{x}_k^H) = \mathbf{u}_k\mathbf{u}_k^H + \mathbf{v}_k\mathbf{v}_k^H. \tag{4.7}$$

We measure the multi-target sensing performance by using beampattern matching error and mean-squared cross correlation [124]. Specifically, the beampattern matching error quantifies the disparity between the desired radiation pattern and the actual measured pattern. Let $\{\psi(\theta_{kq})\}_{q=1}^{Q}$ denote the pre-designed beampattern of SCD k, the SCD k's beampattern matching error between the obtained beampattern and the pre-

designed beampattern is given by

$$\xi_k = \frac{1}{Q}\sum_{q=1}^{Q} |\varsigma_k \psi(\theta_{kq}) - \mathbf{a}_t^H(\theta_{kq})\mathbf{W}_k\mathbf{a}_t(\theta_{kq})|^2, \tag{4.8}$$

where ς_k is the scaling factor of SCD k and $\{\theta_{kq}\}_{q=1}^{Q}$ are the sampled angle grids. The mean-squared cross correlation is used to quantify the correlation between two signals. For high-quality multi-target sensing, there should be a significant difference between the signals in different target directions, i.e., a low cross correlation value should be held, which facilitates the effective separation and extraction of the sensing echoes from different directions. The mean-squared cross correlation of SCD k's transmit signal is given by

$$\zeta_k = \frac{2}{M^2 - M}\sum_{i=1}^{M}\sum_{i'=i+1}^{M} |\mathbf{a}_t^H(\theta_{ki})\mathbf{W}_k\mathbf{a}_t(\theta_{ki'})|^2, \tag{4.9}$$

We measure the cooperative sensing performance by using the sensing estimation rate, which is defined as the cancellation of the uncertainty in the target parameters per second. Based on eq. (4.5), the sensing estimation rate S_k of SCD k for sensing target m is characterized as

$$S_{km} = \frac{\delta}{2\mu}\log_2\left(1 + \frac{2\mu B\mathbf{c}_{km}^H\mathbf{A}_{km}\mathbf{W}_k\mathbf{A}_{km}^H\mathbf{c}_{km}}{\mathbf{c}_{km}^H\mathbf{\Lambda}_{km}\mathbf{c}_{km}}\right), \tag{4.10}$$

where δ denotes the radar duty factor, and μ denotes the radar pulse duration. Vector $\mathbf{c}_{km} \in \mathbb{C}^{N_r \times 1}$ denotes the receive beamforming of SCD k for sensing target m. Vector $\mathbf{\Lambda}$ is the interference of SCD k for sensing target m, and it can be expressed as

$$\mathbf{\Lambda}_{km} = \mathbf{A}_k^{\text{ITF}}\mathbf{W}_k(\mathbf{A}_k^{\text{ITF}})^H + \sum_{m' \neq m}\mathbf{A}_{km'}\mathbf{W}_k\mathbf{A}_{km'}^H + \sigma_k^2\mathbf{I}_N. \tag{4.11}$$

According to [81], the optimal receivers $\mathbf{c}_{km}^*$ is given by

$$\mathbf{c}_{km}^* = \arg\max\frac{\mathbf{c}_{km}^H\mathbf{A}_{km}\mathbf{W}_k\mathbf{A}_{km}^H\mathbf{c}_{km}}{\mathbf{c}_{km}^H\mathbf{\Lambda}_{km}\mathbf{c}_{km}} = \mathbf{\Lambda}_{km}^{-1}\mathbf{a}_r(\theta_{km}). \tag{4.12}$$

By substituting eq. (4.12) into eq. (4.10), we can rewrite S_{km} as

$$S_{km} = \frac{\delta}{2\mu} \log_2 \left(1 + 2\mu B \mathbf{x}_k^H \mathbf{A}_{km}^H \mathbf{\Lambda}_{km}^{-1} \mathbf{A}_{km} \mathbf{x}_k\right). \tag{4.13}$$

4.2.2 Problem Formulation

We aim at maximizing the total throughput of the SCDs considering the fairness (MTCF), while guaranteeing the requirements of both multi-target sensing and cooperative sensing for the given targets. To this end, we conduct a joint optimization of the SCDs' beamforming vectors $\{\mathbf{u}_k\}_{k\in\mathcal{K}}$, $\{\mathbf{v}_k\}_{k\in\mathcal{K}}$, and the time allocation $\{t_k\}_{k\in\mathcal{K}}$.

$$\begin{aligned}
\text{(MTCF):}\ & \max \sum_{k\in\mathcal{K}} \ln(R_k t_k) \\
\text{subject to:}\ & \sum_{k\in\mathcal{K}} t_k \le T, t_k \ge 0, && (4.14)\\
& \sum_{k\in\mathcal{K}} S_{km} t_k \ge S_m^{\text{req}}, \forall m \in \mathcal{M}, && (4.15)\\
& \xi_k \le \xi^{\max}, \forall k \in \mathcal{K}, && (4.16)\\
& \zeta_k \le \zeta^{\max}, \forall k \in \mathcal{K}, && (4.17)\\
& \mathbf{Tr}(\mathbf{W}_k) \le P_k^{\max}, \forall k \in \mathcal{K}, && (4.18)\\
\text{variables:}\ & \{\mathbf{u}_k\}_{k\in\mathcal{K}}, \{\mathbf{v}_k\}_{k\in\mathcal{K}}, \text{ and } \{t_k\}_{k\in\mathcal{K}}.
\end{aligned}$$

In the objective function, we use $\ln(\cdot)$ function as the utility of SCD k for delivering its data volume in Phase k, and maximize the total utility of the SCDs. This objective function facilitates the fairness of the throughput of different devices, which leads to a balanced allocation of data transmission opportunities. Constraint (4.14) ensures that the total time allocation cannot exceed the maximum time T. Constraint (4.15) guarantees the minimum cooperative sensing requirement S_m^{req} for arbitrary target m. Constraint (4.16) ensures that the beampattern matching error of SCD k cannot exceed the maximum error $\xi^{\max}$. Constraint (4.17) ensures that the value of mean-squared cross correlation of SCD k's transmit signal cannot exceed a required level $\zeta^{\max}$. Constraints (4.16) and (4.17) guarantee the SCD k's multi-target sensing performance. Constraint (4.18) ensures that the total power consumption of SCD k cannot exceed its power capacity $P_k^{\max}$.

4.3 Proposed Algorithms for Solving Problem (MTCF)

4.3.1 Decomposition of Problem (MTCF)

Problem (MTCF) is a strictly non-convex optimization problem since the beamforming variables and time allocation variables are coupled in both the objective function and constraints, which is difficult to solve directly. To address this issue, we first decompose the original Problem (MTCF) into two subproblems, including a subproblem for beamforming optimization (BO) and a subproblem for time allocation (TA), which are shown as follows.

$$\begin{aligned}
&\text{(MTCF-BO):}\ \max \sum_{k\in\mathcal{K}} \ln(R_k t_k) \\
&\quad \text{subject to: constraints } (4.15), (4.16), (4.17) \text{ and } (4.18), \\
&\quad \text{variables: } \{\mathbf{u}_k\}_{k\in\mathcal{K}} \text{ and } \{\mathbf{v}_k\}_{k\in\mathcal{K}}.
\end{aligned}$$

$$\begin{aligned}
&\text{(MTCF-TA):}\ \max \sum_{k\in\mathcal{K}} \ln(R_k t_k) \\
&\quad \text{subject to: constraints } (4.14) \text{ and } (4.15), \\
&\quad \text{variables: } \{t_k\}_{k\in\mathcal{K}}.
\end{aligned}$$

Then, we solve the two subproblems iteratively by adopting the block coordinate descent method. The details for solving these two subproblems are shown in Section 4.3.2 and Section 4.3.3.

4.3.2 Algorithm for Solving Problem (MTCF-BO)

Problem (MTCF-BO) is still a strictly non-convex problem since the objective function and constraints (4.15)-(4.17) are non-convex. We first identify the solution feature of $\mathbf{v}_k$ as follows.

Proposition 7. *The optimal solution of Problem (MTCF-BO) has the feature as*

$$\{\mathbf{v}_k^*\}_{k\in\mathcal{K}} = \mathbf{0}. \tag{4.19}$$

Proof. We consider Problem (MTCF-BO), which is under the given $\{\mathbf{u}_k\}_{k\in\mathcal{K}}$, as follows

$$\begin{aligned}
&\text{(BO-v)}: \max \sum_{k\in\mathcal{K}} \ln\left(t_k B \log_2\left(1+\frac{|\mathbf{g}_k^H\mathbf{u}_k|^2}{|\mathbf{g}_k^H\mathbf{v}_k|^2+\sigma_0^2}\right)\right)\\
&\text{subject to: constraints } (4.15), (4.16), (4.17) \text{ and } (4.18),\\
&\text{variables: } \{\mathbf{v}_k\}_{k\in\mathcal{K}}.
\end{aligned}$$

We notice the following important features. On the one hand, the objective function aims to minimize $\{|\mathbf{g}_k^H\mathbf{v}_k|^2\}_{k\in\mathcal{K}}$ and maximize $\{|\mathbf{g}_k^H\mathbf{u}_k|^2\}_{k\in\mathcal{K}}$. On the other hand, $\{\mathbf{u}_k\}_{k\in\mathcal{K}}$ and $\{\mathbf{v}_k\}_{k\in\mathcal{K}}$ play the same role in constraints (4.15)-(4.18), i.e., for arbitrary $\{\mathbf{v}_k\}_{k\in\mathcal{K}} \neq \mathbf{0}$, we can transfer its power to $\{\mathbf{u}_k\}_{k\in\mathcal{K}}$ without changing the feasible region constituted by constraints (4.15)-(4.18). Therefore, we can conclude that the optimal solution of $\{\mathbf{v}_k\}_{k\in\mathcal{K}}$ in Problem (MTCF-BO) is $\{\mathbf{v}_k^*\}_{k\in\mathcal{K}} = \mathbf{0}$. □

Proposition 7 implies that the communication signal can be entirely repurposed for sensing, without the necessity to design the additional dedicated sensing signal for this scenario, which can simplify the system design of the ISAC device and the deployment of the ISAC system in practical applications. By substituting this solution into Problem (MTCF-BO), we can derive the following problem

$$\begin{aligned}
&\text{(BO-E)}: \max \sum_{k\in\mathcal{K}} \ln\left(t_k B \log_2\left(1+\frac{\mathbf{u}_k^H\mathbf{G}_k\mathbf{u}_k}{\sigma_0^2}\right)\right)\\
&\text{subject to: constraints } (4.15), (4.16), (4.17) \text{ and } (4.18),\\
&\text{variables: } \{\mathbf{u}_k\}_{k\in\mathcal{K}}.
\end{aligned}$$

In Problem (BO-E), we define $\mathbf{G}_k \triangleq \mathbf{g}_k\mathbf{g}_k^H$, and $\mathbf{W}_k$ is rewritten as $\mathbf{W}_k = \mathbf{u}_k\mathbf{u}_k^H$. Next, we use successive convex approximation (SCA) to address the non-convexity of the objective function and constraints (4.15)-(4.17), and thus transform Problem (BO-E) into a tractable form.

Proposition 8. *S_{km} in eq. (4.13) can be equivalently transformed into $\hat{S}_{km}$ as follows*

$$\hat{S}_{km} = 2\sqrt{\delta B(1+\gamma_{km})}\mathrm{Re}\{\mathbf{u}_k^H \mathbf{A}_{km}^H \mathbf{f}_{km}\} - 2\mu B||\mathbf{f}_{km}^H \mathbf{A}_{km}\mathbf{u}_k||_F^2 - ||\mathbf{f}_{km}^H \mathbf{A}_k^{\mathrm{ITF}}\mathbf{u}_k||_F^2 - \sum_{m'\neq m} ||\mathbf{f}_{km}^H \mathbf{A}_{km'}\mathbf{u}_k||_F^2 - \sigma_k^2||\mathbf{f}_{km}||_F^2 + \frac{\delta}{2\mu}\log_2(1+\gamma_{km}) - \frac{\delta}{2\mu}\gamma_{km}, \tag{4.20}$$

where $\{\gamma_{km}\}_{k\in\mathcal{K},m\in\mathcal{M}}$ *and* $\{\mathbf{f}_{km}\}_{k\in\mathcal{K},m\in\mathcal{M}}$ *are auxiliary variables and their optimal values can be given by*

$$\gamma_{km}^* = 2\mu B \mathbf{u}_k^H \mathbf{A}_{km}^H \mathbf{\Lambda}_{km}^{-1} \mathbf{A}_{km}\mathbf{u}_k, \tag{4.21}$$

$$\mathbf{f}_{km}^* = \sqrt{\delta B(1+\gamma_{km})}(2\mu B \mathbf{A}_{km}\mathbf{u}_k\mathbf{u}_k^H\mathbf{A}_{km}^H + \mathbf{\Lambda}_{km})^{-1}\mathbf{A}_{km}\mathbf{u}_k. \tag{4.22}$$

Proof. By using Lagrangian dual transform method, we introduce the auxiliary variables $\{\gamma_{km}\}_{k\in\mathcal{K},m\in\mathcal{M}}$ and rewrite S_{km} in eq. (4.13) as

$$\tilde{S}_{km} = \delta B(1+\gamma_{km})\mathbf{u}_k^H \mathbf{A}_{km}^H \mathbf{D}_{km}^{-1}\mathbf{A}_{km}\mathbf{u}_k + \frac{\delta}{2\mu}\log_2(1+\gamma_{km}) - \frac{\delta}{2\mu}\gamma_{km}, \tag{4.23}$$

where $\mathbf{D}_{km}$ is given by

$$\mathbf{D}_{km} = 2\mu B \mathbf{A}_{km}\mathbf{u}_k\mathbf{u}_k^H\mathbf{A}_{km}^H + \mathbf{\Lambda}_{km}. \tag{4.24}$$

It can be identified that $\tilde{S}_{km}$ is a concave function of $\{\gamma_{km}\}_{k\in\mathcal{K},m\in\mathcal{M}}$ under the given $\{\mathbf{u}_k\}_{k\in\mathcal{K}}$ [82]. The first derivative of $\tilde{S}_{km}$ regarding $\{\gamma_{km}\}_{k\in\mathcal{K},m\in\mathcal{M}}$ is given by

$$\frac{\partial\tilde{S}_{km}}{\gamma_{km}} = \delta B \mathbf{u}_k^H \mathbf{A}_{km}^H \mathbf{D}_{km}^{-1}\mathbf{A}_{km}\mathbf{u}_k - \frac{\delta\gamma_{km}}{2\mu(1+\gamma_{km})}. \tag{4.25}$$

By using Sherman-Morrison formula, eq. (4.25) can be rewritten as

$$\begin{aligned}\frac{\partial\tilde{S}_{km}}{\gamma_{km}} &= -\frac{2\mu\delta B^2 \mathbf{u}_k^H \mathbf{A}_{km}^H \mathbf{\Lambda}_{km}^{-1}\mathbf{A}_{km}\mathbf{u}_k\mathbf{u}_k^H\mathbf{A}_{km}^H\mathbf{\Lambda}_{km}^{-1}\mathbf{A}_{km}\mathbf{u}_k}{1+2\mu B\mathbf{u}_k^H\mathbf{A}_{km}^H\mathbf{\Lambda}_{km}^{-1}\mathbf{A}_{km}\mathbf{u}_k} \\ &\quad + \delta B\mathbf{u}_k^H\mathbf{A}_{km}^H\mathbf{\Lambda}_{km}^{-1}\mathbf{A}_{km}\mathbf{u}_k - \frac{\delta\gamma_{km}}{2\mu(1+\gamma_{km})} \\ &= \frac{\delta B\mathbf{u}_k^H\mathbf{A}_{km}^H\mathbf{\Lambda}_{km}^{-1}\mathbf{A}_{km}\mathbf{u}_k}{1+2\mu B\mathbf{u}_k^H\mathbf{A}_{km}^H\mathbf{\Lambda}_{km}^{-1}\mathbf{A}_{km}\mathbf{u}_k} - \frac{\delta\gamma_{km}}{2\mu(1+\gamma_{km})}.\end{aligned} \tag{4.26}$$

By setting $\frac{\partial \tilde{S}_{km}}{\gamma_{km}} = 0$, we can derive that the optimal solution of $\{\gamma_{km}\}_{k\in\mathcal{K},m\in\mathcal{M}}$ can be expressed as

$$\gamma_{km}^{*} = 2\mu B \mathbf{u}_k^H \mathbf{A}_{km}^H \mathbf{\Lambda}_{km}^{-1} \mathbf{A}_{km} \mathbf{u}_k. \tag{4.27}$$

Since eq. (4.23) is still non-convex, we further use multi-dimensional quadratic transform method [125] to rewrite $\tilde{S}_{km}$ as

$$\begin{aligned} \hat{S}_{km} =& 2\sqrt{\delta B(1+\gamma_{km})}\mathrm{Re}\{\mathbf{u}_k^H \mathbf{A}_{km}^H \mathbf{f}_{km}\} - \mathbf{f}_{km}^H \mathbf{D}_{km} \mathbf{f}_{km} \\ &+ \frac{\delta}{2\mu}\log_2(1+\gamma_{km}) - \frac{\delta}{2\mu}\gamma_{km}, \end{aligned} \tag{4.28}$$

where $\{\mathbf{f}_{km}\}_{k\in\mathcal{K},m\in\mathcal{M}} \in \mathbb{C}^{N_r\times 1}$ is the auxiliary vector. By substituting eq. (4.24) into eq. (4.28), we obtain

$$\begin{aligned} \hat{S}_{km} =& 2\sqrt{\delta B(1+\gamma_{km})}\mathrm{Re}\{\mathbf{u}_k^H \mathbf{A}_{km}^H \mathbf{f}_{km}\} - 2\mu B||\mathbf{f}_{km}^H \mathbf{A}_{km}\mathbf{u}_k||_F^2 - ||\mathbf{f}_{km}^H \mathbf{A}_k^{\mathrm{ITF}}\mathbf{u}_k||_F^2 \\ &- \sum_{m'\neq m} ||\mathbf{f}_{km}^H \mathbf{A}_{km'}\mathbf{u}_k||_F^2 - \sigma_k^2||\mathbf{f}_{km}||_F^2 + \frac{\delta}{2\mu}\log_2(1+\gamma_{km}) - \frac{\delta}{2\mu}\gamma_{km}. \end{aligned} \tag{4.29}$$

According to the criterion of multi-dimensional quadratic transform [125], the optimal solution of $\{\mathbf{f}_{km}\}_{k\in\mathcal{K},m\in\mathcal{M}}$ is

$$\mathbf{f}_{km}^{*} = \sqrt{\delta B(1+\gamma_{km})}\mathbf{D}_{km}^{-1}\mathbf{A}_{km}\mathbf{u}_k. \tag{4.30}$$

Thus, we complete the proof. □

It can be identified that eq. (4.20) is a concave function of $\{\mathbf{u}_k\}_{k\in\mathcal{K}}$ under the given $\{\gamma_{km}\}_{k\in\mathcal{K},m\in\mathcal{M}}$ and $\{\mathbf{f}_{km}\}_{k\in\mathcal{K},m\in\mathcal{M}}$ since the first term of eq. (4.20) is affine and the other terms in eq. (4.20) are concave.

We introduce the auxiliary variables $\{l_{kq}\}_{k\in\mathcal{K},m\in\mathcal{M}}$ that satisfy

$$|\varsigma_k \psi(\theta_{kq}) - \mathbf{a}_t^H(\theta_{kq})\mathbf{u}_k\mathbf{u}_k^H\mathbf{a}_t(\theta_{kq})| \leq l_{kq}, \forall k, q. \tag{4.31}$$

Then, we can transform constraint (4.16) into the following three constraints

$$||\mathbf{a}_t^H(\theta_{kq})\mathbf{u}_k||_F^2 - \varsigma_k\psi(\theta_{kq}) \leq l_{kq}, \forall k, q, \tag{4.32}$$

$$\varsigma_k\psi(\theta_{kq}) - \mathbf{a}_t^H(\theta_{kq})\mathbf{u}_k\mathbf{u}_k^H\mathbf{a}_t(\theta_{kq}) \leq l_{kq}, \forall k, q, \tag{4.33}$$

$$\frac{1}{Q}\sum_{q=1}^{Q} l_{kq}^2 \leq \xi^{\max}, \forall k, m. \tag{4.34}$$

Constraint (4.32) is convex since the square of the Frobenius-norm is convex, and constraint (4.34) is convex. Next, we design the surrogate functions [126] for non-convex constraints (4.9) and (4.33) as well as the objective function.

Proposition 9. *The surrogate functions for constraint (4.17) and constraint (4.33) can be respectively expressed as*

$$\begin{aligned}\hat{\Omega}_1 = &\sum_{i=1}^{M}\sum_{i'=i+1}^{M} |\mathbf{a}_t^H(\theta_{ki})\overline{\mathbf{u}}_k\overline{\mathbf{u}}_k^H\mathbf{a}_t(\theta_{ki'})|^2 + \\ &\sum_{i=1}^{M}\sum_{i'=i+1}^{M} 4\mathrm{Re}\{(\mathbf{a}_t^H(\theta_{ki})\overline{\mathbf{u}}_k\overline{\mathbf{u}}_k^H\mathbf{a}_t(\theta_{ki'}))(\overline{\mathbf{u}}_k^H\mathbf{a}_t(\theta_{ki'})\mathbf{a}_t^H(\theta_{ki})(\mathbf{u}_k - \overline{\mathbf{u}}_k))\},\end{aligned} \tag{4.35}$$

$$\hat{\Omega}_2 = \varsigma_k\psi(\theta_{kq}) - \mathbf{a}_t^H(\theta_{kq})\overline{\mathbf{u}}_k\overline{\mathbf{u}}_k^H\mathbf{a}_t(\theta_{kq}) - 2\mathrm{Re}\{\overline{\mathbf{u}}_k^H\mathbf{a}_t(\theta_{kq})\mathbf{a}_t^H(\theta_{kq})(\mathbf{u}_k - \overline{\mathbf{u}}_k)\}, \forall k, q, \tag{4.36}$$

where $\overline{\mathbf{u}}_k$ is the solution of $\mathbf{u}_k$ obtained by the previous iteration in solving the surrogate problem.

Proof. We rewrite $|\mathbf{a}_t^H(\theta_{ki})\mathbf{u}_k\mathbf{u}_k^H\mathbf{a}_t(\theta_{ki'})|^2$ in eq. (4.9) as

$$\Omega_1 = (\mathbf{Tr}(\mathbf{u}_k\mathbf{u}_k^H\mathbf{a}_t(\theta_{ki'})\mathbf{a}_t^H(\theta_{ki})))^2. \tag{4.37}$$

The complex-valued derivatives of Ω_1 is given by

$$\frac{\partial\Omega_1}{\partial\mathbf{u}_k} = 2(\mathbf{a}_t^H(\theta_{ki})\mathbf{u}_k\mathbf{u}_k^H\mathbf{a}_t(\theta_{ki'}))(\mathbf{a}_t(\theta_{ki'})\mathbf{a}_t^H(\theta_{ki}))^T\mathbf{u}_k^\dagger, \tag{4.38}$$

$$\frac{\partial\Omega_1}{\partial\mathbf{u}_k^\dagger} = 2(\mathbf{a}_t^H(\theta_{ki})\mathbf{u}_k\mathbf{u}_k^H\mathbf{a}_t(\theta_{ki'}))(\mathbf{a}_t(\theta_{ki'})\mathbf{a}_t^H(\theta_{ki}))\mathbf{u}_k. \tag{4.39}$$

We use the first-order Taylor expansion of $\{\mathbf{u}_k\}_{k\in\mathcal{K}}$ in eq. (4.37) and derive the surro-

gate function $\hat{\Omega}_1$ as the upper bound which is given by

$$\begin{aligned}
&\sum_{i=1}^{M}\sum_{i'=i+1}^{M}\Omega_1 \leq \hat{\Omega}_1 = \sum_{i=1}^{M}\sum_{i'=i+1}^{M}\Bigg(|\mathbf{a}_t^H(\theta_{ki})\overline{\mathbf{u}}_k\overline{\mathbf{u}}_k^H\mathbf{a}_t(\theta_{ki'})|^2+ \\
&2(\mathbf{a}_t^H(\theta_{ki})\mathbf{u}_k\mathbf{u}_k^H\mathbf{a}_t(\theta_{ki'}))\overline{\mathbf{u}}_k^H(\mathbf{a}_t(\theta_{ki'})\mathbf{a}_t^H(\theta_{ki}))(\mathbf{u}_k-\overline{\mathbf{u}}_k)+ \\
&2(\mathbf{a}_t^H(\theta_{ki})\mathbf{u}_k\mathbf{u}_k^H\mathbf{a}_t(\theta_{ki'}))\overline{\mathbf{u}}_k^T(\mathbf{a}_t(\theta_{ki'})\mathbf{a}_t^H(\theta_{ki}))^T(\mathbf{u}_k^\dagger-\overline{\mathbf{u}}_k^\dagger)\Bigg) \qquad (4.40)\\
&=\sum_{i=1}^{M}\sum_{i'=i+1}^{M}|\mathbf{a}_t^H(\theta_{ki})\overline{\mathbf{u}}_k\overline{\mathbf{u}}_k^H\mathbf{a}_t(\theta_{ki'})|^2+\sum_{i=1}^{M}\sum_{i'=i+1}^{M}4\mathrm{Re} \\
&\{(\mathbf{a}_t^H(\theta_{ki})\overline{\mathbf{u}}_k\overline{\mathbf{u}}_k^H\mathbf{a}_t(\theta_{ki'}))(\overline{\mathbf{u}}_k^H\mathbf{a}_t(\theta_{ki'})\mathbf{a}_t^H(\theta_{ki})(\mathbf{u}_k-\overline{\mathbf{u}}_k))\},
\end{aligned}$$

where $\overline{\mathbf{u}}_k$ is the solution of $\mathbf{u}_k$ obtained by the previous iteration in solving the surrogate problem.

We rewrite the left side of eq. (4.33) as

$$\Omega_2 = \varsigma_k\psi(\theta_{kq}) - \mathbf{Tr}(\mathbf{u}_k\mathbf{u}_k^H\mathbf{a}_t(\theta_{kq})\mathbf{a}_t^H(\theta_{kq})). \qquad (4.41)$$

We use the first-order Taylor expansion of $\{\mathbf{u}_k\}_{k\in\mathcal{K}}$ in eq. (4.41) and derive the surrogate function $\hat{\Omega}_2$ as the upper bound which can be expressed as

$$\begin{aligned}
\Omega_2 \leq \hat{\Omega}_2 &= \varsigma_k\psi(\theta_{kq}) - \mathbf{a}_t^H(\theta_{kq})\overline{\mathbf{u}}_k\overline{\mathbf{u}}_k^H\mathbf{a}_t(\theta_{kq}) - \overline{\mathbf{u}}_k^H\mathbf{a}_t(\theta_{kq})\mathbf{a}_t^H(\theta_{kq})(\mathbf{u}_k-\overline{\mathbf{u}}_k) \\
&\quad - \overline{\mathbf{u}}_k^T\mathbf{a}_t(\theta_{kq})\mathbf{a}_t^H(\theta_{kq})(\mathbf{u}_k^\dagger-\overline{\mathbf{u}}_k^\dagger) \\
&= \varsigma_k\psi(\theta_{kq}) - \mathbf{a}_t^H(\theta_{kq})\overline{\mathbf{u}}_k\overline{\mathbf{u}}_k^H\mathbf{a}_t(\theta_{kq}) - 2\mathrm{Re}\{\overline{\mathbf{u}}_k^H\mathbf{a}_t(\theta_{kq})\mathbf{a}_t^H(\theta_{kq})(\mathbf{u}_k-\overline{\mathbf{u}}_k)\},
\end{aligned} \qquad (4.42)$$

where $\overline{\mathbf{u}}_k$ is the solution of $\mathbf{u}_k$ obtained by the previous iteration in solving the surrogate problem. Thus, we complete the proof. □

Then, we use the first-order Taylor expansion of $\{\mathbf{u}_k\}_{k\in\mathcal{K}}$ for eq. (4.6) and define the surrogate function $\hat{R}_k$ as

$$\hat{R}_k = B\log_2(1+\frac{\overline{\mathbf{u}}_k^H\mathbf{G}_k\overline{\mathbf{u}}_k}{\sigma_0^2}) + \frac{2\mathrm{Re}\{\overline{\mathbf{u}}_k^H\mathbf{G}_k(\mathbf{u}_k-\overline{\mathbf{u}}_k)\}}{\sigma_0^2+\overline{\mathbf{u}}_k^H\mathbf{G}_k\overline{\mathbf{u}}_k}, \qquad (4.43)$$

where $\overline{\mathbf{u}}_k$ is the solution of $\mathbf{u}_k$ obtained by the previous iteration in solving the surro-

gate problem.

After the above operations, we can establish the surrogate problem for Problem (BO-E) as follows.

$$\text{(BO-E-Sur):}\ \max \Upsilon = \sum_{k\in\mathcal{K}} \ln\left(t_k \hat{R}_k\right)$$

$$\text{subject to: constraints } (4.18), (4.32) \text{ and } (4.34),$$

$$\sum_{k\in\mathcal{K}} \hat{S}_{km} t_k \geq S_m^{\text{req}}, \forall m \in \mathcal{M}, \tag{4.44}$$

$$\hat{\Omega}_1 \leq \frac{M^2 - M}{2} \zeta^{\max}, \forall k \in \mathcal{K}, \tag{4.45}$$

$$\hat{\Omega}_2 \leq l_{kq}, \forall k, q, \tag{4.46}$$

$$\text{variables: } \{\mathbf{u}_k\}_{k\in\mathcal{K}} \text{ and } \{l_{kq}\}_{\forall k,q}.$$

We identify the convexity of Problem (BO-E-Sur) and prove it with the following proposition.

Proposition 10. *Problem (BO-E-Sur) is a strictly convex optimization problem with respect to* $\{\mathbf{u}_k\}_{\forall k}$ *and* $\{l_{kq}\}_{\forall k,q}$.

Proof. It can be identified that $\hat{R}_k$ is affine with respect to $\{\mathbf{u}_k\}_{k\in\mathcal{K}}$. We conclude that the objective function of Problem (BO-E-Sur) is a concave function of $\{\mathbf{u}_k\}_{k\in\mathcal{K}}$ based on the theory of convexity preserving operations [82]. Moreover, constraints (4.18), (4.44), (4.45) and (4.46) are convex regarding $\{\mathbf{u}_k\}_{\forall k}$, constraint (4.34) is convex regarding $\{l_{kq}\}_{\forall k,q}$, constraint (4.32) is convex regarding $\{\mathbf{u}_k\}_{\forall k}$ and $\{l_{kq}\}_{\forall k,q}$. Therefore, Problem (BO-E-Sur) is a strictly convex optimization problem with respect to $\{\mathbf{u}_k\}_{\forall k}$ and $\{l_{kq}\}_{\forall k,q}$. □

Based on Proposition 10, we can obtain the solution of Problem (MTCF-BO) by solving Problem (BO-E-Sur) with CVX [82] in an iterative manner. The details for solving Problem (MTCF-BO) are presented in Algorithm 7.

4.3.3 Algorithm for Solving Problem (MTCF-TA)

It can be verified that Problem (MTCF-TA) is a strictly convex optimization since the objective function of Problem (MTCF-TA) is concave and both constraints (4.14)

Algorithm 7 : To solve Problem (MTCF-BO) and obtain $\mathbf{u}_k^*$

1: **Initialization:** Initialize $\{\mathbf{u}_k[0]\}_{k\in\mathcal{K}}$. Calculate $\Upsilon[0] = \sum_{k\in\mathcal{K}} \ln\left(t_k \hat{R}_k[0]\right)$. Set $n = 0$. Set the convergence accuracy Δ as a very small positive number.
2: **repeat**
3: Update $n = n + 1$.
4: With the value of $\{\mathbf{u}_k[n-1]\}_{k\in\mathcal{K}}$, update $\{\gamma_{km}[n]\}_{\forall k,m}$ according to eq. (4.21) and update $\{\mathbf{f}_{km}[n]\}_{\forall k,m}$ according to eq. (4.22).
5: Solve Problem (BO-E-Sur) with $\{\mathbf{u}_k[n-1]\}_{k\in\mathcal{K}}$, $\{\gamma_{km}[n]\}_{\forall k,m}$ and $\{\mathbf{f}_{km}[n]\}_{\forall k,m}$ by using CVX and obtain $\{\mathbf{u}_k[n]\}_{k\in\mathcal{K}}$.
6: Calculate $\Upsilon[n] = \sum_{k\in\mathcal{K}} \ln\left(t_k \hat{R}_k[n]\right)$.
7: **until** $|\Upsilon[n] - \Upsilon[n-1]| < \Delta$
8: Set $\{\mathbf{u}_k^* = \mathbf{u}_k[n]\}_{k\in\mathcal{K}}$.
9: **Output:** $\{\mathbf{u}_k^*\}_{k\in\mathcal{K}}$.

and (4.15) are affine. Therefore, we can construct a Lagrange function as follows

$$\mathcal{L} = -\sum_{k\in\mathcal{K}} \ln(R_k t_k) + \lambda\left(\sum_{k\in\mathcal{K}} t_k - T\right) + \sum_{m\in\mathcal{M}} \rho_m \left(S_m^{\text{req}} - \sum_{k\in\mathcal{K}} S_{km} t_k\right) - \sum_{k\in\mathcal{K}} \pi_k t_k, \tag{4.47}$$

where λ, $\{\rho_m\}_{m\in\mathcal{M}}$ and $\{\pi_k\}_{k\in\mathcal{K}}$ denote the dual variables. According to Karush-Kuhn-Tucker (KKT) conditions, the optimal solution of Problem (MTCF-TA) should satisfy

$$\frac{\partial \mathcal{L}}{\partial t_k} = -\frac{1}{t_k} + \lambda - \sum_{m\in\mathcal{M}} \rho_m S_{km} - \pi_k = 0, \forall k \in \mathcal{K}, \tag{4.48}$$

$$\lambda\left(\sum_{k\in\mathcal{K}} t_k - T\right) = 0, \lambda \geq 0, \tag{4.49}$$

$$\rho_m \left(S_m^{\text{req}} - \sum_{k\in\mathcal{K}} S_{km} t_k\right) = 0, \rho_m \geq 0, \forall m \in \mathcal{M}, \tag{4.50}$$

$$\pi_k t_k = 0, \pi_k \geq 0, \forall k \in \mathcal{K}. \tag{4.51}$$

From eq. (4.51), we conclude that $\pi_k = 0, \forall k$ since $t_k \neq 0, \forall k$. Then, based on eq. (4.48), we can derive that

$$t_k^* = \frac{1}{\lambda - \sum_{m\in\mathcal{M}} \rho_m S_{km}}, \forall k \in \mathcal{K}. \tag{4.52}$$

Eq. (4.52) indicates that the optimal time allocation t_k is increasing with respect to S_{km} under the given $\{\rho_m\}_{m\in\mathcal{M}}$ and λ. Moreover, it can be shown by contradiction that the optimal time allocation always holds

$$\sum_{k\in\mathcal{K}} t_k = T. \tag{4.53}$$

Next we discuss the two possible cases regarding the optimal values of $\{\rho_m\}_{m\in\mathcal{M}}$ as follows.

Case I with $\{\rho_m\}_{\forall m} = 0$

In this case, there exists $t_k^* = \frac{1}{\lambda}$, and the optimal time allocation and the maximum value of the objective function can be expressed as

$$t_k^* = \frac{T}{K}, \forall k \in \mathcal{K}, \tag{4.54}$$

$$f^{\text{obj}} = \sum_{k\in\mathcal{K}} \ln(\frac{R_k T}{K}). \tag{4.55}$$

This case implies that the same time is allocated to the SCDs and the cooperative sensing constraint is always satisfied. Therefore, the value of eq. (4.55) denotes the maximum transmitted data volume when accounting for the fairness.

Case II with at least one $\rho_m > 0$

We introduce set $\mathcal{M}_\rho = \{m|\rho_m > 0, m \in \mathcal{M}\} \subseteq \mathcal{M}$, and thus $\{\rho_m\}_{m\in\mathcal{M}\setminus\mathcal{M}_\rho} = 0$. In this case, according to complementary slackness condition in eq. (4.50), we have

$$\sum_{k\in\mathcal{K}} S_{km} t_k = S_m^{\text{req}}, \forall m \in \mathcal{M}_\rho. \tag{4.56}$$

By substituting eq. (4.52) into eqs. (4.53) and (4.56), we derive that

$$\sum_{k\in\mathcal{K}} (\lambda - \sum_{m\in\mathcal{M}} \rho_m S_{km})^{-1} - T = 0, \tag{4.57}$$

$$\sum_{k\in\mathcal{K}} S_{km} (\lambda - \sum_{m\in\mathcal{M}} \rho_m S_{km})^{-1} - S_m^{\text{req}} = 0, \forall m \in \mathcal{M}_\rho, \tag{4.58}$$

$$\lambda - \sum_{m \in \mathcal{M}} \rho_m S_{km} > 0, \forall k \in \mathcal{K}. \tag{4.59}$$

We can obtain the optimal dual variables λ and $\{\rho_m\}_{m \in \mathcal{M}_\rho}$ by jointly solving eqs. (4.57)-(4.59). Since both eqs. (4.57) and (4.58) are nonlinear with respect to the dual variables, we use Newton's method to numerically obtain solutions for the dual variables.

Let $\boldsymbol{\omega} = [\lambda, \rho_1, ..., \rho_m]^T, m \in \mathcal{M}_\rho$ and $\boldsymbol{\Theta}(\boldsymbol{\omega}) = [\Theta_0(\boldsymbol{\omega}), \Theta_1(\boldsymbol{\omega}), ..., \Theta_m(\boldsymbol{\omega})]^T, m \in \mathcal{M}_\rho$, where $\Theta_0(\boldsymbol{\omega})$ is given by eq. (4.57) and $\{\Theta_m(\boldsymbol{\omega})\}_{m \in \mathcal{M}_\rho}$ is given by eq. (4.58). According to Newton's method, $\boldsymbol{\omega}_n$ at n-th iteration can be updated as

$$\boldsymbol{\omega}[n] = \boldsymbol{\omega}[n-1] - \kappa \boldsymbol{\Xi}^{-1}(\boldsymbol{\omega}[n-1]) \boldsymbol{\Theta}(\boldsymbol{\omega}[n-1]), \tag{4.60}$$

where κ denotes the step-size, and $\boldsymbol{\Xi}(\cdot)$ is given by

$$\boldsymbol{\Xi}(\boldsymbol{\omega}) = \begin{bmatrix} \frac{\partial \Theta_0}{\partial \lambda}, & \frac{\partial \Theta_0}{\partial \rho_1}, & ..., & \frac{\partial \Theta_0}{\partial \rho_m} \\ \frac{\partial \Theta_1}{\partial \lambda}, & \frac{\partial \Theta_1}{\partial \rho_1}, & ..., & \frac{\partial \Theta_1}{\partial \rho_m} \\ ..., & ..., & ..., & ... \\ \frac{\partial \Theta_m}{\partial \lambda}, & \frac{\partial \Theta_m}{\partial \rho_1}, & ..., & \frac{\partial \Theta_m}{\partial \rho_m} \end{bmatrix}, m \in \mathcal{M}_\rho. \tag{4.61}$$

The elements in eq. (4.61) are given by

$$\frac{\partial \Theta_0}{\partial \lambda} = -\sum_{k \in \mathcal{K}} (\lambda - \sum_{m \in \mathcal{M}} \rho_m S_{km})^{-2}, \tag{4.62}$$

$$\frac{\partial \Theta_0}{\partial \rho_m} = \sum_{k \in \mathcal{K}} S_{km} (\lambda - \sum_{m \in \mathcal{M}} \rho_m S_{km})^{-2}, \forall m \in \mathcal{M}_\rho, \tag{4.63}$$

$$\frac{\partial \Theta_m}{\partial \lambda} = -\sum_{k \in \mathcal{K}} S_{km} (\lambda - \sum_{m \in \mathcal{M}} \rho_m S_{km})^{-2}, \forall m \in \mathcal{M}_\rho, \tag{4.64}$$

$$\frac{\partial \Theta_m}{\partial \rho_m} = \sum_{k \in \mathcal{K}} S_{km}^2 (\lambda - \sum_{m \in \mathcal{M}} \rho_m S_{km})^{-2}, \forall m \in \mathcal{M}_\rho. \tag{4.65}$$

By iteratively updating λ and $\{\rho_m\}_{m \in \mathcal{M}_\rho}$ according to eq. (4.60), we can obtain the optimal value of the dual variables. Then, the optimal time allocation is calculated by eq. (4.52).

We define the maximum cooperative sensing requirement of target m as

$$S_m^{\max} = \max_k \{S_{km}\} T, \forall m \in \mathcal{M}, \tag{4.66}$$

which is obtained by allocating all the time to the SCD that achieves the maximum sensing estimation rate for target m. Therefore, for arbitrary value S_m^{cur}, it holds $0 \leq S_m^{\text{cur}} \leq S_m^{\max}, \forall m$ to guarantee the feasibility of cooperative sensing constraint for target m in Problem (MTCF-TA). Moreover, the optimal value of Problem (MTCF-TA) is non-increasing with respect to $\{S_m^{\text{cur}}\}_{m\in\mathcal{M}}$, since the feasible region constructed by constraints (4.14) and (4.15) becomes smaller when $\{S_m^{\text{cur}}\}_{m\in\mathcal{M}}$ increases.

Let $S_m^{\text{tem}} = \sum_{k\in\mathcal{K}} \frac{S_{km}T}{K}$. It also satisfies $0 \leq S_m^{\text{tem}} \leq S_m^{\max}, \forall m$. We introduce set $\mathcal{M}_a = \{m | S_m^{\text{tem}} < S_m^{\text{req}} \leq S_m^{\max}\}$ to denote the active cooperative sensing constraints. Then, the optimal solution of Problem (MTCF-TA) can be discussed in the following three cases.

Case II.A with $0 \leq S_m^{\text{req}} \leq S_m^{\text{tem}}, \forall m$

In this case, constraint (4.15) is inactive. Thus, it is evident that the optimal solution is achieved by allocating time in equal proportions and the optimal objective value is given by eq. (4.55).

Case II.B with $0 \leq S_m^{\text{req}} < S_m^{\max}, \forall m$ **and at least one** $S_m^{\text{req}} > S_m^{\text{tem}}$

In this case, there are $|\mathcal{M}_a|$ active cooperative sensing constraints. For revealing the feasibility of Problem (MTCF-TA), we consider Problem (MTCF-TA-Fea) as follows

$$\begin{aligned} \text{(MTCF-TA-Fea):}\ & \max \sum_{k\in\mathcal{K}} \ln(R_k t_k) \\ & \text{subject to: constraints } (4.14) \text{ and } (4.56), \\ & \text{variables: } \{t_k\}_{k\in\mathcal{K}}. \end{aligned}$$

Let $\mathbf{s}_m = [S_{1m}, ..., S_{Km}], \forall m \in \mathcal{M}_a$, $\mathbf{S} = [\mathbf{s}_1, ..., \mathbf{s}_m]^T$, $\forall m \in \mathcal{M}_a$ and $\mathbf{S}^{\text{req}} = [S_1^{\text{req}}, ..., S_m^{\text{req}}]^T, \forall m \in \mathcal{M}_a$. Problem (MTCF-TA-Fea) is feasible if constraint (4.56) yields a non-empty region, i.e., $\text{rank}(\mathbf{S}) = \text{rank}([\mathbf{S}, \mathbf{S}^{\text{req}}])$. Therefore, we can use

eq. (4.60) to obtain the optimal dual variables and calculate the optimal solution of Problem (MTCF-TA) according to eq. (4.52) in the feasible region.

Case II.C with $0 \leq S_m^{\text{req}} \leq S_m^{\max}, \forall m$ **and at least one** $S_m^{\text{req}} = S_m^{\max}$

In this case, there are $|\mathcal{M}_a|$ active cooperative sensing constraints. Based on the analysis in Case B, we conclude that problem is feasible if and only if $\text{rank}(\mathbf{S}) = \text{rank}([\mathbf{S}, \mathbf{S}^{\text{req}}])$ holds. Then, the optimal solution is achieved by allocating all time to the SCD with the maximum sensing estimation rate.

Based on the above analysis, we provide a detailed algorithm for solving Problem (MTCF-TA) in Algorithm 8.

Algorithm 8 : To solve Problem (MTCF-TA) and obtain t_k^*

if $0 \leq S_m^{\text{req}} \leq S_m^{\text{tem}}, \forall m$ **then**
  Case A: Calculate the optimal time allocation according to eq. (4.54).
else if $0 \leq S_m^{\text{req}} < S_m^{\max}, \forall m$, at least one $S_m^{\text{req}} > S_m^{\text{tem}}$, and $\text{rank}(\mathbf{S}) = \text{rank}([\mathbf{S}, \mathbf{S}^{\text{req}}])$ **then**
  Initialization: Initialize $\boldsymbol{\omega}[0] = [\lambda[0], \rho_1[0], ..., \rho_m[0]]^T = [\frac{K}{T}, 0, ..., 0]^T, \forall m \in \mathcal{M}_a$. Set $n = 0$. Set the updating step-size κ as a very small positive number. Set the convergence accuracy Δ as a very small positive number.
  repeat
    Update $n = n + 1$.
    Update $\boldsymbol{\omega}[n]$ according to eq. (4.60).
  until $||\boldsymbol{\omega}[n] - \boldsymbol{\omega}[n-1]|| < \Delta$
  Case B: Calculate the optimal time allocation according to eq. (4.52).
else if $0 \leq S_m^{\text{req}} \leq S_m^{\max}, \forall m$, at least one $S_m^{\text{req}} = S_m^{\max}$, and $\text{rank}(\mathbf{S}) = \text{rank}([\mathbf{S}, \mathbf{S}^{\text{req}}])$ **then**
  Case C: Allocate all the time to the SCD with the maximum sensing estimation rate for target m.
else
  Problem (MTCF-TA) is infeasible.
end if
Output: $\{t_k^*\}_{k \in \mathcal{K}}$.

4.3.4 Algorithm for Solving Problem (MTCF)

Finally, we iteratively execute Algorithm 7 and Algorithm 8 to reach the solution of Problem (MTCF). The overall algorithm is shown in Algorithm 9. It is worth to notice that the proposed Algorithm 9 is a centralized optimization algorithm for the implementation of the fairness-aware cooperative sensing. Therefore, we assume that the BS works as a controller to allocate the optimal resources for the SCDs by collect-

ing their information, and thus to maximize the system-wise utility. We will further investigate the implementation of multi-device multi-target cooperative sensing in a distributed manner in our future work.

Algorithm 9 : To solve Problem (MTCF) and obtain $\mathbf{u}_k^*$ and t_k^*.

1: **Initialization:** Set the initial feasible point. Set the convergence threshold ϵ.
2: **repeat**
3: Execute Algorithm 7 to obtain the beamforming solutions.
4: Execute Algorithm 8 to obtain the time allocation solutions.
5: **until** the increasement of the objective value is smaller than ϵ.

Complexity Analysis: The complexity of Algorithm 7 is dominated by Step 5 for solving Problem (BO-E-Sur) with CVX. We can express the complexity of Algorithm 7 which solves Problem (BO-E-Sur) by the path-following method [127] as $\mathcal{O}(KN_t + KM)$. The main complexity of Algorithm 8 lies in Steps 4 to 9 (i.e., Case B), which is given by $\mathcal{O}(M^3)$. Therefore, the overall complexity is expressed as $\mathcal{O}(KN_t + KM + M^3)$.

4.4 Numerical Results

4.4.1 Simulation Setup

We present simulation results to demonstrate the performance advantage of our fairness-aware design for ISAC-enabled multi-device cooperative sensing systems. We consider the scenario of $M = 4$ targets, $J = 3$ clutters and $K = 4$ SCDs which each SCD equipped with $N_t = 10$ transmit antennas and $N_r = 15$ receive antennas. The SCDs are uniformly distributed in the radius of $\{\varepsilon_k\}_{k\in\mathcal{K}} \in [50, 100]$m centered on the BS, and the targets and clutters are randomly located in the radius of $\{\varepsilon_m\}_{m\in\mathcal{M}\cup\mathcal{J}} \in [150, 200]$m. We consider the channels between the SCDs and the BS obey the Rayleigh fading with the path loss of $\{\nu_k\}_{k\in\mathcal{K}} = 40 + 30\log_{10}\varepsilon_k$ and the channel between the SCDs and targets are assumed to hold a line-of-sight link with the pass loss of $\{\nu_m\}_{k\in\mathcal{K}} = 40 + 25\log_{10}\varepsilon_m$. Moreover, we set channel bandwidth $B = 10$MHz, $\sigma_k^2 = \sigma_0^2 = -80$dBm, $\delta = 0.01$, and $\mu = 2\times10^{-5}$. We set the maximum time $T = 1$s and the average power capacity of the heterogeneous SCDs as 4W. The residual self-interference channel at the SCDs is set as $\{[\mathbf{H}_k^{\mathrm{SI}}]_{\tilde{r},\tilde{t}}\}_{k\in\mathcal{K}} = \sqrt{\eta_{\tilde{r},\tilde{t}}}e^{-j2\pi\frac{\overline{\phi}_{\tilde{r},\tilde{t}}}{\overline{\chi}}}$, where $\eta_{\tilde{r},\tilde{t}} = -110$ dB denotes the self-interference channel coefficient and $\overline{\phi}_{\tilde{r},\tilde{t}}$ rep-

resents the spatial separation between the $\tilde{r}$-th receive antenna and the $\tilde{t}$-th transmit antenna [128]. To ensure the reliability and statistical significance of the results, each set of results in this section is averaged over 50 independent simulation runs.

4.4.2 Evaluation of the Proposed Algorithm

The comparison benchmark algorithms are as follows.

- SDR-MMFA algorithm: In SDR-MMFA algorithm, the semidefinite relaxation (SDR) [129] is adopted to solve Problem (MTCF-BO) and the Gaussian randomization is used to recover the Rank-1 solution from the solution obtained by SDR. Then, we use the max-min fairness allocation (MMFA) [130] to solve Problem (MTCF-TA).

- DLP-WFA algorithm: In DLP-WFA algorithm, we use the double-layer penalty (DLP)-based method [131] to solve Problem (MTCF-BO), and use the water-filling-based allocation (WFA) [132] to allocate the time for different SCDs and thus solve Problem (MTCF-TA).

Figures 4.2 to 4.7 validate the performance advantages of the proposed algorithm for solving the joint optimization of beamforming and time allocation over the two benchmarks under different settings. Figure 4.2 and Figure 4.3 evaluate the total throughput with different numbers of SCDs and targets. Figure 4.4 shows the system performance with different values of the maximum time. Figure 4.5 shows the system performance with different values of the average power capacity. Figure 4.6 demonstrates the system utility under different cooperative sensing requirements. Figure 4.7 demonstrates the system utility under different maximum beampattern matching errors for multi-target sensing. It can be observed that the fair total throughput increases with the number of SCDs, the value of the maximum time, the value of the average power capacity, and the value of the maximum multi-target sensing beampattern matching error, and decreases with the number of targets and cooperative sensing requirement. In particular, the average gains obtained by our proposed algorithm over the benchmarks (i.e., SDR-MMFA and DLP-WFA) are marked at the top of six figures. The results in Figures 4.2 to 4.7 indicate that our proposed algorithm achieves a superior

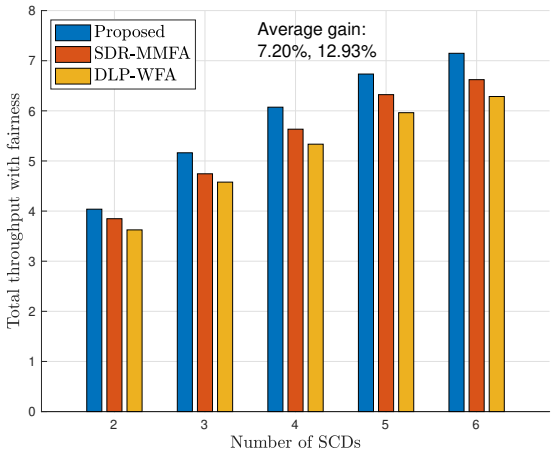

Fig. 4.2: Performance advantages under different numbers of SCDs

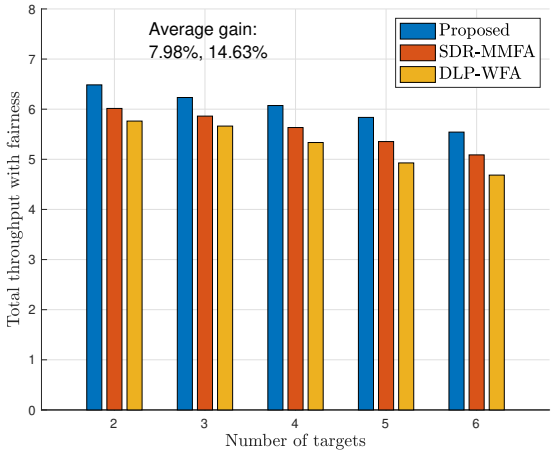

Fig. 4.3: Performance advantages under different numbers of targets

performance in comparison with the benchmarks.

4.4.3 Evaluation of the Fairness-aware Cooperative Sensing

The comparison benchmark schemes are as follows.

- FSSCS scheme: In full spectrum sharing cooperative sensing (FSSCS) scheme, the SCDs perform cooperative sensing towards multiple targets with full spectrum sharing and send data to the BS simultaneously, where each SCD suffers interference from other SCDs' signals.

- FDCCS scheme: In frequency division-based clustering cooperative sensing (FDCCS) scheme, the SCDs and targets are clustered into several clusters according to distance. Then, the SCDs perform cooperative sensing towards tar-

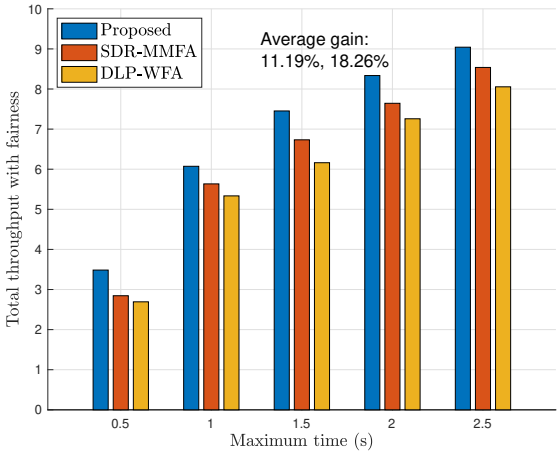

Fig. 4.4: Performance advantages under different values of the maximum time

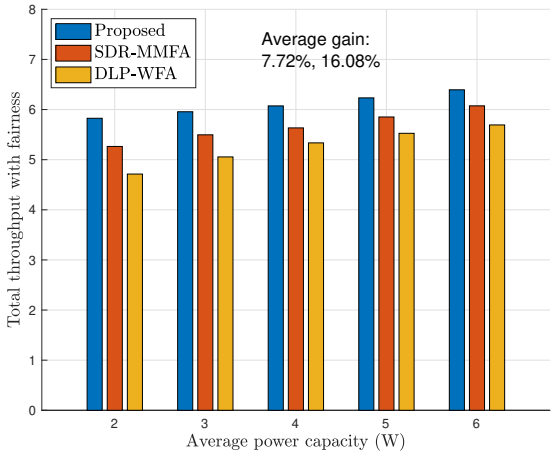

Fig. 4.5: Performance advantages under different values of the average power

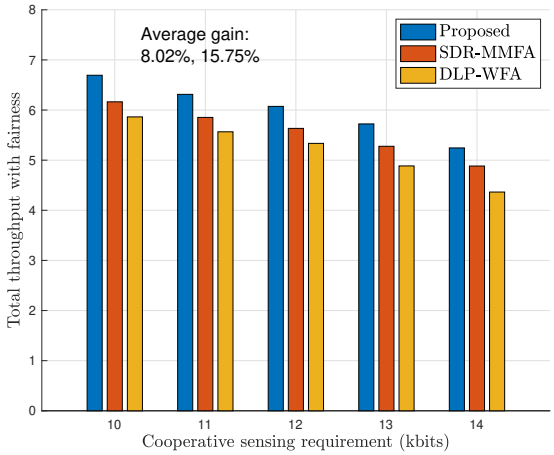

Fig. 4.6: Performance advantages under different cooperative sensing requirements

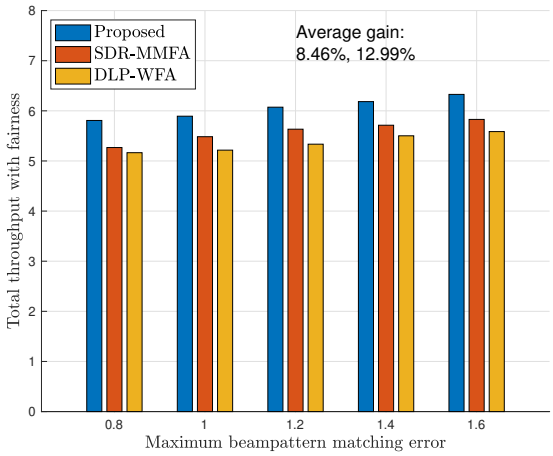

Fig. 4.7: Performance advantages under different values of the maximum multi-target sensing beampattern matching error

gets within the same cluster and send data to the BS simultaneously. Each cluster has a pre-assigned frequency band, and the frequency bands between different clusters are orthogonal to each other, and thus there is no co-channel interference between different clusters.

Figures 4.8 and 4.9 verify the performance advantages of the proposed fairness-aware cooperative sensing design. In Figure 4.8, we plot the total throughput achieved by the schemes with different cooperative sensing requirements. In Figure 4.9, we plot the total cooperative sensing quality achieved by the schemes with different maximum multi-target sensing beampattern matching errors. In particular, the average gains obtained by our proposed scheme over the benchmarks (i.e., FSSCS and FD-CCS) are marked at the top of two figures. Figures 4.8 and 4.9 demonstrate that our fairness-aware cooperative sensing scheme outperforms the benchmark schemes in both throughput and cooperative sensing accuracy.

Figure 4.10 verifies the fairness advantages of our proposed cooperative sensing scheme. To evaluate the fairness performance, we use the metric of Jain's fairness index, which can quantifies the fairness in throughput achieved among SCDs [133]. Jain's Fairness Index is defined as

$$JFI(x_1, x_2, ..., x_n) = \frac{(\sum_{i=1}^{n} x_i)^2}{n \sum_{i=1}^{n} x_i^2}. \tag{4.67}$$

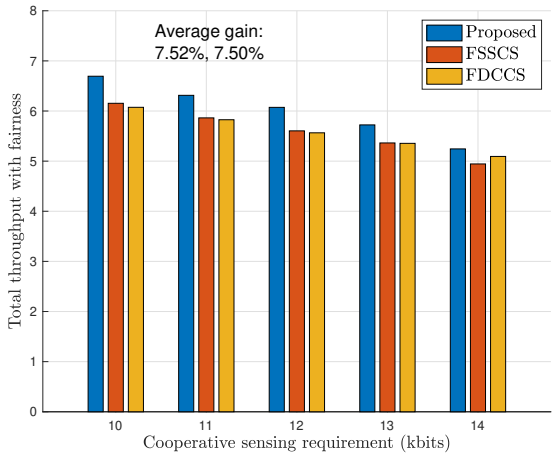

Fig. 4.8: Performance advantages of our fairness-aware cooperative sensing scheme in throughput

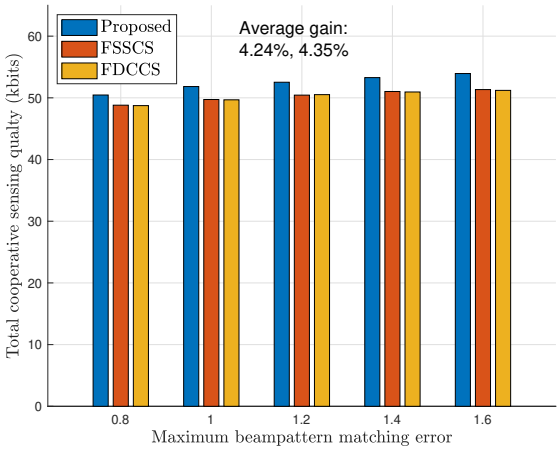

Fig. 4.9: Performance advantages of our fairness-aware cooperative sensing scheme in sensing accuracy

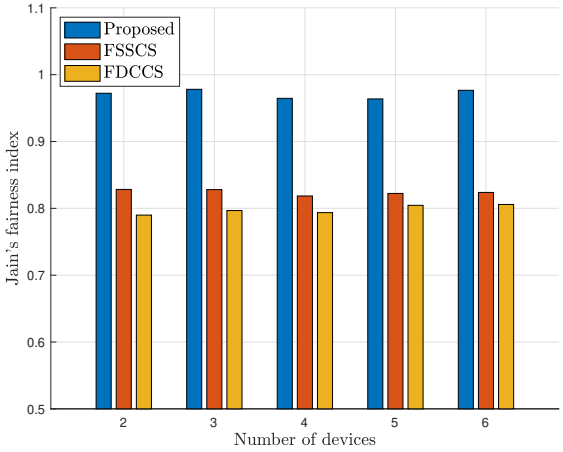

Fig. 4.10: Fairness advantages of our proposed cooperative sensing scheme

where x_i denotes the achieved performance of the i-th SCD, and n is the total number of SCDs. The index ranges from $\frac{1}{n}$ (the worst case) to 1 (the best case), with higher values indicating better fairness. It can be observed that our proposed cooperative sensing scheme outperforms the benchmark schemes in the data transmission fairness. The higher fairness index indicates that our approach allocates resources among devices in a more fairness manner and avoids significant differences in data transmission performance.

4.5 Conclusion

In this chapter, we have proposed a fairness-aware design for ISAC-enabled multi-device cooperative sensing system, in which the SCDs engage in cooperative sensing towards multiple targets in a time-division manner while simultaneously delivering data to the BS. We have formulated a joint beamforming optimization for both sensing and transmission and the time allocation for different SCDs, aiming at maximizing the fair total throughput. To address its non-convexity, we have adopted a decomposition-based framework and identified the solution features of the decomposed subproblems. We further proposed an efficient algorithm for solving it. The numerical results validate the effectiveness of our proposed approach and demonstrate the performance advantages of our fairness-aware ISAC-enabled multi-device cooperative sensing in improving both the throughput and cooperative sensing accuracy.

Chapter 5

Integrated Sensing and Two-Tier Task Offloading via NOMA: An Energy-Minimization Design

5.1 Introduction

The rapid developments of next-generation communication technologies have yielded tremendous revolutions in emerging immersive services such as Metaverse, smart healthcare, and autonomous driving, which necessitate diverse quality of services including high-precision sensing, ultra-reliable communications, and low-latency computing [134]. Mobile edge computing (MEC), which allows edge computing users with limited processing capabilities to offload tasks to nearby edge servers, has been considered as an effective solution for reducing computing latency [135–137]. Concurrently, integrated sensing and communication (ISAC) provides a key paradigm for achieving simultaneous high-throughput transmission and high-precision sensing within limited spectrum resources [138–141]. Consequently, the convergence of these technologies into integrated sensing, communication, and computing (ISCC) networks is expected to play a crucial role in future wireless networks, offering enhanced collaboration capabilities and efficient resource utilization. In particular, realizing the full potential of ISCC requires careful design of interference mitigation and resource allocation strategies.

Non-orthogonal multiple access (NOMA), which allows multiple users to be served simultaneously on the same resource block, has been considered as a spectrum-efficient approach to enable massive connectivity in next-generation wireless networks [142]. By using superposition coding (SC) at the transmitter side and further using successive interference cancellation (SIC) at the receiver side, NOMA can mitigate users' co-channel interference, which has attracted a lot of research interests in exploiting NOMA for various wireless services [143–147]. In particular, NOMA has been regarded as a promising solution for alleviating severe inter-functionalities interference in ISCC systems under massive connectivity.

With the exponential growth of network traffic and environmental sensing data, a single-tier edge computing framework relying solely on local edge servers cannot

meet the escalating demands of ISCC networks. Leveraging multi-tier cooperative edge computing, where edge servers and cloudlet servers are jointly utilized for task processing, enables an efficient and balanced utilization of computing resources across different tiers, thereby avoiding the severe processing delay due to the potential congestion caused by overloading. In this chapter, we investigate a NOMA-assisted integrated sensing and two-tier task offloading (ISTTO) framework, in which an ISCC access point (AP) provides task offloading services for a group of edge computing users via NOMA while performing the radar sensing towards a target in both tiers. The signals in the two tiers are illustrated as follows. In Tier-I, the AP transmits a sensing signal to sense the target. Meanwhile, the AP receives both the sensing echo and all edge computing users' offloading signals. In Tier-II, the AP transmits the ISAC signal (including the dedicated sensing signal and the offloading signals), which is used to offload the workloads to a group of cloudlet servers and perform the radar sensing simultaneously. Our framework poses two important challenges as follows. First, the sensing and offloading signals interfere with each other in Tier-I, while only the dedicated sensing signal interferes to the offloading signals in Tier-II. It is crucial to design different NOMA mechanisms for alleviating different inter-functionalities interferences and thus improve the performances of both sensing and offloading. Second, in the two-tier framework, there exists a tradeoff between the sensing accuracy and the computational offloading latency by properly tuning the durations of Tier-I and Tier-II. Specifically, the longer durations of Tier-I and Tier-II allow for a larger amount of sensing estimation information, and consequently yield an improved estimation of the target. However, blindly increasing the durations leads to the longer computational offloading latency. It is crucial to find the optimal durations in both tiers to achieve a balanced tradeoff between the sensing accuracy and computational offloading latency. Our detailed contributions are summarized as follows.

- We propose a NOMA-assisted ISTTO framework in which the ISCC AP provides task offloading services for a group of edge computing users via NOMA while performing sensing towards a target. Based on the proposed two-tier offloading procedures, we design different NOMA mechanisms in Tier-I and Tier-

II to alleviate different inter-functionalities interferences. We formulate a joint optimization of the AP's transmit beamforming, the two-tier dedicated sensing signals, the edge computing users' transmit powers, the two-tier durations, the offloading strategies and the edge server's processing-rate, with the objective of minimizing the total energy consumption of all edge computing users and the AP with the edge server, while guaranteeing the required sensing performance over the total duration.

- To address the non-convexity of the formulated optimization problem, we adopt a decomposition-based approach. Specifically, we identify the hidden monotonic feature of the problem with respect to the Tier-I duration and propose a polyblock approximation-based algorithm to obtain the optimal Tier-I duration. Meanwhile, we identify the Rank-1 feature of the dedicated sensing signal of Tier-I and propose an alternating optimization-based algorithm for obtaining its solution. We also propose a successive convex approximation-based algorithm for obtaining the solutions of the AP's transmit beamforming, the dedicated sensing signal of Tier-II, and the offloading strategies of Tier-II.

- We present the numerical results to verify the performances of our proposed algorithms. Compared with the benchmark algorithms, our algorithm yields a superior performance in energy minimization while reaching the close-to-optimal solution in an efficient manner. Moreover, numerical results verify the performance advantages of our NOMA-assisted ISTTO scheme. Compared with the benchmark schemes, our NOMA-assisted ISTTO scheme achieves better performances in both sensing performance and task offloading performance.

The remainder of this chapter is organized as follows. Section 5.2 depicts the system model and problem formulation. Section 5.3 illustrate the decomposition of the original problem and identify the features of the solutions. We propose the corresponding algorithms for solving the problem in Section 5.3. Numerical Results are presented in Section 5.4 and Section 5.5 concludes this chapter. Table 5.1 summarizes the key notations used in this chapter.

Table 5.1: Key notations

Notations	Definitions
D_k^{tot}	Total workloads of ECU k.
x_k^{I}	Transmit signal of ECU k in Tier-I.
$\mathbf{x}_0^{\text{I}}$	Transmit signal of the AP in Tier-I.
$\mathbf{y}_0^{\text{I}}$	Received signal at the AP in Tier-I.
$\mathbf{x}_0^{\text{II}}$	Transmit signal of the AP in Tier-II.
y_i^{II}	Received signal at CS i in Tier-II.
$\mathbf{y}_0^{\text{II}}$	Received signal at the AP in Tier-II.
$\mathbf{s}_0^{\text{I}}$	Dedicated sensing signal in Tier-I.
$\mathbf{s}_0^{\text{II}}$	Dedicated sensing signal in Tier-II.
p_k	Transmit power of ECU k in Tier-I.
$\mathbf{w}_i$	Transmit beamforming of the AP for CS i.
t^{I}	Duration of Tier-I.
t^{II}	Duration of Tier-II.
d_{ki}	ECU k's offloading decisions in Tier-II.
ϱ_k	The ES's processing-rate for ECU k's workloads.
R_k^{I}	Achievable rate from ECU k to the AP in Tier-I.
$\mathbf{\Gamma}_k$	Total interference for receiving ECU k's data in Tier-I.
R_i^{II}	Achievable rate from the AP to CS i in Tier-II.
Q^{I}	Sensing estimation rate for sensing in Tier-I.
Q^{II}	Sensing estimation rate for sensing in Tier-II.
$\mathbf{\Lambda}$	Total interference for sensing in Tier-I.
$\mathbf{\Psi}$	Total interference for sensing in Tier-II.
l_k	Total latency for completing ECU k's workloads.
E_k^{off}	Energy consumption of ECU k.
E^{AP}	Energy consumption of the AP.
E_k^{ES}	Energy consumption of the ES for ECU k's workloads.
$L_k^{\max}$	Latency requirement for ECU k's workloads.
$T^{\max}$	Maximum available radio interface time.
Q^{req}	Sensing requirement over the total duration.

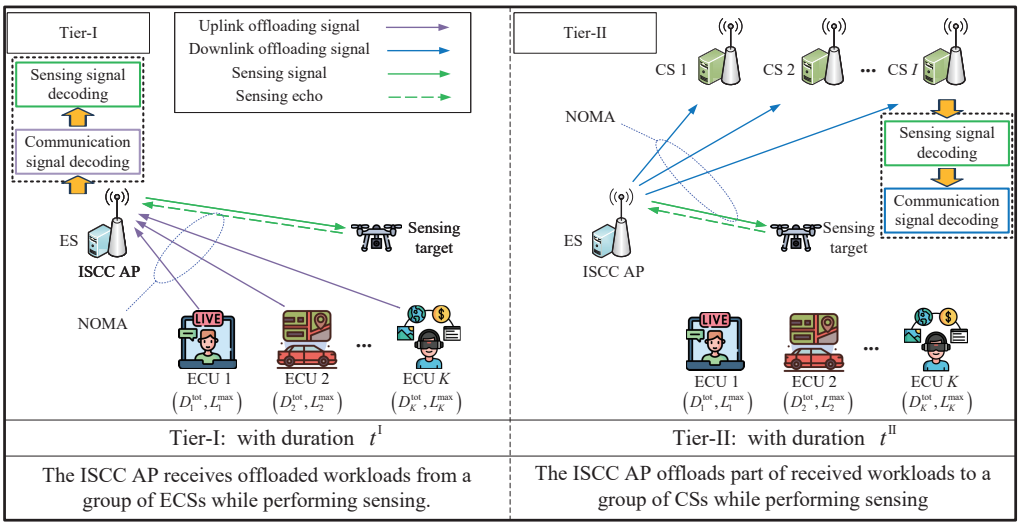

Fig. 5.1: NOMA-assisted integrated sensing and two-tier task offloading framework

5.2 System Model of Integrated Sensing and Two-Tier Task Offloading

5.2.1 System Model

As shown in Figure 5.1, we consider a NOMA-assisted ISTTO system including an ISCC AP with N_t transmit antennas and N_r receive antennas, a group of single-antenna edge computing users (ECUs) represented by $\mathcal{K} = \{1, 2, ..., K\}$, and a group of cloudlet servers (CSs) represented by $\mathcal{I} = \{1, 2, ..., I\}$. The ISCC AP performs radar sensing towards a specific target with an angle of θ_0 (e.g., estimating the UAV flight data for path planning) and guarantees a sensing estimation information denoted by Q^{req}. Each ECU $k \in \mathcal{K}$ has a task D_k^{tot} to be completed with the corresponding latency constraint $L_k^{\max}$. The ISCC AP is equipped with an edge server (ES) that can provide the task offloading services for the ECUs. Moreover, the ES can further offload part of its received workloads to the CSs. Figure 5.1 demonstrates the operations of ECUs and the ISCC AP in two tiers.

- In Tier-I with the duration of t^{I}, the ECUs offload their entire workloads to the ES. The ISCC AP transmits a sensing signal to sense the target. Meanwhile, the ISCC AP receives both the sensing echo and all ECUs' offloading signals via NOMA.

- In Tier-II with the duration of t^{II}, the ISCC AP transmits the ISAC signal via

NOMA. The ISAC signal serves for two purposes, i.e., offloading part of the received workloads to multiple CSs and performing the radar sensing towards the target.

5.2.2 Modeling of Tier-I

In Tier-I, all ECUs transmit the offloading signals for offloading their respective workloads $\{D_k^{\text{tot}}\}_{k\in\mathcal{K}}$ to the ISCC AP. Meanwhile, the ISCC AP transmits a sensing signal towards a sensing target at the angle of θ_0.

Signal Model

The transmitted signal of ECU k can be expressed as

$$x_k^{\text{I}} = \sqrt{p_k} s_k, \tag{5.1}$$

where p_k denotes the transmit power for delivering the information symbol s_k with $\mathbb{E}\{|s_k|^2\} = 1$. The transmitted sensing signal of the ISCC AP in Tier-I can be expressed as

$$\mathbf{x}_0^{\text{I}} = \mathbf{s}_0^{\text{I}}, \tag{5.2}$$

where $\mathbf{s}_0^{\text{I}} \in \mathbb{C}^{N_t\times 1}$ denotes the dedicated sensing signal with covariance $\mathbf{S}_0^{\text{I}} = \mathbb{E}\{\mathbf{s}_0^{\text{I}}(\mathbf{s}_0^{\text{I}})^H\}$. We next model the sensing channel for the ISCC AP regarding the sensing target. Assume that both the transmitting and receiving uniform linear arrays of the ISCC AP have half-wavelength antenna spacing. Then, the transmit steering vector and the receive steering vector on direction θ can be given by

$$\mathbf{a}_t(\theta) = \frac{1}{\sqrt{N_t}}\left[1, e^{j\pi\sin\theta}, ..., e^{j\pi(N_t-1)\sin\theta}\right]^T, \tag{5.3}$$

$$\mathbf{a}_r(\theta) = \frac{1}{\sqrt{N_r}}\left[1, e^{j\pi\sin\theta}, ..., e^{j\pi(N_r-1)\sin\theta}\right]^T. \tag{5.4}$$

We consider that there exists M clutters under the angles of $\{\theta_m\}_{m=1}^M$, and the AP has the prior knowledge of the target and clutters. Therefore, the received signal at the AP can be expressed as

$$\mathbf{y}_0^{\mathrm{I}} = \underbrace{\sum_{k\in\mathcal{K}} \mathbf{g}_k\sqrt{p_k}s_k}_{\text{signal from all ECUs}} + \underbrace{\beta_0\mathbf{a}_r(\theta_0)\mathbf{a}_t^H(\theta_0)\mathbf{x}_0^{\mathrm{I}}}_{\text{sensing echo from the desired target}} + \underbrace{\sum_{m=1}^{M}\beta_m\mathbf{a}_r(\theta_m)\mathbf{a}_t^H(\theta_m)\mathbf{x}_0^{\mathrm{I}}}_{\text{clutter interference}} + \underbrace{\mathbf{H}_{\mathrm{SI}}\mathbf{x}_0^{\mathrm{I}} + \mathbf{n}_0}_{\text{self-interference and noise}}, \tag{5.5}$$

where $\mathbf{g}_k \in \mathbb{C}^{N_r\times 1}$ denotes the channel from ECU k to the ISCC AP. The complex amplitudes $\{\beta_m\}_{m=0,1,\ldots,M}$ are primarily determined by the factors such as the path loss and radar cross-section. $\mathbf{H}_{\mathrm{SI}} \in \mathbb{C}^{N_r\times N_t}$ denotes the residual self-interference channel at the ISCC AP. $\mathbf{n}_0$ denotes the noise with variance σ_0^2. For the sake of clear notations, we further define $\mathbf{A}_s = \beta_0\mathbf{a}_r(\theta_0)\mathbf{a}_t^H(\theta_0)$ and $\mathbf{A}_c = \sum_{m=1}^{M}\beta_m\mathbf{a}_r(\theta_m)\mathbf{a}_t^H(\theta_m) + \mathbf{H}_{\mathrm{SI}}$.

Offloading Transmission Rate and Sensing Estimation Rate

In Tier-I, NOMA is exploited for decoding the offloading signals from the ECUs at the ISCC AP. The use of NOMA not only achieves the capacity for uplink transmission in multi-antenna systems, but also enables the ISCC AP to analyze the sensing echo in a communication-interference-free manner via the SIC, which thus reduces the inter-functionalities interference at the ISCC AP and enhances the accuracy of sensing. Without loss of any generality, we use the permutation Φ^{I} to map the decoding order of the workloads offloaded by ECU k to the ISCC AP in Tier-I. For instance, $\Phi^{\mathrm{I}}(j) < \Phi^{\mathrm{I}}(k)$ means that the data from ECU j is decoded and canceled from the received signal before decoding the data from ECU k. With this decoding order, based on eq. (5.5), the achievable offloading transmission rate R_k^{I} from ECU k to the ISCC AP is given by

$$R_k^{\mathrm{I}} = B^{\mathrm{I}}\log_2\left(1 + \frac{p_k\mathbf{c}_k^H\mathbf{g}_k\mathbf{g}_k^H\mathbf{c}_k}{\mathbf{c}_k^H\mathbf{\Gamma}_k\mathbf{c}_k}\right), \forall k \in \mathcal{K}, \tag{5.6}$$

where B^{I} denotes the transmission channel bandwidth in Tier-I, and $\mathbf{c}_k \in \mathbb{C}^{N_r\times 1}$ denotes the ISCC AP's communication receive beamforming. In eq. (5.6), $\mathbf{\Gamma}_k$ denotes the total interference for receiving ECU k's data, and it can be expressed as

$$\mathbf{\Gamma}_k = \sum_{\Phi^{\mathrm{I}}(j)>\Phi^{\mathrm{I}}(k)} p_j \mathbf{g}_j \mathbf{g}_j^H + \mathbf{A}_s \mathbf{S}_0^{\mathrm{I}} \mathbf{A}_s^H + \mathbf{A}_c \mathbf{S}_0^{\mathrm{I}} \mathbf{A}_c^H + \sigma_0^2 \mathbf{I}_N. \tag{5.7}$$

According to [81], the optimal receiver $\mathbf{c}_k^*$ is given by

$$\mathbf{c}_k^* = \arg\max \frac{p_k \mathbf{c}_k^H \mathbf{g}_k \mathbf{g}_k^H \mathbf{c}_k}{\mathbf{c}_k^H \mathbf{\Gamma}_k \mathbf{c}_k} = \mathbf{\Gamma}_k^{-1} \mathbf{g}_k, \forall k \in \mathcal{K}. \tag{5.8}$$

By substituting $\mathbf{c}_k^*$ into eq. (5.6), the achievable offloading transmission rate R_k^{I} can be rewritten as

$$R_k^{\mathrm{I}} = B^{\mathrm{I}} \log_2 \left(1 + p_k \mathbf{g}_k^H \mathbf{\Gamma}_k^{-1} \mathbf{g}_k\right), \forall k \in \mathcal{K}. \tag{5.9}$$

With the duration of t^{I} in Tier-I, the offloading transmission rate R_k^{I} should satisfy

$$t^{\mathrm{I}} R_k^{\mathrm{I}} = D_k^{\mathrm{tot}}, \forall k \in \mathcal{K}. \tag{5.10}$$

We utilize the sensing estimation rate to measure the radar sensing performance, which is defined as the cancellation of the uncertainty in the target parameters per second. Based on eq. (5.5), after decoding the transmission signal from all ECUs, the sensing estimation rate Q^{I} of the ISCC AP for sensing the target in Tier-I is

$$Q^{\mathrm{I}} = \frac{\delta}{2\mu} \log_2 \left(1 + \frac{2\mu B^{\mathrm{I}} \mathbf{u}^H \mathbf{A}_s \mathbf{S}_0^{\mathrm{I}} \mathbf{A}_s^H \mathbf{u}}{\mathbf{u}^H \mathbf{\Lambda} \mathbf{u}}\right), \tag{5.11}$$

where δ represents the duty factor, and μ represents the pulse duration. Vector $\mathbf{u}$ denotes the ISCC AP's sensing receive beamforming. In eq. (5.11), $\mathbf{\Lambda}$ denotes the total interference of the ISCC AP for sensing the target in Tier-I, and it can be expressed as

$$\mathbf{\Lambda} = \mathbf{A}_c \mathbf{S}_0^{\mathrm{I}} \mathbf{A}_c^H + \sigma_0^2 \mathbf{I}_N. \tag{5.12}$$

According to [81], the optimal receiver $\mathbf{u}^*$ is given by

$$\mathbf{u}^* = \arg\max \frac{\mathbf{u}^H \mathbf{A}_s \mathbf{S}_0^{\mathrm{I}} \mathbf{A}_s^H \mathbf{u}}{\mathbf{u}^H \mathbf{\Lambda} \mathbf{u}} = \mathbf{\Lambda}^{-1} \mathbf{a}_r(\theta_0). \tag{5.13}$$

By substituting $\mathbf{u}^*$ into eq. (5.11), we can rewrite Q^{I} as

$$Q^{\mathrm{I}} = \frac{\delta}{2\mu} \log_2(1 + 2\mu B^{\mathrm{I}} (\mathbf{s}_0^{\mathrm{I}})^H \mathbf{A}_s^H \mathbf{\Lambda}^{-1} \mathbf{A}_s \mathbf{s}_0^{\mathrm{I}}). \tag{5.14}$$

5.2.3 Modeling of Tier-II

After the ISCC AP receives the workloads from all ECUs, in Tier-II, the ISCC AP offloads part of its received workloads to multiple CSs and performs the radar sensing simultaneously.

Signal model

The transmitted ISAC signal of the ISCC AP in Tier-II can be expressed as

$$\mathbf{x}_0^{\mathrm{II}} = \sum_{i \in \mathcal{I}} \mathbf{w}_i z_i + \mathbf{s}_0^{\mathrm{II}}, \tag{5.15}$$

where $\mathbf{w}_i \in \mathbb{C}^{N_t \times 1}$ denotes the transmit beamforming for CS i and z_i with $\mathbb{E}\{|z_i|^2\} = 1$ denotes the symbol for CS i. Meanwhile, in eq. (5.15), $\mathbf{s}_0^{\mathrm{II}}$ denotes a dedicated sensing signal with covariance $\mathbf{S}_0^{\mathrm{II}} = \mathbb{E}\{\mathbf{s}_0^{\mathrm{II}}(\mathbf{s}_0^{\mathrm{II}})^H\}$ for achieving the enhanced sensing performance in the scenario of multiple downlink users. The received signal at CS i is given by

$$y_i^{\mathrm{II}} = \mathbf{h}_i^H \mathbf{w}_i z_i + \sum_{j \in \mathcal{I}, j \neq i} \mathbf{h}_i^H \mathbf{w}_j z_j + \mathbf{h}_i^H \mathbf{s}_0^{\mathrm{II}} + n_i, \tag{5.16}$$

where $\mathbf{h}_i \in \mathbb{C}^{N_t \times 1}$ denotes the channel gain between the ISCC AP and CS i, and n_i denotes the noise with variance σ_i^2. The received signal at the ISCC AP in Tier-II is given by

$$\mathbf{y}_0^{\mathrm{II}} = \mathbf{A}_s \mathbf{x}_0^{\mathrm{II}} + \mathbf{A}_c \mathbf{x}_0^{\mathrm{II}} + \mathbf{n}_0. \tag{5.17}$$

Offloading Transmission Rate and Sensing Estimation Rate

In Tier-II, the ISCC AP exploits the downlink NOMA ISAC signal for sensing the target and offloading part of its received workloads to different cloudlet servers simultaneously. However, the dedicated sensing signal impairs the communication performance from the ISCC AP to CSs. To address this issue, we design a NOMA decoding scheme which can remove the interference from the dedicated sensing signal to the downlink offloading signals. In particular, to guarantee that the dedicated sensing signal is decoded before decoding the communication signals, the following condition should be satisfied

$$|\mathbf{h}_i^H \mathbf{s}_0^{\mathrm{II}}|^2 \geq |\mathbf{h}_i^H \mathbf{w}_i|^2, \forall i \in \mathcal{I}. \tag{5.18}$$

We use the permutation Φ^{II} to map the decoding order of the workloads offloaded by the ISCC AP to the CSs. After removing the interference from the dedicated sensing signal, based on eq. (5.16), the offloading transmission rate R_i^{II} achieved by CS i can be expressed as

$$R_i^{\mathrm{II}} = B^{\mathrm{II}} \log_2 \left(1 + \frac{|\mathbf{h}_i^H \mathbf{w}_i|^2}{\sum_{\Phi^{\mathrm{II}}(j) > \Phi^{\mathrm{II}}(i)} |\mathbf{h}_i^H \mathbf{w}_j|^2 + \sigma_i^2} \right), \forall i \in \mathcal{I}, \tag{5.19}$$

where B^{II} denotes the transmission channel bandwidth in Tier-II. We use d_{ki} to denote the ECU k's workloads offloaded from the ISCC AP to CS i, with the duration of t^{II} in Tier-II, R_i^{II} should satisfy

$$t^{\mathrm{II}} R_i^{\mathrm{II}} \geq \sum_{k \in \mathcal{K}} d_{ki}, \forall i \in \mathcal{I}. \tag{5.20}$$

Similar to eq. (5.14), the sensing estimation rate Q^{II} of the ISCC AP for sensing the target in Tier-II can be expressed as

$$Q^{\mathrm{II}} = \frac{\delta}{2\mu} \log_2 \left(1 + 2\mu B^{\mathrm{II}} (\mathbf{x}_0^{\mathrm{II}})^H \mathbf{A}_s^H \mathbf{\Psi}^{-1} \mathbf{A}_s \mathbf{x}_0^{\mathrm{II}} \right), \tag{5.21}$$

where $\mathbf{\Psi}$ denotes the total interference of the ISCC AP for sensing the target in Tier-II, and it can be expressed as

$$\mathbf{\Psi} = \mathbf{A}_c \mathbf{x}_0^{\mathrm{II}} (\mathbf{x}_0^{\mathrm{II}})^H \mathbf{A}_c^H + \sigma_0^2 \mathbf{I}_N. \tag{5.22}$$

5.2.4 Modeling of Latency and Energy Consumption

The energy consumption of ECU k for its offloading transmission is given by

$$E_k^{\mathrm{off}} = p_k t^{\mathrm{I}}, \forall k \in \mathcal{K}. \tag{5.23}$$

For ECU k, the latency for completing its workloads is determined by two parts, including the latency l_k^{ES} for processing at the ES, and the latency l_k^{CS} for processing at the CSs. The latency for processing ECU k's workloads at the ES can be expressed as

$$l_k^{\text{ES}} = t^{\text{I}} + \frac{\upsilon_k (D_k^{\text{tot}} - \sum_{i \in \mathcal{I}} d_{ki})}{\varrho_k}, \forall k \in \mathcal{K}, \tag{5.24}$$

where υ_k denotes the number of CPU cycles for processing one bit of D_k^{tot} and ϱ_k denotes the ES's processing-rate allocated for processing ECU k's offloaded workloads. The ES's energy consumption for processing ECU k's workloads can be expressed as

$$E_k^{\text{ES}} = \epsilon \varrho_k^2 \upsilon_k (D_k^{\text{tot}} - \sum_{i \in \mathcal{I}} d_{ki}), \forall k \in \mathcal{K}, \tag{5.25}$$

where ϵ is the power consumption coefficient of the ES. The energy consumption of the ISCC AP for performing sensing in Tier-I and further offloading to the CSs while performing sensing in Tier-II is given by

$$E^{\text{AP}} = \mathbf{Tr}\left(\mathbf{S}_0^{\text{I}}\right) t^{\text{I}} + \mathbf{Tr}\left(\sum_{i \in \mathcal{I}} \mathbf{w}_i \mathbf{w}_i^H + \mathbf{S}_0^{\text{II}}\right) t^{\text{II}}. \tag{5.26}$$

The latency for processing ECU k's workloads at the CSs can be expressed as

$$l_k^{\text{CS}} = t^{\text{I}} + t^{\text{II}} + \max_i \{\frac{\upsilon_k d_{ki}}{\varsigma_{ki}}\}, \forall k \in \mathcal{K}, \tag{5.27}$$

where ς_{ki} denotes the CS i's processing-rate allocated for processing the offloaded workloads from ECU k.

Based on the above modelings, the total latency l_k for completing ECU k's workloads is given by

$$l_k = \max\{l_k^{\text{ES}}, l_k^{\text{CS}}\}, \forall k \in \mathcal{K}. \tag{5.28}$$

The total energy consumption of the ECUs and the ISCC AP with the ES is given by

$$E^{\text{tot}} = \underbrace{\sum_{k \in \mathcal{K}} E_k^{\text{off}}}_{\text{ECUs}} + \underbrace{E^{\text{AP}} + \sum_{k \in \mathcal{K}} E_k^{\text{ES}}}_{\text{ISCC AP and ES}}. \tag{5.29}$$

5.2.5 Problem Formulation

We focus on an energy-minimization design (EMD) for the ECUs and the ISCC AP with the ES, including all ECUs' offloading energy consumption in Tier-I, the ES's local processing energy consumption, and the energy consumption of the ISCC AP for performing the radar sensing in Tier-I and further offloading to the CSs while performing sensing in Tier-II. To accomplish this objective, we jointly optimize the transmit beamforming $\{\mathbf{w}_i\}_{i\in\mathcal{I}}$, the dedicated sensing signals $\mathbf{s}_0^{\mathrm{I}}$ and $\mathbf{s}_0^{\mathrm{II}}$, the ECUs' transmit powers $\{p_k\}_{k\in\mathcal{K}}$, the two-tier durations t^{I} and t^{II}, the Tier-II offloading data volume $\{d_{ki}\}_{k\in\mathcal{K},i\in\mathcal{I}}$, and the ES's processing-rate $\{\varrho_k\}_{k\in\mathcal{K}}$ as follows.

$$\text{(EMD):}\ \min E^{\mathrm{tot}}$$

$$\text{subject to: constraints } (5.10), (5.18), \text{ and } (5.20),$$

$$l_k \le L_k^{\max}, \forall k \in \mathcal{K}, \tag{5.30}$$

$$p_k \le P_k^{\max}, \forall k \in \mathcal{K}, \tag{5.31}$$

$$\mathbf{Tr}\left(\mathbf{S}_0^{\mathrm{I}}\right) \le P^{\mathrm{AP,max}}, \tag{5.32}$$

$$\mathbf{Tr}\left(\sum_{i\in\mathcal{I}} \mathbf{w}_i\mathbf{w}_i^H + \mathbf{S}_0^{\mathrm{II}}\right) \le P^{\mathrm{AP,max}}, \tag{5.33}$$

$$0 \le \sum_{i\in\mathcal{I}} d_{ki} \le D_k^{\max}, \forall k \in \mathcal{K}, \tag{5.34}$$

$$0 \le t^{\mathrm{I}} \le T^{\max}, \tag{5.35}$$

$$0 \le t^{\mathrm{II}} \le T^{\max}, \tag{5.36}$$

$$t^{\mathrm{I}}Q^{\mathrm{I}} + t^{\mathrm{II}}Q^{\mathrm{II}} \ge Q^{\mathrm{req}}, \tag{5.37}$$

$$0 \le \sum_{k\in\mathcal{K}} \varrho_k \le \varrho^{\max}, \tag{5.38}$$

$$\text{variables: } \{\mathbf{w}_i\}_{i\in\mathcal{I}}, \mathbf{s}_0^{\mathrm{I}}, \mathbf{s}_0^{\mathrm{II}}, \{p_k\}_{k\in\mathcal{K}}, t^{\mathrm{I}}, t^{\mathrm{II}}, \{d_{ki}\}_{k\in\mathcal{K},i\in\mathcal{I}}, \text{ and } \{\varrho_k\}_{k\in\mathcal{K}}.$$

Constraint (5.30) guarantees that the overall latency in completing ECU k's workloads cannot exceed the latency requirement $L_k^{\max}$. Constraint (5.31) provides an up-

per bound for ECU k's transmit power. Constraints (5.32) and (5.33) ensure that ISCC AP's transmit power cannot exceed its power capacity $P^{\text{AP,max}}$. Constraint (5.34) guarantees that the tasks of ECU k offloaded from the ES to the CSs cannot exceed those offloaded to the ES. Constraints (5.35) and (5.36) mean that both Tier-I duration and Tier-II duration cannot exceed a specified upper-bound $T^{\max}$ (i.e., the duration for occupying the radio interface). Constraint (5.37) guarantees the required sensing estimation information Q^{req} over the total duration $t^{\text{I}} + t^{\text{II}}$. Constraint (5.38) implies that the ES's total allocated processing-rate for all ECUs cannot exceed its computing capacity $\varrho^{\max}$.

5.3 Proposed Algorithms for Problem (EMD)

5.3.1 Problem Reformulation

It can be found that Problem (EMD) is a strictly non-convex optimization problem. Thus, it is very difficult to solve Problem (EMD) directly. To this end, we first reformulate Problem (EMD) to obtain its equivalent form.

By putting eq. (5.9) into constraint (5.10), we derive

$$p_k(t^{\text{I}}, \mathbf{S}_0^{\text{I}}) = \left(\mathbf{g}_k^H \mathbf{\Omega}^{-1} \mathbf{g}_k\right)^{-1} \left(2^{\frac{D_k^{\text{tot}}}{t^{\text{I}} B^{\text{I}}}} - 1\right) 2^{\frac{\sum_{\Phi^{\text{I}}(j) > \Phi^{\text{I}}(k)} D_j^{\text{tot}}}{t^{\text{I}} B^{\text{I}}}}, \tag{5.39}$$

where

$$\mathbf{\Omega} = \mathbf{A}_s \mathbf{S}_0^{\text{I}} \mathbf{A}_s^H + \mathbf{A}_c \mathbf{S}_0^{\text{I}} \mathbf{A}_c^H + \sigma_0^2 \mathbf{I}_N. \tag{5.40}$$

Proposition 11. *The optimal solution of* $\{\varrho_k\}_{k \in \mathcal{K}}$ *is given by*

$$\varrho_k^* = \frac{\upsilon_k (D_k^{\text{tot}} - \sum_{i \in \mathcal{I}} d_{ki})}{L_k^{\max} - t^{\text{I}}}, \forall k \in \mathcal{K}. \tag{5.41}$$

Proof. With eq. (5.28), constraint (5.30) can be transformed into

$$\frac{\upsilon_k (D_k^{\text{tot}} - \sum_{i \in \mathcal{I}} d_{ki})}{L_k^{\max} - t^{\text{I}}} \leq \varrho_k, \forall k \in \mathcal{K}, \tag{5.42}$$

$$\frac{\upsilon_k d_{ki}}{\varsigma_{ki}} \leq L_k^{\max} - t^{\text{I}} - t^{\text{II}}, \forall k \in \mathcal{K}, i \in \mathcal{I}. \tag{5.43}$$

It can be identified that the objective function of Problem (EMD) increases monotoni-

cally with respect to $\{\varrho_k\}_{k\in\mathcal{K}}$. Therefore, in the feasible solution interval, minimizing the total energy consumption is equivalent to finding the minimum value of $\{\varrho_k\}_{k\in\mathcal{K}}$. According to the lower-bounds given in eq. (5.42), the optimal values of $\{\varrho_k\}_{k\in\mathcal{K}}$ are given in eq. (5.41). □

With the optimal solution of $\{\varrho_k\}_{k\in\mathcal{K}}$, we can rewrite eq. (5.25) as

$$E_k^{\text{ES}} = \frac{\epsilon \upsilon_k^3 (D_k^{\text{tot}} - \sum_{i\in\mathcal{I}} d_{ki})^3}{(L_k^{\max} - t^{\text{I}})^2}, \forall k \in \mathcal{K}. \tag{5.44}$$

After the above operations, Problem (EMD) can be equivalently transformed into Problem (EMD-E) as follows.

(EMD-E): $\min E^{\text{tot}}$

subject to: constraints $(5.18), (5.20), (5.32), (5.33), (5.34), (5.35),$

$(5.36),$ and $(5.37),$

$$p_k(t^{\text{I}}, \mathbf{S}_0^{\text{I}}) \le P_k^{\max}, \forall k \in \mathcal{K}, \tag{5.45}$$

$$0 \le \sum_{k\in\mathcal{K}} \frac{\upsilon_k (D_k^{\text{tot}} - \sum_{i\in\mathcal{I}} d_{ki})}{L_k^{\max} - t^{\text{I}}} \le \varrho^{\max}, \tag{5.46}$$

$$\frac{\upsilon_k d_{ki}}{\varsigma_{ki}} \le L_k^{\max} - t^{\text{I}} - t^{\text{II}}, \forall k \in \mathcal{K}, i \in \mathcal{I}, \tag{5.47}$$

variables: $\{\mathbf{w}_i\}_{i\in\mathcal{I}}, \mathbf{s}_0^{\text{I}}, \mathbf{s}_0^{\text{II}}, t^{\text{I}}, t^{\text{II}},$ and $\{d_{ki}\}_{k\in\mathcal{K}, i\in\mathcal{I}}$.

5.3.2 Decomposition of Problem (EMD-E)

Problem (EMD-E) is still a strictly non-convex optimization problem. To address this difficulty, we propose the following decomposition approach.

1) Bottom-problem under the given t^{II}: Given the duration t^{II} of Tier-II, Problem (EMD-E) turns into Problem (EMD-BOT) as follows.

(EMD-BOT): $E^{\text{tot,min}} = \min E^{\text{tot}}$

subject to: constraints $(5.18), (5.20), (5.32), (5.33), (5.34), (5.35),$

$(5.37), (5.45), (5.46),$ and $(5.47),$

variables: $\{\mathbf{w}_i\}_{i\in\mathcal{I}}, \mathbf{s}_0^{\text{I}}, \mathbf{s}_0^{\text{II}}, t^{\text{I}},$ and $\{d_{ki}\}_{k\in\mathcal{K}, i\in\mathcal{I}}$.

2) Top-problem to optimize t^{II}: After solving Problem (EMD-BOT) and obtaining the value of $E^{\text{tot,min}}$ with the given t^{II}, we then continue to optimize t^{II}, which results in the following optimization problem.

$$\begin{aligned}\text{(EMD-TOP):}\ & \min E^{\text{tot,min}} \\ \text{subject to: constraint}\ & (5.36), \\ \text{variable:}\ & t^{\text{II}}.\end{aligned}$$

5.3.3 Decomposition of Problem (EMD-BOT)

In Problem (EMD-BOT), the duration t^{I} of Tier-I, the dedicated sensing signals $\mathbf{s}_0^{\text{I}}$ and $\mathbf{s}_0^{\text{II}}$, and the transmit beamforming $\{\mathbf{w}_i\}_{i\in\mathcal{I}}$ show a strong coupling effect in both the objective function and constraints. To solve Problem (EMD-BOT) efficiently, we propose the following decomposition of Problem (EMD-BOT) based on the block coordinated descent (BCD) method.

1) Sub-problem to optimize t^{I} under the given $\{\mathbf{w}_i\}_{i\in\mathcal{I}}$, $\mathbf{s}_0^{\text{I}}$, $\mathbf{s}_0^{\text{II}}$, and $\{d_{ki}\}_{k\in\mathcal{K},i\in\mathcal{I}}$.

$$\begin{aligned}\text{(Sub-t):}\ & \min E^{\text{tot}} \\ \text{subject to: constraints}\ & (5.35), (5.37), (5.45), (5.46),\ \text{and}\ (5.47), \\ \text{variable:}\ & t^{\text{I}}.\end{aligned}$$

2) Sub-problem to optimize $\{\mathbf{w}_i\}_{i\in\mathcal{I}}$, $\mathbf{s}_0^{\text{II}}$, and $\{d_{ki}\}_{k\in\mathcal{K},i\in\mathcal{I}}$ under the given t^{I} and $\mathbf{s}_0^{\text{I}}$.

$$\begin{aligned}\text{(Sub-w):}\ & \min E^{\text{tot}} \\ \text{subject to: constraints}\ & (5.18), (5.20), (5.33), (5.34), (5.37), (5.46),\ \text{and}\ (5.47), \\ \text{variables:}\ & \{\mathbf{w}_i\}_{i\in\mathcal{I}}, \mathbf{s}_0^{\text{II}},\ \text{and}\ \{d_{ki}\}_{k\in\mathcal{K},i\in\mathcal{I}}.\end{aligned}$$

3) Sub-problem to optimize $\mathbf{s}_0^{\text{I}}$ under the given t^{I}, $\{\mathbf{w}_i\}_{i\in\mathcal{I}}$, $\mathbf{s}_0^{\text{II}}$, and $\{d_{ki}\}_{k\in\mathcal{K},i\in\mathcal{I}}$.

$$\begin{aligned}\text{(Sub-s):}\ & \min E^{\text{tot}} \\ \text{subject to: constraints}\ & (5.32), (5.37),\ \text{and}\ (5.45),\end{aligned}$$

variable: $\mathbf{s}_0^{\mathrm{I}}$.

According to the criterion of the BCD method, the three sub-problems (i.e., Problem (Sub-t), Problem (Sub-w) and Problem (Sub-s)) are solved iteratively to obtain the solution of Problem (EMD-BOT). The key advantage of using the above decomposition lies in that we can solve the subproblem optimally in an individual manner.

5.3.4 Proposed Algorithm for Solving Problem (Sub-t)

Although Problem (Sub-t) is still non-convex, we have an observation regarding its objective function as follows.

Proposition 12. *The objective function of Problem (Sub-t) is the difference between two monotonic functions with respect to* t^{I}.

Proof. The objective function of Problem (Sub-t) consists of three parts, i.e., all ECUs' energy consumption $\sum_{k\in\mathcal{K}} E_k^{\mathrm{off}}$ for offloading, the ISCC AP's energy consumption E^{AP} within two tiers, and ES's energy consumption $\sum_{k\in\mathcal{K}} E_k^{\mathrm{ES}}$ for processing. According to eq. (5.26) and eq. (5.44), it can be observed that E^{AP} and $\sum_{k\in\mathcal{K}} E_k^{\mathrm{ES}}$ are increasing with respect to t^{I}. Next we show that $\sum_{k\in\mathcal{K}} E_k^{\mathrm{off}}$ is decreasing with respect to t^{I}.

The first derivative of E_k^{off} with respect to t^{I} can be expressed as

$$\begin{aligned}\frac{\mathrm{d}E_k^{\mathrm{off}}}{\mathrm{d}t^{\mathrm{I}}} = {} & 2^{\frac{\sum_{\Phi^{\mathrm{I}}(j)\geq\Phi^{\mathrm{I}}(k)} D_j^{\mathrm{tot}}}{t^{\mathrm{I}}B^{\mathrm{I}}}}\left(1-\frac{\sum_{\Phi^{\mathrm{I}}(j)\geq\Phi^{\mathrm{I}}(k)} D_j^{\mathrm{tot}}}{t^{\mathrm{I}}B^{\mathrm{I}}}\ln 2\right)\\ & -2^{\frac{\sum_{\Phi^{\mathrm{I}}(j)>\Phi^{\mathrm{I}}(k)} D_j^{\mathrm{tot}}}{t^{\mathrm{I}}B^{\mathrm{I}}}}\left(1-\frac{\sum_{\Phi^{\mathrm{I}}(j)>\Phi^{\mathrm{I}}(k)} D_j^{\mathrm{tot}}}{t^{\mathrm{I}}B^{\mathrm{I}}}\ln 2\right).\end{aligned} \tag{5.48}$$

Let $f^{'} = 2^q(1-q\ln 2)$. By the first derivative of $f^{'}$ with respect to q, we can discover that

$$\frac{\mathrm{d}f^{'}}{\mathrm{d}q} = -q2^q(\ln 2)^2 < 0, \tag{5.49}$$

which means $f^{'}$ is decreasing with respect to q. With eq. (5.49), we can derive that

$$\frac{\mathrm{d}E_k^{\mathrm{off}}}{\mathrm{d}t^{\mathrm{I}}} < 0, \tag{5.50}$$

which proves that $\sum_{k\in\mathcal{K}} E_k^{\text{off}}$ is decreasing with respect to t^{I}. Thus, we can rewrite the objective function of Problem (Sub-t) as

$$E^{\text{tot}} = E^{\text{AP}} + \sum_{k\in\mathcal{K}} E_k^{\text{ES}} - (-\sum_{k\in\mathcal{K}} E_k^{\text{off}}), \tag{5.51}$$

which is the difference between two monotonically increasing functions with respect to t^{I}. □

With the hidden monotonic feature of Problem (Sub-t) in Proposition 12, we can establish Problem (Sub-t) as a canonical monotonic optimization form by introducing an auxiliary variable α^{dif} and a new function $F(t^{\text{I}}, \alpha^{\text{dif}})$. For the sake of clear expression, we define

$$f(t^{\text{I}}) = E^{\text{AP}} + \sum_{k\in\mathcal{K}} E_k^{\text{ES}}. \tag{5.52}$$

According to Proposition 12 and constraint (5.35), we have

$$f(t^{\text{I}}) \leq E^{\max} = f(T^{\max}). \tag{5.53}$$

Then, α^{dif} and $F(t^{\text{I}}, \alpha^{\text{dif}})$ can be respectively defined as

$$\alpha^{\text{dif}} = E^{\max} - f(t^{\text{I}}), \tag{5.54}$$

$$F(t^{\text{I}}, \alpha^{\text{dif}}) = -\sum_{k\in\mathcal{K}} E_k^{\text{off}} + \alpha^{\text{dif}}. \tag{5.55}$$

After the above operations, we can derive the following equivalent form of Problem (Sub-t).

$$\begin{aligned} \text{(MO-t):}\ & \max F(t^{\text{I}}, \alpha^{\text{dif}}) \\ \text{subject to:}\ & \text{constraints } (5.35), (5.37), (5.45), (5.46), \text{and } (5.47), \\ & 0 \leq \alpha^{\text{dif}} \leq E^{\max} - f(t^{\text{I}}), \\ \text{variables:}\ & t^{\text{I}} \text{ and } \alpha^{\text{dif}}. \end{aligned} \tag{5.56}$$

In Problem (MO-t), we transform eq. (5.54) of α^{dif} into constraint (5.56) to estab-

lish a canonical monotonic optimization problem. Nevertheless, in our Algorithm-PA below, the intersection can be obtained on the upper boundary with bisection search in Step 5, which means that α^{dif} always achieves its maximum value, i.e., $\alpha^{\text{dif}} = E^{\max} - f(t^{\text{I}})$. Therefore, the transformation from eq. (5.54) to constraint (5.56) does not change the optimality of the problem.

Proposition 13. *Problem (MO-t) is a canonical form of monotonic optimization problem with respect to t^{I} and α^{dif}.*

Proof. The proof is based on the monotonic optimization theory. Specifically, the objective function is increasing in $(t^{\text{I}}, \alpha^{\text{dif}})$. Moreover, the feasible region is the intersection of a normal set (defined in eq. (5.57)) and a conormal set (defined in eq. (5.58)). Therefore, Problem (MO-t) is a canonical monotonic optimization form [148, 149]. □

Algorithm 10 : To solve Problem (Sub-t) and obtain optimal $t^{\text{I},*}$.

1: **Initialization:** Initialize the vertex set $\mathcal{V}^0 = \{(T^{\max}, E^{\max})\}$. Set the current best value $\text{CBV}^0 = -\infty$ and the current best solution $\mathbf{CBS}^0$ as an empty set. Set the iteration number $\tau = 0$. Set ξ_1 as a very small positive number.
2: **repeat**
3: Update $\tau = \tau + 1$.
4: Find the vertex $\mathbf{z}^\tau = \arg\max\{F(t^{\text{I}}, \alpha^{\text{dif}}) | (t^{\text{I}}, \alpha^{\text{dif}}) \in \mathcal{V}^{\tau-1}\}$ from $\mathcal{V}^{\tau-1}$.
5: Use bisection search to find the projection of $\mathbf{z}^\tau$ on the boundary of $\mathcal{M}$, which is denoted as $\pi_{\mathcal{M}}(\mathbf{z}^\tau)$.
6: **if** $|\pi_{\mathcal{M}}(\mathbf{z}^\tau) - \mathbf{z}^\tau| \leq \xi_1$ **then**
7: Update $\mathbf{CBS}^\tau = \mathbf{z}^\tau$ and $\text{CBV}^\tau = F(\mathbf{z}^\tau)$.
8: **else**
9: **if** $\pi_{\mathcal{M}}(\mathbf{z}^\tau) \in \mathcal{M} \cap \mathcal{N}$ and $F(\pi_{\mathcal{M}}(\mathbf{z}^\tau)) \geq \text{CBV}^{\tau-1}$ **then**
10: Update $\mathbf{CBS}^\tau = \pi_{\mathcal{M}}(\mathbf{z}^\tau)$ and $\text{CBV}^\tau = F(\pi_{\mathcal{M}}(\mathbf{z}^\tau))$.
11: **else**
12: Update $\mathbf{CBS}^\tau = \mathbf{CBS}^{\tau-1}$ and $\text{CBV}^\tau = \text{CBV}^{\tau-1}$.
13: **end if**
14: Set $\mathbf{z}^{\text{temp}} = \pi_{\mathcal{M}}(\mathbf{z}^\tau)$ and update $\mathcal{V}^\tau = \{\mathcal{V}^{\tau-1} \backslash \mathbf{z}^\tau\} \cup \{(\mathbf{z}^\tau(1), \mathbf{z}^{\text{temp}}(2)), (\mathbf{z}^{\text{temp}}(1), \mathbf{z}^\tau(2))\}$.
15: Remove from $\mathcal{V}^\tau$ the improper vertices and the vertices $\{\mathbf{v} \in \mathcal{V}^\tau | \mathbf{v} \notin \mathcal{N}\}$.
16: **end if**
17: **until** $|F(\mathbf{z}^\tau) - \mathbf{CBV}^\tau| \leq \xi_1$.
18: **Output:** Output the optimal solution $(t^{\text{I},*}, \alpha^{\text{dif},*}) = \mathbf{CBS}_j$ for Problem (MO-t). Notice that $t^{\text{I},*}$ is also the solution for Problem (Sub-t).

Based on the monotonicity in constraints (5.35), (5.37), (5.45), (5.46), (5.47) and

(5.56), we can establish the following normal set $\mathcal{M}$ and conormal set $\mathcal{N}$.

$$\mathcal{M} = \{(t^{\mathrm{I}}, \alpha^{\mathrm{dif}}) | \text{Constraints } (5.35), (5.46), (5.47), (5.56)\}, \tag{5.57}$$

$$\mathcal{N} = \{(t^{\mathrm{I}}, \alpha^{\mathrm{dif}}) | \text{Constraints } (5.37), (5.45)\}. \tag{5.58}$$

Exploiting the feature of Problem (MO-t) in Proposition 13, we propose Algorithm 10, which is based on the idea of polyblock approximation [148, 149], for finding the optimal solution $(t^{\mathrm{I},*}, \alpha^{\mathrm{dif},*})$ that can minimize $F(t^{\mathrm{I}}, \alpha^{\mathrm{dif}})$. The obtained $t^{\mathrm{I},*}$ is sufficient to be the optimal Tier-I duration for Problem (Sub-t). The details for solving Problem (Sub-t) are presented in Algorithm 10.

5.3.5 Proposed Algorithm for Solving Problem (Sub-w)

To solve Problem (Sub-w), we first define $\mathbf{W}_i \triangleq \mathbf{w}_i \mathbf{w}_i^H, \forall i$ with $\text{Rank}(\mathbf{W}_i) = 1, \forall i$ and $\mathbf{H}_i \triangleq \mathbf{h}_i \mathbf{h}_i^H, \forall i$. With this definition, constraint (5.20) can be rewritten as

$$\log_2 \left(1 + \frac{\mathbf{Tr}(\mathbf{H}_i \mathbf{W}_i)}{\sum_{\Phi^{\mathrm{II}}(j) > \Phi^{\mathrm{II}}(i)} \mathbf{Tr}(\mathbf{H}_i \mathbf{W}_j) + \sigma_i^2} \right) \geq \frac{\sum_{k \in \mathcal{K}} d_{ki}}{t^{\mathrm{II}} B^{\mathrm{II}}}. \tag{5.59}$$

After some mathematical operations, constraint (5.37) can be expressed as

$$\mathbf{a}_t^H(\theta_0) \left(\sum_{i \in \mathcal{I}} \mathbf{W}_i + \mathbf{S}_0^{\mathrm{II}} \right) \mathbf{a}_t(\theta_0) \mathbf{a}_r^H(\theta_0) \mathbf{\Psi}^{-1} \mathbf{a}_r(\theta_0) \geq \kappa^{\mathrm{req}}, \tag{5.60}$$

where

$$\kappa^{\mathrm{req}} = \frac{1}{2\mu B^{\mathrm{II}}} \left(2^{\frac{2\mu(Q^{\mathrm{req}} - t^{\mathrm{I}} Q^{\mathrm{I}})}{\delta t^{\mathrm{II}}}} - 1 \right). \tag{5.61}$$

Then, Problem (Sub-w) can be equivalently reformulated as follows.

(Sub-w'): $\min E^{\mathrm{tot}}$

subject to: constraints $(5.34), (5.46), (5.47), (5.59),$ and (5.60),

$$\mathbf{Tr}(\mathbf{H}_i \mathbf{S}_0^{\mathrm{II}}) \geq \mathbf{Tr}(\mathbf{H}_i \mathbf{W}_i), \forall i \in \mathcal{I}, \tag{5.62}$$

$$\mathbf{Tr} \left(\sum_{i \in \mathcal{I}} \mathbf{W}_i + \mathbf{S}_0^{\mathrm{II}} \right) \leq P^{\mathrm{AP,max}}, \tag{5.63}$$

$$\text{Rank}(\mathbf{W}_i) = 1, \forall i \in \mathcal{I}, \text{Rank}(\mathbf{S}_0^{\mathrm{II}}) = 1, \tag{5.64}$$

variables: $\{\mathbf{W}_i \succeq 0\}_{i\in\mathcal{I}}, \mathbf{S}_0^{\text{II}} \succeq 0$, and $\{d_{ki}\}_{k\in\mathcal{K},i\in\mathcal{I}}$.

The difficulty of solving Problem (Sub-w') lies in the non-convexity of constraints (5.59), (5.60) and (5.64). To this end, we perform the operations of SCA to handle constraints (5.59) and (5.60) to obtain a more tractable form. Focusing on constraint (5.59), we rewrite its left-hand side as

$$\chi_i = \log_2\left(\sum_{\Phi^{\text{II}}(j)\geq\Phi^{\text{II}}(i)} \mathbf{Tr}(\mathbf{H}_i\mathbf{W}_j) + \sigma_i^2\right) - \log_2\left(\sum_{\Phi^{\text{II}}(j)>\Phi^{\text{II}}(i)} \mathbf{Tr}(\mathbf{H}_i\mathbf{W}_j) + \sigma_i^2\right). \tag{5.65}$$

By performing the first-order Taylor expansion of $\{\mathbf{W}_i\}_{i\in\mathcal{I}}$ in the second term of eq. (5.65), for the τ-th iteration of the SCA, we obtain the lower bound as

$$\begin{aligned}\chi_i \geq \chi_i^{\text{lb}} \triangleq\ & \log_2\left(\sum_{\Phi^{\text{II}}(j)\geq\Phi^{\text{II}}(i)} \mathbf{Tr}(\mathbf{H}_i\mathbf{W}_j) + \sigma_i^2\right) \\ & - \log_2\left(\sum_{\Phi^{\text{II}}(j)>\Phi^{\text{II}}(i)} \mathbf{Tr}(\mathbf{H}_i\mathbf{W}_j^{\tau-1}) + \sigma_i^2\right) \\ & - \frac{\sum_{\Phi^{\text{II}}(j)>\Phi^{\text{II}}(i)} \mathbf{Tr}(\mathbf{H}_i(\mathbf{W}_j - \mathbf{W}_j^{\tau-1}))}{(\sum_{\Phi^{\text{II}}(j)>\Phi^{\text{II}}(i)} \mathbf{Tr}(\mathbf{H}_i\mathbf{W}_j^{\tau-1}) + \sigma_i^2)\ln 2},\end{aligned} \tag{5.66}$$

where $\{\mathbf{W}_i^{\tau-1}\}_{i\in\mathcal{I}}$ denotes the solutions attained in the $(\tau-1)$-th iteration. With eq. (5.66), constraint (5.59) can be replaced by a convex constraint as

$$\chi_i^{\text{lb}} \geq \frac{\sum_{k\in\mathcal{K}} d_{ki}}{t^{\text{II}}B^{\text{II}}}. \tag{5.67}$$

Next, we focus on constraint (5.60). Due to $\sum_{i\in\mathcal{I}}\mathbf{W}_i + \mathbf{S}_0^{\text{II}} \succeq 0$ and $\kappa^{\text{req}} > 0$, we derive $\mathbf{a}_t^H(\theta_0)\left(\sum_{i\in\mathcal{I}}\mathbf{W}_i + \mathbf{S}_0^{\text{II}}\right)\mathbf{a}_t(\theta_0) > 0$. Therefore, we can transform constraint (5.60) into a difference of convex form as

$$\mathbf{a}_r^H(\theta_0)\mathbf{\Psi}^{-1}\mathbf{a}_r(\theta_0) \geq \kappa^{\text{req}}\left(\mathbf{a}_t^H(\theta_0)\left(\sum_{i\in\mathcal{I}}\mathbf{W}_i + \mathbf{S}_0^{\text{II}}\right)\mathbf{a}_t(\theta_0)\right)^{-1}. \tag{5.68}$$

By performing the first-order Taylor expansion of the left-hand side in eq. (5.68), for

the τ-th iteration of the SCA, we obtain the lower bound as

$$\begin{aligned}&\mathbf{a}_r^H(\theta_0)\boldsymbol{\Psi}^{-1}\mathbf{a}_r(\theta_0) \geq J^{\text{lb}} \triangleq \mathbf{a}_r^H(\theta_0)(\boldsymbol{\Psi}^{\tau-1})^{-1}\mathbf{a}_r(\theta_0)\\&- \mathbf{a}_r^H(\theta_0)(\boldsymbol{\Psi}^{\tau-1})^{-1}\left(\boldsymbol{\Psi} - (\boldsymbol{\Psi}^{\tau-1})\right)(\boldsymbol{\Psi}^{\tau-1})^{-1}\mathbf{a}_r(\theta_0),\end{aligned} \tag{5.69}$$

where

$$\boldsymbol{\Psi}^{\tau-1} = \mathbf{A}_c\left(\sum_{i\in\mathcal{I}}\mathbf{W}_i^{\tau-1} + (\mathbf{S}_0^{\text{II}})^{\tau-1}\right)\mathbf{A}_c^H + \sigma_0^2\mathbf{I}_N \tag{5.70}$$

denotes the solution obtained in the $(\tau-1)$-th iteration. With eq. (5.69), constraint (5.60) can be replaced by a convex constraint as

$$J^{\text{lb}} \geq \kappa^{\text{req}}\left(\mathbf{a}_t^H(\theta_0)\left(\sum_{i\in\mathcal{I}}\mathbf{W}_i + \mathbf{S}_0^{\text{II}}\right)\mathbf{a}_t(\theta_0)\right)^{-1}. \tag{5.71}$$

Then, we employ the technique of semidefinite relaxation (SDR) and temporarily do not consider the Rank-1 constraint (5.64). As a result, Problem (Sub-w') can be solved by iteratively solving the following surrogate problem.

$$\begin{aligned}&\text{(Surrogate-w):}\ \min E^{\text{tot}}\\&\quad\text{subject to: constraints } (5.34), (5.46), (5.47), (5.62), (5.63),\\&\qquad\qquad (5.67),\ \text{and } (5.71),\\&\quad\text{variables: } \{\mathbf{W}_i \succeq 0\}_{i\in\mathcal{I}}, \mathbf{S}_0^{\text{II}} \succeq 0, \text{and } \{d_{ki}\}_{k\in\mathcal{K},i\in\mathcal{I}}.\end{aligned}$$

Proposition 14. *Problem (Surrogate-w) is a strictly convex optimization problem with respect to* $\{\mathbf{W}_i\}_{i\in\mathcal{I}}$, $\mathbf{S}_0^{\text{II}}$ *and* $\{d_{ki}\}_{k\in\mathcal{K},i\in\mathcal{I}}$.

Proof. It can be identified that the objective function in Problem (Surrogate-w) is strictly convex with respect to $\{\mathbf{W}_i\}_{i\in\mathcal{I}}$, $\mathbf{S}_0^{\text{II}}$ and $\{d_{ki}\}_{k\in\mathcal{K},i\in\mathcal{I}}$. It can also be identified that constraint (5.71) is convex with respect to $\{\mathbf{W}_i\}_{i\in\mathcal{I}}$ and $\mathbf{S}_0^{\text{II}}$ due to the function $\mathbf{a}^H\mathbf{X}^{-1}\mathbf{a}$ is convex with respect to $\mathbf{X}$ for $\mathbf{X}\succ 0$. Constraints (5.62), (5.63), (5.67) and (5.71) result in a convex feasible set for $\{\mathbf{W}_i\}_{i\in\mathcal{I}}$, $\mathbf{S}_0^{\text{II}}$ and $\{d_{ki}\}_{k\in\mathcal{K},i\in\mathcal{I}}$. Constraints (5.34), (5.46) and (5.47) are all affine. Therefore, it can be concluded that Problem (Surrogate-w) is a strictly convex optimization problem with respect to $\{\mathbf{W}_i\}_{i\in\mathcal{I}}$, $\mathbf{S}_0^{\text{II}}$

and $\{d_{ki}\}_{k\in\mathcal{K},i\in\mathcal{I}}$. $\square$

Based on Proposition 14, Problem (Surrogate-w) can be solved efficiently with some existing solvers for convex optimizations, e.g., CVX. We solve Problem (Surrogate-w) in an iterative manner and denote the obtained solution after convergence as $\{\{\widehat{\mathbf{W}}_i\}_{i\in\mathcal{I}}, \widehat{\mathbf{S}}_0^{\mathrm{II}}, \{\widehat{d}_{ki}\}_{k\in\mathcal{K},i\in}$ Then, we can construct the Rank-1 solution from the solution set $\{\{\widehat{\mathbf{W}}_i\}_{i\in\mathcal{I}}, \widehat{\mathbf{S}}_0^{\mathrm{II}}, \{\widehat{d}_{ki}\}_{k\in\mathcal{K},i\in\mathcal{I}}\}$ and obtain the solution of Problem (Sub-w) as follows.

Proposition 15. *Based on the solution* $\{\{\widehat{\mathbf{W}}_i\}_{i\in\mathcal{I}}, \widehat{\mathbf{S}}_0^{\mathrm{II}}, \{\widehat{d}_{ki}\}_{k\in\mathcal{K},i\in\mathcal{I}}\}$*, the* Rank-1 *solution, i.e., the solution of Problem (Sub-w), can be constructed as*

$$\mathbf{w}_i^* = \left(\mathbf{h}_i^H \widehat{\mathbf{W}}_i \mathbf{h}_i\right)^{-\frac{1}{2}} \widehat{\mathbf{W}}_i \mathbf{h}_i, \forall i \in \mathcal{I}, \tag{5.72}$$

$$\mathbf{S}_0^{\mathrm{II},*} = \sum_{i\in\mathcal{I}} \widehat{\mathbf{W}}_i + \widehat{\mathbf{S}}_0^{\mathrm{II}} - \sum_{i\in\mathcal{I}} \mathbf{w}_i^* (\mathbf{w}_i^*)^H, \tag{5.73}$$

$$d_{ki}^* = \widehat{d}_{ki}, \forall k \in \mathcal{K}, i \in \mathcal{I}. \tag{5.74}$$

Proof. To prove Proposition 15, we first show that $\{\{\mathbf{w}_i^*\}_{i\in\mathcal{I}}, \mathbf{S}_0^{\mathrm{II},*}, \{d_{ki}^*\}_{k\in\mathcal{K},i\in\mathcal{I}}\}$ is a feasible solution to Problem (Sub-w). Given an arbitrary vector $\mathbf{c} \in \mathbb{C}^{N_t\times 1}$, the following equation holds

$$\begin{aligned}
&\mathbf{c}^H \left(\widehat{\mathbf{W}}_i - \mathbf{w}_i^* (\mathbf{w}_i^*)^H\right) \mathbf{c} \\
&= \mathbf{c}^H \left(\widehat{\mathbf{W}}_i - (\mathbf{h}_i^H \widehat{\mathbf{W}}_i \mathbf{h}_i)^{-1} \widehat{\mathbf{W}}_i \mathbf{h}_i \mathbf{h}_i^H \widehat{\mathbf{W}}_i^H\right) \mathbf{c} \\
&= \mathbf{c}^H \widehat{\mathbf{W}}_i \mathbf{c} - (\mathbf{h}_i^H \widehat{\mathbf{W}}_i \mathbf{h}_i)^{-1} |\mathbf{c}^H \widehat{\mathbf{W}}_i \mathbf{h}_i|^2 \\
&\overset{(a)}{\geq} \mathbf{c}^H \widehat{\mathbf{W}}_i \mathbf{c} - (\mathbf{h}_i^H \widehat{\mathbf{W}}_i \mathbf{h}_i)^{-1} \mathbf{c}^H \widehat{\mathbf{W}}_i \mathbf{c} \mathbf{h}_i^H \widehat{\mathbf{W}}_i \mathbf{h}_i = 0, \forall i \in \mathcal{I},
\end{aligned} \tag{5.75}$$

where the inequality (a) is derived from the Cauchy-Schwarz inequality. Thus, we have $\{\mathbf{W}_i \succeq 0\}_{i\in\mathcal{I}}$. Due to $\widehat{\mathbf{S}}_0^{\mathrm{II}} \succeq 0$ and eq. (5.73), we have $\mathbf{S}_0^{\mathrm{II},*} \succeq 0$. Moreover, it can be shown that

$$\begin{aligned}
\mathbf{h}_i^H \mathbf{W}_i^* \mathbf{h}_i &= \mathbf{h}_i^H \mathbf{w}_i^* (\mathbf{w}_i^*)^H \mathbf{h}_i \\
&= (\mathbf{h}_i^H \widehat{\mathbf{W}}_i \mathbf{h}_i)^{-1} \mathbf{h}_i^H \widehat{\mathbf{W}}_i \mathbf{h}_i \mathbf{h}_i^H \widehat{\mathbf{W}}_i \mathbf{h}_i \\
&= \mathbf{h}_i^H \widehat{\mathbf{W}}_i \mathbf{h}_i, \forall i \in \mathcal{I}.
\end{aligned} \tag{5.76}$$

From eq. (5.73), the following equation holds

$$\sum_{i\in\mathcal{I}} \mathbf{w}_i^*(\mathbf{w}_i^*)^H + \mathbf{S}_0^{\mathrm{II},*} = \sum_{i\in\mathcal{I}} \widehat{\mathbf{W}}_i + \widehat{\mathbf{S}}_0^{\mathrm{II}}, \tag{5.77}$$

which indicates that $\{\{\mathbf{w}_i^*\}_{i\in\mathcal{I}}, \mathbf{S}_0^{\mathrm{II},*}, \{d_{ki}^*\}_{k\in\mathcal{K},i\in\mathcal{I}}\}$ and $\{\{\widehat{\mathbf{W}}_i\}_{i\in\mathcal{I}}, \widehat{\mathbf{S}}_0^{\mathrm{II}}, \{\widehat{d}_{ki}\}_{k\in\mathcal{K},i\in\mathcal{I}}\}$ yield the same feasible domain. Then, according to eqs. (5.74) and (5.77), it is obvious that the objective function values of Problem (Sub-t) are identical for sets $\{\{\mathbf{w}_i^*\}_{i\in\mathcal{I}}, \mathbf{S}_0^{\mathrm{II},*}, \{d_{ki}^*\}_{k\in\mathcal{K},i\in\mathcal{I}}\}$ and $\{\{\widehat{\mathbf{W}}_i\}_{i\in\mathcal{I}}, \widehat{\mathbf{S}}_0^{\mathrm{II}}, \{\widehat{d}_{ki}\}_{k\in\mathcal{K},i\in\mathcal{I}}\}$, which completes the proof. □

With Proposition 15, we can derive the solution of Problem (Sub-w) from the solution of Problem (Surrogate-w). The details for solving Problem (Sub-w) are presented in Algorithm 11.

Algorithm 11 : To solve Problem (Sub-w) and obtain $\{\mathbf{w}_i^*\}_{i\in\mathcal{I}}$, $\mathbf{S}_0^{\mathrm{II},*}$ and $\{d_{ki}^*\}_{k\in\mathcal{K},i\in\mathcal{I}}$.

1: **Initialization:** Initialize $\{\{\mathbf{W}_i^0\}_{i\in\mathcal{I}}, \mathbf{S}_0^{\mathrm{II},0}, \{d_{ki}^0\}_{k\in\mathcal{K},i\in\mathcal{I}}\}$. Set the iteration number $\tau = 0$. Set ξ_2 as a very small positive number.
2: **repeat**
3: Update $\tau = \tau + 1$.
4: Solve Problem (Surrogate-w) with $\{\{\mathbf{W}_i^{\tau-1}\}_{i\in\mathcal{I}}, \mathbf{S}_0^{\mathrm{II},\tau-1}, \{d_{ki}^{\tau-1}\}_{k\in\mathcal{K},i\in\mathcal{I}}\}$ by CVX and obtain $\{\{\mathbf{W}_i^{\tau}\}_{i\in\mathcal{I}}, \mathbf{S}_0^{\mathrm{II},\tau}, \{d_{ki}^{\tau}\}_{k\in\mathcal{K},i\in\mathcal{I}}\}$.
5: **until** *Convergence*.
6: Calculate $\{\mathbf{w}_i^*\}_{i\in\mathcal{I}}$ according to eq. (5.72). Calculate $\mathbf{S}_0^{\mathrm{II},*}$ according to eq. (5.73). Calculate $\{d_{ki}^*\}_{k\in\mathcal{K},i\in\mathcal{I}}$ according to eq. (5.74).
7: **Output:** Output the solution $\{\mathbf{w}_i^*\}_{i\in\mathcal{I}}$, $\mathbf{S}_0^{\mathrm{II},*}$ and $\{d_{ki}^*\}_{k\in\mathcal{K},i\in\mathcal{I}}$ for Problem (Sub-w).

5.3.6 Proposed Algorithm for Solving Problem (Sub-s)

To solve Problem (Sub-s), we define $\boldsymbol{\omega} \triangleq \mathbf{A}_s^H\mathbf{u}$, $\boldsymbol{\rho} \triangleq \mathbf{A}_c^H\mathbf{u}$ and $\varphi \triangleq \sigma_0^2\mathbf{u}^H\mathbf{u}$. Then, constraint (5.37) can be rewritten as

$$\boldsymbol{\omega}^H\mathbf{S}_0^{\mathrm{I}}\boldsymbol{\omega} \geq \psi^{\mathrm{req}}\left(\boldsymbol{\rho}^H\mathbf{S}_0^{\mathrm{I}}\boldsymbol{\rho} + \varphi\right), \tag{5.78}$$

where

$$\psi^{\mathrm{req}} = \frac{1}{2\mu B^{\mathrm{I}}}\left(2^{\frac{2\mu(Q^{\mathrm{req}} - t^{\mathrm{II}}Q^{\mathrm{II}})}{\delta t^{\mathrm{I}}}} - 1\right). \tag{5.79}$$

With eq. (5.13), we can reformulate Problem (Sub-s) into

$$\begin{aligned} &\text{(Sub-s')}: \min \mathbf{Tr}(\mathbf{S}_0^{\mathrm{I}}) \\ &\text{subject to: constraints } (5.32), (5.45), \text{ and } (5.78), \\ &\qquad \mathrm{Rank}(\mathbf{S}_0^{\mathrm{I}}) = 1, \\ &\text{variable: } \mathbf{S}_0^{\mathrm{I}} \succeq 0. \end{aligned} \tag{5.80}$$

After omitting the Rank-1 constraint (5.80), Problem (Sub-s') can be identified as a standard semidefinite programming (SDP), and thus be solved directly by CVX. Thus, we can solve Problem (Sub-s) by optimizing $\mathbf{S}_0^{\mathrm{I}}$ in Problem (Sub-s') and updating $\mathbf{u}$ according to eq. (5.13) in an alternating manner. The detailed procedures for solving Problem (Sub-s) are presented in Algorithm 12.

Algorithm 12 : To solve Problem (Sub-s) and obtain $\mathbf{S}_0^{\mathrm{I},*}$.

1: **Initialization:** Initialize $\mathbf{S}_0^{\mathrm{I},0}$. Set the iteration number $\tau = 0$. Set ξ_3 as a very small positive number.
2: **repeat**
3: Update $\tau = \tau + 1$.
4: Update $\mathbf{u}^\tau$ with $\mathbf{S}_0^{\mathrm{I},\tau-1}$ according to eq. (5.13).
5: Solve Problem (Sub-s') with $\mathbf{u}^\tau$ by CVX and obtain $\mathbf{S}_0^{\mathrm{I},\tau}$.
6: **until** *Convergence*.
7: **Output:** Output the solution $\mathbf{S}_0^{\mathrm{I},*} = \mathbf{S}_0^{\mathrm{I},\tau}$ for Problem (Sub-s).

Although we temporarily do not consider the Rank-1 constraint (5.80) when solving Problem (Sub-s'), we identify the following feature.

Proposition 16. *The solution* $\mathbf{S}_0^{\mathrm{I},*}$ *obtained by Algorithm 12 always satisfy*

$$\mathrm{Rank}(\mathbf{S}_0^{\mathrm{I},*}) = 1. \tag{5.81}$$

Proof. Problem (Sub-s'), without accounting for the Rank-1 constraint (5.80), is a

standard convex SDP, we can construct the Lagrangian function as

$$\begin{aligned}\mathcal{L}(\mathbf{S}_0^{\mathrm{I}}, \varepsilon, \iota, \{\lambda_k\}_{k\in\mathcal{K}}, \mathbf{O}) &= \varepsilon(\mathbf{Tr}(\mathbf{S}_0^{\mathrm{I}}) - P^{\mathrm{AP,max}}) \\ &+ \mathbf{Tr}(\mathbf{S}_0^{\mathrm{I}}) + \iota\left(\psi^{\mathrm{req}}\left(\boldsymbol{\rho}^H\mathbf{S}_0^{\mathrm{I}}\boldsymbol{\rho} + \varphi\right) - \boldsymbol{\omega}^H\mathbf{S}_0^{\mathrm{I}}\boldsymbol{\omega}\right) \\ &+ \sum_{k\in\mathcal{K}}\lambda_k\left(\varpi - \mathbf{g}_k^H\boldsymbol{\Omega}\mathbf{g}_k P_k^{\max}\right) - \mathbf{Tr}(\mathbf{O}\mathbf{S}_0^{\mathrm{I}}),\end{aligned} \tag{5.82}$$

where

$$\varpi = \left(2^{\frac{D_k^{\mathrm{tot}}}{t^{\mathrm{I}}B^{\mathrm{I}}}} - 1\right)2^{\frac{\sum_{\Phi^{\mathrm{I}}(j)>\Phi^{\mathrm{I}}(k)} D_j^{\mathrm{tot}}}{t^{\mathrm{I}}B^{\mathrm{I}}}}. \tag{5.83}$$

In eq. (5.82), $\varepsilon \geq 0$, $\iota \geq 0$, $\{\lambda_k \geq 0\}_{k\in\mathcal{K}}$ and $\mathbf{O} \succeq 0$ denote the Lagrange multipliers. With eq. (5.82), the Lagrange dual function is given by

$$\begin{aligned}g(\varepsilon, \iota, \{\lambda_k\}_{k\in\mathcal{K}}, \mathbf{O}) &= \inf_{\mathbf{S}_0^{\mathrm{I}}} \mathcal{L}(\mathbf{S}_0^{\mathrm{I}}, \iota, \{\lambda_k\}_{k\in\mathcal{K}}, \mathbf{O}) \\ &= \inf_{\mathbf{S}_0^{\mathrm{I}}} \mathbf{Tr}(\mathbf{V}\mathbf{S}_0^{\mathrm{I}}) + g^{'},\end{aligned} \tag{5.84}$$

where

$$\begin{aligned}\mathbf{V} =& \mathbf{I}_N + \varepsilon\mathbf{I}_N + \iota\psi^{\mathrm{req}}\boldsymbol{\rho}\boldsymbol{\rho}^H - \iota\boldsymbol{\omega}\boldsymbol{\omega}^H - \mathbf{O} \\ &- \sum_{k\in\mathcal{K}}\lambda_k P_k^{\max}(\mathbf{g}_k\mathbf{A}_s\mathbf{A}_s^H\mathbf{g}_k^H + \mathbf{g}_k\mathbf{A}_c\mathbf{A}_c^H\mathbf{g}_k^H),\end{aligned} \tag{5.85}$$

$$g^{'} = \iota\psi^{\mathrm{req}}\varphi + \sum_{k\in\mathcal{K}}\lambda_k(\varpi - \sigma_0^2 P_k^{\max}\mathbf{g}_k^H\mathbf{g}_k) - \varepsilon P^{\mathrm{AP,max}}. \tag{5.86}$$

According to [82], we have $\mathbf{V} = \mathbf{0}$, and thus we have

$$\mathbf{O} = \mathbf{I}_N + \varepsilon\mathbf{I}_N + \iota\psi^{\mathrm{req}}\boldsymbol{\rho}\boldsymbol{\rho}^H - \iota\boldsymbol{\omega}\boldsymbol{\omega}^H - \sum_{k\in\mathcal{K}}\lambda_k P_k^{\max}(\mathbf{g}_k\mathbf{A}_s\mathbf{A}_s^H\mathbf{g}_k^H + \mathbf{g}_k\mathbf{A}_c\mathbf{A}_c^H\mathbf{g}_k^H). \tag{5.87}$$

Since the Lagrange multipliers ε, ι and $\{\lambda_k\}_{k\in\mathcal{K}}$ are non-negative, we conclude that

$$\mathrm{Rank}(\mathbf{O}) \geq N_t - 1. \tag{5.88}$$

Moreover, the related Karush-Kuhn-Tucker (KKT) conditions of Problem (Sub-s') can

be expressed as

$$\boldsymbol{\omega}^H \mathbf{S}_0^{\mathrm{I},*} \boldsymbol{\omega} \geq \psi^{\mathrm{req}} \left(\boldsymbol{\rho}^H \mathbf{S}_0^{\mathrm{I},*} \boldsymbol{\rho} + \varphi \right), \tag{5.89}$$

$$\mathbf{O}^* \mathbf{S}_0^{\mathrm{I},*} = \mathbf{0}. \tag{5.90}$$

Combining eqs. (5.88) and (5.90), we have $\mathrm{Rank}(\mathbf{S}_0^{\mathrm{I},*}) \leq 1$. Since $\varphi > 0$, we can derive from eq. (5.89) that $\mathrm{Rank}(\mathbf{S}_0^{\mathrm{I},*}) \neq 0$. Finally, we conclude that $\mathrm{Rank}(\mathbf{S}_0^{\mathrm{I},*}) = 1$. □

Thanks to Proposition 16, it is unnecessary to recover the Rank-1 solution of $\mathbf{S}_0^{\mathrm{I}}$, which reduces the complexity of Algorithm 12.

5.3.7 Proposed Algorithm for Solving Problem (EMD-TOP)

After solving Problem (EMD-BOT) and obtaining $E^{\mathrm{tot,min}}$ by iteratively solving three sub-problems, i.e., Problem (Sub-t), Problem (Sub-w) and Problem (Sub-s), we continue to determine the solution of Problem (EMD-TOP), i.e., finding the optimal t^{II} that minimizes the total energy consumption. The challenge for solving Problem (EMD-TOP) lies in the lack of an analytical expression for $E^{\mathrm{tot,min}}$. Therefore, we execute a linear search over the variable t^{II} within its viable interval according to constraint (5.36), which thus solves Problem (EMD-TOP) numerically. The detailed procedures for solving Problem (EMD-TOP) are presented in Algorithm 13.

Notice that our algorithm operates in a master-slave manner in which Algorithm 13 works as a master routine to invoke the other algorithms. In each round of the iterations, Algorithm 13 invokes Algorithm 10, Algorithm 11 and Algorithm 12 as three subroutines and executes them iteratively to obtain $E^{\mathrm{tot,min}}$ for each given t^{II}.

5.4 Numerical Results

Numerical results are provided to validate the performance advantages of our NOMA-assisted ISTTO system. Specifically, we consider that the AP is equipped with $N_t = 10$ transmit antennas and $N_r = 15$ receive antennas. The desired target is located at $\theta_0 = 0^\circ$ and $M = 4$ undesired clutters are under angles of $\{-50^\circ, -30^\circ, 30^\circ, 50^\circ\}$.

Algorithm 13 : To solve Problem (EMD-TOP) and obtain $\{\{\mathbf{w}_i^*\}_{i\in\mathcal{I}}, \mathbf{S}_0^{\mathrm{I},*}, \mathbf{S}_0^{\mathrm{II},*}, \{d_{ki}^*\}_{k\in\mathcal{K},i\in\mathcal{I}}, t^{\mathrm{I},*}, t^{\mathrm{II},*}\}$.

Initialization: Initialize $t^{\mathrm{II}} = 0$. Set Δt as a small step-size. Set ξ_4 as a very small positive number. Set the current best value CBV $= \infty$ and current best solution **CBS** as an empty set.
while $t^{\mathrm{II}} \leq T^{\max}$ **do**
  repeat
    Using Algorithm 10 to solve Problem (Sub-t) and obtain $t^{\mathrm{I},*}$.
    Using Algorithm 11 to solve Problem (Sub-w) and obtain $\{\mathbf{w}_i^*\}_{i\in\mathcal{I}}$, $\mathbf{S}_0^{\mathrm{II},*}$ and $\{d_{ki}^*\}_{k\in\mathcal{K},i\in\mathcal{I}}$.
    Using Algorithm 12 to solve Problem (Sub-s) and obtain $\mathbf{S}_0^{\mathrm{I},*}$.
  until *Convergence*.
  Calculate $E^{\mathrm{tot,min}}$ based on $\{t^{\mathrm{I},*}, \{\mathbf{w}_i^*\}_{i\in\mathcal{I}}, \mathbf{S}_0^{\mathrm{I},*}, \mathbf{S}_0^{\mathrm{II},*}, \{d_{ki}^*\}_{k\in\mathcal{K},i\in\mathcal{I}}\}$.
  if $E^{\mathrm{tot,min}} <$ CBV **then**
    Update CBV=$E^{\mathrm{tot,min}}$.
    Update **CBS** $= \{\{\mathbf{w}_i^*\}_{i\in\mathcal{I}}, \mathbf{S}_0^{\mathrm{I},*}, \mathbf{S}_0^{\mathrm{II},*}, \{d_{ki}^*\}_{k\in\mathcal{K},i\in\mathcal{I}}, t^{\mathrm{I},*}, t^{\mathrm{II}}\}$.
  end if
  Update $t^{\mathrm{II}} = t^{\mathrm{II}} + \Delta t$.
end while
Output: Output the optimal value CBV as the minimum total energy consumption, and the optimal solutions **CBS**.

The ECUs and CSs are randomly located within a radius of $\{\overline{d}_k\}_{k\in\mathcal{K}} \in [50, 150]$ m and $\{\overline{d}_i\}_{i\in\mathcal{I}} \in [200, 300]$ m, respectively, from the center of the AP, and the target and clutters are located with a radius of $\{\overline{d}_m\}_{m=0,1,\ldots,M} \in [150, 200]$ m. We consider the channels between the ECUs and the AP and between the AP and the CSs obey the Rayleigh fading with the path loss of $\{L_j^{\mathrm{R}}\}_{j\in\mathcal{K}\cup\mathcal{I}} = 40 + 30\log_{10}\overline{d}_j$, while the channels between the AP and target/clutters are assumed to hold a line-of-sight link with the path loss of $\{L_m^{\mathrm{LoS}}\}_{m=0,1,\ldots,M} = 40 + 25\log_{10}\overline{d}_m$ [87]. Moreover, we set the bandwidth $B^{\mathrm{I}} = B^{\mathrm{II}} = 10$ MHz, the duty factor $\delta = 0.01$, the pulse duration $\mu = 2 \times 10^{-5}$ s, $\nu_k = 1 \times 10^3$ cycles/bit, $\epsilon = 1 \times 10^{-28}$, and set $\sigma_0^2 = \sigma_i^2 = -80$ dBm. The residual self-interference channel at the AP is set as $[\mathbf{H}_{\mathrm{SI}}]_{m,n} = \sqrt{\aleph_{m,n}} e^{-j2\pi\frac{\hat{d}_{m,n}}{\lambda}}$, where $\aleph_{m,n} = -110$ dB denotes the self-interference channel coefficient and $\hat{d}_{m,n}$ represents the spatial separation between the m-th receive antenna and the n-th transmit antenna [128].

Figure 5.2 validates the convergence performance of the proposed Algorithm 13 under the different ECU numbers and CS numbers. Figure 5.2 demonstrates that the objective value of Problem (EMD) converges rapidly within 8 iterations for all tested

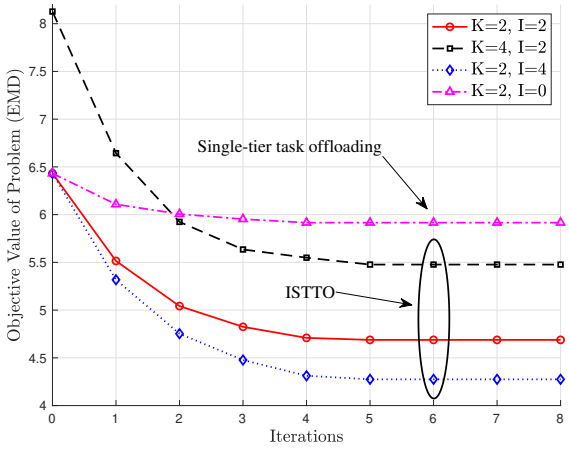

Fig. 5.2: Convergence performance of the proposed Algorithm 13

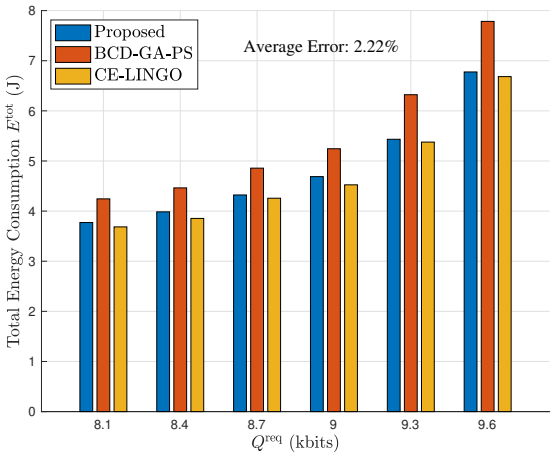

Fig. 5.3: Performance advantages of the proposed Algorithm 13

cases. Meanwhile, it can be observed that the total energy consumption increases with the growing number of ECUs and decreases with the growing number of CSs, which can be explained as follows. Under the same computational offloading latency constraints, the increased number of ECUs results in higher total workloads, and a larger energy consumption is required to guarantee the more stringent offloading and computing requirements. The increased number of the CSs provides more flexible offloading options for the AP, and thus alleviates the computing burden on the AP.

To verify the accuracy and effectiveness of our proposed algorithm, we compare our algorithm with the following two benchmark algorithms.

- BCD-GA-PS algorithm. We utilize the BCD method to divide Problem (EMD) into two sub-problems as follows. The first sub-problem is to optimize variables

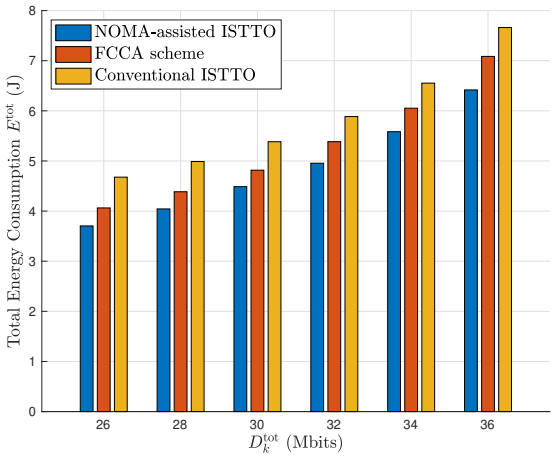

Fig. 5.4: Performance advantages under different D_k^{tot}

$\{t^{\text{I}}, t^{\text{II}}, \{d_{ki}\}\}$, which is solved by the genetic algorithm (GA) [110]. The second sub-problem is to optimize $\{\{\mathbf{w}_i\}, \mathbf{s}_0^{\text{I}}, \mathbf{s}_0^{\text{II}}\}$, which is solved by the pattern search (PS) algorithm [150].

- CE-LINGO algorithm. We utilize the cross-entropy (CE) algorithm to find the optimal $\{t^{\text{I},*}, t^{\text{II},*}, \{d_{ki}^*\}\}$ [107]. For each given $\{t^{\text{I}}, t^{\text{II}}, \{d_{ki}\}\}$, we obtain the solution $\{\{\mathbf{w}_i\}, \mathbf{s}_0^{\text{I}}, \mathbf{s}_0^{\text{II}}\}$ by LINGO [90]. According to the criterion of CE and LINGO, the solution obtained by CE-LINGO algorithm can be regarded as the optimal solution of Problem (EMD).

Figure 5.3 shows the comparison between our proposed Algorithm 13 and two benchmark algorithms versus different sensing estimation information requirements. It can be observed that our Algorithm 13 outperforms the BCD-GA-PS algorithm in energy minimization while reaching the close-to-optimal solution compared to the CE-LINGO algorithm. We mark the average error between the results obtained by our Algorithm 13 and those obtained by CE-LINGO algorithm at the top of Figure 5.3. The results show that the average error does not exceed 3%, which verifies the accuracy of our algorithm.

Figures 5.4 and 5.5 show the performance advantages of the proposed NOMA-assisted ISTTO in comparison with two benchmark resource allocation schemes, i.e., 1) fixed computing capacity allocation (FCCA) scheme, in which the ES allocates a fixed computing capacity to each ECU and 2) conventional ISTTO, in which both tiers

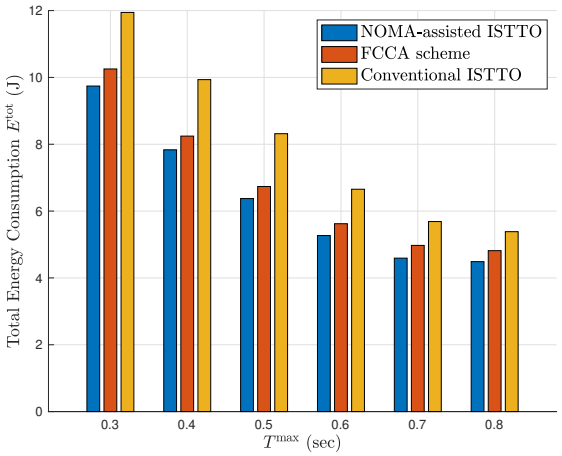

Fig. 5.5: Performance advantages under different $T^{\max}$

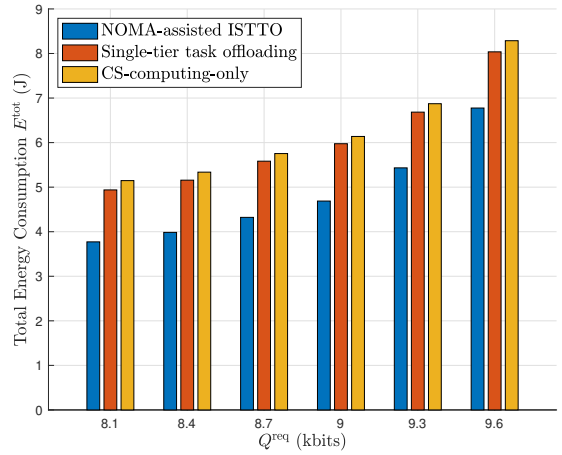

Fig. 5.6: Performance advantages under different Q^{req}

of transmissions do not use NOMA. Figure 5.4 shows that the total energy consumption is increasing with respect to the value of D_k^{tot}. Figure 5.5 shows that the total energy consumption is decreasing with respect to the value of the maximum available radio interface time $T^{\max}$. It can be seen that compared to the FCCA scheme, our proposed NOMA-assisted ISTTO can achieve a lower energy consumption due to the optimized computing capacity allocation of the ES. Moreover, our NOMA-assisted ISTTO scheme significantly outperforms conventional ISTTO scheme due to the fact that leveraging NOMA alleviates the inter-functionalities interference of two-tier transmissions and thus improves both sensing and offloading performances.

Figures 5.6 and 5.7 demonstrate the performance advantages of our NOMA-assisted ISTTO in comparison with two benchmark offloading schemes including the single-

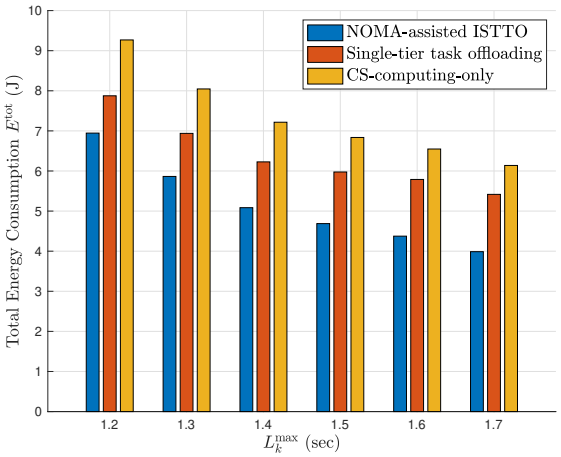

Fig. 5.7: Performance advantages under different $L_k^{\max}$

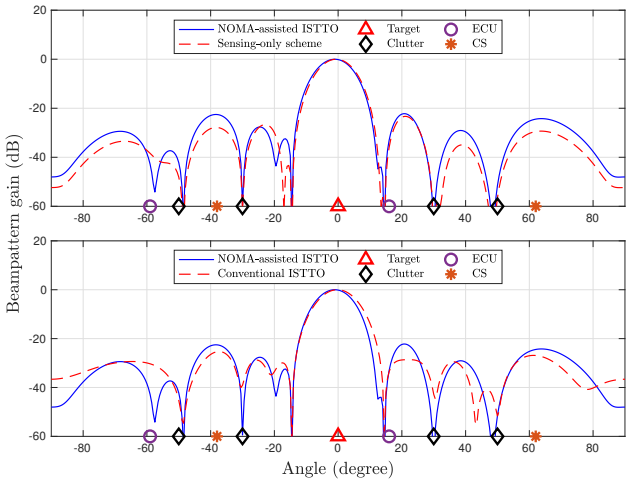

Fig. 5.8: Beampattern gain of NOMA-assisted ISTTO scheme

tier task offloading scheme and the CS-computing-only scheme (all ECUs' workloads are only processed at the CSs). It can be observed that our NOMA-assisted ISTTO outperforms two benchmark offloading schemes, which indicates that our ISTTO framework can achieve a lower energy consumption than the benchmark schemes under the same computational offloading latency constraints and the sensing requirement. This is due to the fact that the two-tier task offloading framework enables an efficient and balanced utilization of the computing resources across different tiers.

Figure 5.8 shows the beampattern gain of our NOMA-assisted ISTTO scheme, which can be defined as

$$P^{\text{BG}}(\theta) = |(\mathbf{u}^*)^H \mathbf{a}_r(\theta) \mathbf{a}_t^H(\theta) \mathbf{x}_0^{\text{II},*}|^2, \tag{5.91}$$

where the optimal sensing receiver is normalized as $||\mathbf{u}^*|| = 1$. We set $K = 2$ ECUs and $I = 2$ CSs as the tested scenario, and we mark the angles of all ECUs, CSs, target and clutters in both sub-figures of Figure 5.8. In the top sub-figure of Figure 5.8, we compare the beampattern gain achieved by our NOMA-assisted ISTTO scheme and the sensing-only scheme. It can be observed that our NOMA-assisted ISTTO scheme achieves dominant peaks in the directions of the CSs and the target, while maintaining a low power leakage in the directions of the ECUs and the clutters, which reduces the severe interference caused by reflected signals to the sensing. Compared to the sensing-only scheme, our scheme achieves higher powers in the directions of the CSs, which results in an improved two-tier task offloading performance. The bottom sub-figure of Figure 5.8 shows that compared to conventional ISTTO scheme, our NOMA-assisted ISTTO scheme suppresses the interference from the clutters' and the ECUs' directions better, and thus achieves a better sensing performance while maintaining the power in the directions of the CSs.

5.5 Conclusion

In this chapter, we have proposed a NOMA-assisted integrated sensing and two-tier task offloading system, in which the ISCC AP provides task offloading services for the ECUs while performing sensing towards a target. We have proposed a joint optimization of the AP's transmit beamforming, the two-tier dedicated sensing signals, the two-tier computation offloading strategies and the associated allocations of the communication and computing resources, with the aim of achieving an energy-minimizing design. Despite the non-convexity of the formulated joint optimization problem, we have exploited a decomposition-based framework and proposed the corresponding algorithms for solving it. Numerical results have been provided to validate the accuracy and effectiveness of our algorithms and the performance advantages of our NOMA-assisted ISTTO scheme.

Chapter 6

Conclusion and Future Work

6.1 Conclusion

In this thesis, we have addressed the fundamental challenges of resource efficiency in integrated sensing and communication (ISAC) systems caused by the scarcity of multi-dimensional radio resources. We have investigated four distinct resource-efficient designs spanning the time, frequency, spatial, and functional domains. These schemes aim to break the resource bottlenecks such as temporal rigidity, spectral saturation, spatial inequality, and functional isolation. We have formulated joint optimization problems involving beamforming, scheduling, and multi-dimensional resource allocation to coordinate the conflicting requirements of sensing and communication. Through rigorous mathematical modeling and algorithmic design, we have achieved superior system performance in terms of energy efficiency, sensing efficiency, fairness, and sustainability.

In Chapter 2, we have proposed an energy-efficient sensing scheduling scheme using channel-sharing mechanisms to address the temporal rigidity in ISAC systems. The scheme allows the ISAC base station to dynamically schedule sensing tasks over the downlink channels of conventional cellular users. We have formulated a joint optimization problem of multi-target sensing scheduling and transceiver beamforming to maximize the energy efficiency of radar sensing while guaranteeing the communication throughput. To solve the non-convex problem, we have developed an efficient algorithm based on Dinkelbach's method, semidefinite relaxation (SDR), and a swap-matching mechanism.

In Chapter 3, to tackle the spectral capacity limit, we have proposed a sensing-efficient NOMA-aided ISAC framework. We have introduced a novel metric, i.e., sensing efficiency, to measure the number of successfully sensed targets per time unit. We have formulated a joint optimization problem of beamforming, NOMA transmission duration, and sensing scheduling to maximize this efficiency while satisfying the quality of service for both NOMA users and sensing targets. We have designed a decomposition-based algorithm that utilizes successive convex approximation (SCA)

and penalty function methods for beamforming, a bisection search approach for optimal time duration, and a cross-entropy learning-based algorithm for optimal scheduling.

In Chapter 4, we have addressed the spatial coverage limitations and resource unfairness by proposing a fairness-aware multi-device cooperative sensing scheme. Devices perform cooperative sensing and data transmission in a time-division manner to eliminate interference. We have formulated a joint optimization problem of time allocation and beamforming to maximize the fairness-aware system-wise throughput while guaranteeing multi-target sensing quality. We have derived a semi-analytical expression for the optimal time allocation and developed an efficient block coordinate descent (BCD)-based algorithm to solve the joint optimization problem.

In Chapter 5, we have investigated the integration of sensing, communication, and computing to address functional isolation. We have proposed a NOMA-assisted integrated sensing and two-tier task offloading (ISTTO) framework, where an access point supports edge task processing while performing continuous sensing, with additional offloading capabilities to cloudlet servers. We have addressed the complex inter-functionality interference and the trade-off between sensing accuracy and offloading latency. We have formulated a joint optimization problem of transmit beamforming, dedicated sensing signals, offloading strategies, and associated allocations of the communication and computing resources to minimize the total energy consumption, and designed a decomposition-based algorithm to obtain the optimal solution.

6.2 Future Work

The research presented in this thesis has established a systematic framework for resource-efficient ISAC, primarily focusing on ground-based networks. However, the rapid growth of the low-altitude economy presents a new area characterized by complex environments and dynamic missions. To address the practical challenges of unclear sensing, unreliable control, and difficult collaboration in low-altitude scenarios, future work will focus on multi-modal cooperative sensing, embodied ISAC, and cognitive swarm intelligence.

6.2.1 Robust Multi-Modal Cooperative Sensing for Low-Altitude Environments

As highlighted in the research background, low-altitude sensing faces three main challenges: unclear sensing due to bad weather (rain, fog, low light), inaccurate detection caused by high-speed flight, and incomplete observation due to limited view angles and blocking objects. To overcome these environmental and physical limitations, it is essential to move beyond single-node, single-modal sensing. We propose a comprehensive approach that integrates heterogeneous sensors and multi-view cooperation to achieve robust perception, focusing on the following two aspects:

- All-Weather Multi-Sensor Fusion: Future work will extend the single-modal ISAC framework to multi-modal ISAC, combining radio frequency sensing with vision. We aim to use the advantage of radio frequency signals to penetrate rain and fog, making up for the performance loss of optical sensors in harsh environments. A cooperative learning framework will be developed to mix data from different sensors, ensuring clear perception under all weather conditions.

- Multi-View Cooperative Reconstruction: To address the incomplete sensing problem caused by blocking objects, we will explore multi-view cooperative sensing. By coordinating multiple UAVs to observe a target from different angles, we can build a complete 3D map of the environment. This direction involves optimizing the 3D formation of UAVs to capture the most spatial information, thereby solving the blind spot issue found in single-view perception.

6.2.2 Embodied ISAC: From Sensing to Reliable Action

In complex low-altitude environments, current UAV systems suffer from unreliable target understanding, imprecise action generation, and uncontrollable safety risks. To mitigate these risks and bridge the gap between perception and actuation, future work will transition from open-loop sensing to closed-loop embodied ISAC. This paradigm shift requires joint optimization of information acquisition and physical control, with specific research directions outlined as follows:

- Sensing-Control Closed-Loop Optimization: Unlike traditional ISAC which treats sensing as an output, embodied ISAC treats sensing as an input for control. Fu-

ture work will investigate the joint optimization of ISAC waveforms and flight control policies. The goal is to minimize the action generation error by directly mapping sensing data to precise mechanical operations (e.g., grasping or landing), improving the working efficiency of aerial manipulation.

- Safety-Aware Autonomous Decision Making: To address the uncontrollable safety risks (e.g., collisions), we will develop explainable end-to-end ISAC strategies. By integrating real-time environmental sensing with reliable control theory, the system can autonomously respond to sudden obstacles and ensure safe paths. This research aims to guarantee system-level reliability and safety for autonomous low-altitude flight.

6.2.3 Cognitive Swarm Intelligence: Collaborative Reasoning and Evolution

Low-altitude swarm intelligence currently faces the challenges of data scarcity, poor autonomy, and difficult collaboration. Furthermore, the complexity of tasks requires UAVs to perform cross-level reasoning in environments with little semantic information. Establishing a robust swarm intelligence system in such resource-constrained environments requires a fundamental shift in how knowledge is acquired and processed. We identify two key research pathways to enhance the autonomy and cognitive capabilities of UAV swarms:

- Collaborative Learning for Swarm Evolution: To tackle the data scarcity and poor autonomy issues, future work will propose a distributed collaborative learning framework. By enabling UAVs to share model updates rather than raw data, the swarm can collectively improve its sensing models and adapt to new environments without relying heavily on pre-labeled training data.

- Semantic-Aware Reasoning and Decision: Addressing the spatial complexity and task complexity, we will explore semantic ISAC. This involves moving beyond signal-level processing to semantic-level understanding. We aim to equip UAV swarms with the ability to perform logical reasoning across sensing-reasoning-decision chains, enabling them to understand complex instructions and execute diverse missions with high autonomy.

References

[1] H. Tataria, M. Shafi, A. F. Molisch, M. Dohler, H. Sjöland, and F. Tufvesson, "6G wireless systems: Vision, requirements, challenges, insights, and opportunities," *Proceedings of the IEEE*, vol. 109, no. 7, pp. 1166–1199, 2021.

[2] K. B. Letaief, W. Chen, Y. Shi, J. Zhang, and Y.-J. A. Zhang, "The roadmap to 6G: AI empowered wireless networks," *IEEE Communications Magazine*, vol. 57, no. 8, pp. 84–90, 2019.

[3] D. C. Nguyen, M. Ding, P. N. Pathirana, A. Seneviratne, J. Li, D. Niyato, O. Dobre, and H. V. Poor, "6G internet of things: A comprehensive survey," *IEEE Internet of Things Journal*, vol. 9, no. 1, pp. 359–383, 2022.

[4] J. A. Zhang, F. Liu, C. Masouros, R. W. Heath, Z. Feng, L. Zheng, and A. Petropulu, "An overview of signal processing techniques for joint communication and radar sensing," *IEEE Journal of Selected Topics in Signal Processing*, vol. 15, no. 6, pp. 1295–1315, 2021.

[5] C. De Lima, D. Belot, R. Berkvens, A. Bourdoux, D. Dardari, M. Guillaud, M. Isomursu, E.-S. Lohan, Y. Miao, A. N. Barreto, M. R. K. Aziz, J. Saloranta, T. Sanguanpuak, H. Sarieddeen, G. Seco-Granados, J. Suutala, T. Svensson, M. Valkama, B. Van Liempd, and H. Wymeersch, "Convergent communication, sensing and localization in 6G systems: An overview of technologies, opportunities and challenges," *IEEE Access*, vol. 9, pp. 26 902–26 925, 2021.

[6] J. A. Zhang, M. L. Rahman, K. Wu, X. Huang, Y. J. Guo, S. Chen, and J. Yuan, "Enabling joint communication and radar sensing in mobile networks—a survey," *IEEE Communications Surveys & Tutorials*, vol. 24, no. 1, pp. 306–345, 2022.

[7] S. Lu, F. Liu, Y. Li, K. Zhang, H. Huang, J. Zou, X. Li, Y. Dong, F. Dong, J. Zhu, Y. Xiong, W. Yuan, Y. Cui, and L. Hanzo, "Integrated sensing and communications: Recent advances and ten open challenges," *IEEE Internet of Things Journal*, vol. 11, no. 11, pp. 19 094–19 120, 2024.

[8] W. Zhou, R. Zhang, G. Chen, and W. Wu, "Integrated sensing and communication waveform design: A survey," *IEEE Open Journal of the Communications Society*, vol. 3, pp. 1930–1949, 2022.

[9] A. Liu, Z. Huang, M. Li, Y. Wan, W. Li, T. X. Han, C. Liu, R. Du, D. K. P. Tan, J. Lu, Y. Shen, F. Colone, and K. Chetty, "A survey on fundamental limits of integrated sensing and communication," *IEEE Communications Surveys & Tutorials*, vol. 24, no. 2, pp. 994–1034, 2022.

[10] Y. Cui, F. Liu, X. Jing, and J. Mu, "Integrating sensing and communications for ubiquitous IoT: Applications, trends, and challenges," *IEEE Network*, vol. 35, no. 5, pp. 158–167, 2021.

[11] N. C. Luong, X. Lu, D. T. Hoang, D. Niyato, and D. I. Kim, "Radio resource management in joint radar and communication: A comprehensive survey," *IEEE Communications Surveys & Tutorials*, vol. 23, no. 2, pp. 780–814, 2021.

[12] A. Kaushik, R. Singh, S. Dayarathna, R. Senanayake, M. Di Renzo, M. Dajer, H. Ji, Y. Kim, V. Sciancalepore, A. Zappone, and W. Shin, "Toward integrated sensing and communications for 6G: Key enabling technologies, standardization, and challenges," *IEEE Communications Standards Magazine*, vol. 8, no. 2, pp. 52–59, 2024.

[13] F. Liu, C. Masouros, A. P. Petropulu, H. Griffiths, and L. Hanzo, "Joint radar and communication design: Applications, state-of-the-art, and the road ahead," *IEEE Transactions on Communications*, vol. 68, no. 6, pp. 3834–3862, 2020.

[14] M. F. Keskin, V. Koivunen, and H. Wymeersch, "Limited feedforward waveform design for OFDM dual-functional radar-communications," *IEEE Transactions on Signal Processing*, vol. 69, pp. 2955–2970, 2021.

[15] Q. Zhang, H. Sun, X. Gao, X. Wang, and Z. Feng, "Time-division ISAC enabled connected automated vehicles cooperation algorithm design and performance evaluation," *IEEE Journal on Selected Areas in Communications*, vol. 40, no. 7, pp. 2206–2218, 2022.

[16] Z. Zhang, H. Ren, C. Pan, S. Hong, D. Wang, J. Wang, and X. You, "Target localization in cooperative ISAC systems: A scheme based on 5G NR OFDM signals," *IEEE Transactions on Communications*, vol. 73, no. 5, pp. 3562–3578, 2025.

[17] Z. Wei, J. Piao, X. Yuan, H. Wu, J. A. Zhang, Z. Feng, L. Wang, and P. Zhang, "Waveform design for MIMO-OFDM integrated sensing and communication system: An information theoretical approach," *IEEE Transactions on Communications*, vol. 72, no. 1, pp. 496–509, 2024.

[18] J. Li, X. Shao, F. Chen, S. Wan, C. Liu, Z. Wei, and D. Wing Kwan Ng, "Networked integrated sensing and communications for 6G wireless systems," *IEEE Internet of Things Journal*, vol. 11, no. 17, pp. 29 062–29 075, 2024.

[19] K. Meng, C. Masouros, A. P. Petropulu, and L. Hanzo, "Cooperative ISAC networks: Opportunities and challenges," *IEEE Wireless Communications*, vol. 32, no. 3, pp. 212–219, 2025.

[20] N. Huang, C. Dou, Y. Wu, L. Qian, B. Lin, H. Zhou, and X. Shen, "Mobile edge computing aided integrated sensing and communication with short-packet transmissions," *IEEE Transactions on Wireless Communications*, vol. 23, no. 7, pp. 7759–7774, 2024.

[21] P. Liu, X. Wang, Z. Fei, Y. Wu, J. Xu, and A. Nallanathan, "Latency minimization oriented radio and computation resource allocations for 6G V2X networks with ISCC," *IEEE Transactions on Communications*, vol. 73, no. 12, pp. 15 851–15 865, 2025.

[22] X. Wang, Z. Fei, J. A. Zhang, and J. Xu, "Partially-connected hybrid beamforming design for integrated sensing and communication systems," *IEEE Transactions on Communications*, vol. 70, no. 10, pp. 6648–6660, 2022.

[23] Y. Huang, Y. Fang, X. Li, and J. Xu, "Coordinated power control for network integrated sensing and communication," *IEEE Transactions on Vehicular Technology*, vol. 71, no. 12, pp. 13 361–13 365, 2022.

[24] F. Dong, F. Liu, Y. Cui, W. Wang, K. Han, and Z. Wang, "Sensing as a service in 6G perceptive networks: A unified framework for ISAC resource allocation," *IEEE Transactions on Wireless Communications*, vol. 22, no. 5, pp. 3522–3536, 2023.

[25] Z. He, W. Xu, H. Shen, Y. Huang, and H. Xiao, "Energy efficient beamforming optimization for integrated sensing and communication," *IEEE Wireless Communications Letters*, vol. 11, no. 7, pp. 1374–1378, 2022.

[26] Z. Wang, K. Han, X. Shen, W. Yuan, and F. Liu, "Achieving the performance bounds for sensing and communications in perceptive networks: Optimal bandwidth allocation," *IEEE Wireless Communications Letters*, vol. 11, no. 9, pp. 1835–1839, 2022.

[27] B. Liu, J. Liu, and N. Kato, "Optimal beamformer design for millimeter wave dual-functional radar-communication based V2X systems," *IEEE Journal on Selected Areas in Communications*, vol. 40, no. 10, pp. 2980–2993, 2022.

[28] Z. He, W. Xu, H. Shen, D. W. K. Ng, Y. C. Eldar, and X. You, "Full-duplex communication for ISAC: Joint beamforming and power optimization," *IEEE Journal on Selected Areas in Communications*, vol. 41, no. 9, pp. 2920–2936, 2023.

[29] N. Huang, C. Dou, Y. Wu, L. Qian, B. Lin, and H. Zhou, "Unmanned-aerial-vehicle-aided integrated sensing and computation with mobile-edge computing," *IEEE Internet of Things Journal*, vol. 10, no. 19, pp. 16 830–16 844, 2023.

[30] Z. Yang, S. Bi, and Y.-J. A. Zhang, "Deployment optimization of dual-functional UAVs for integrated localization and communication," *IEEE Transactions on Wireless Communications*, vol. 22, no. 12, pp. 9672–9687, 2023.

[31] Z. Yang, D. Li, N. Zhao, Z. Wu, Y. Li, and D. Niyato, "Secure precoding optimization for NOMA-aided integrated sensing and communication," *IEEE Transactions on Communications*, vol. 70, no. 12, pp. 8370–8382, 2022.

[32] Y. Cui, W. Yuan, Z. Zhang, J. Mu, and X. Li, "On the physical layer of digital twin: An integrated sensing and communications perspective," *IEEE Journal on Selected Areas in Communications*, vol. 41, no. 11, pp. 3474–3490, 2023.

[33] H. T. Nguyen, D. T. Hoang, N. C. Luong, D. Niyato, and D. I. Kim, "A hierarchical game model for OFDM integrated radar and communication systems," *IEEE Transactions on Vehicular Technology*, vol. 70, no. 5, pp. 5077–5082, 2021.

[34] H. Yang, Z. Wei, Z. Feng, C. Qiu, Z. Fang, X. Chen, and P. Zhang, "Queue-aware dynamic resource allocation for the joint communication-radar system," *IEEE Transactions on Vehicular Technology*, vol. 70, no. 1, pp. 754–767, 2021.

[35] Z. Wang, K. Han, J. Jiang, F. Liu, and W. Yuan, "Multi-vehicle tracking and ID association based on integrated sensing and communication signaling," *IEEE Wireless Communications Letters*, vol. 11, no. 9, pp. 1960–1964, 2022.

[36] X. Liu, T. Huang, N. Shlezinger, Y. Liu, J. Zhou, and Y. C. Eldar, "Joint transmit beamforming for multiuser MIMO communications and MIMO Radar," *IEEE Transactions on Signal Processing*, vol. 68, pp. 3929–3944, 2020.

[37] K. Wu, J. A. Zhang, Z. Ni, X. Huang, Y. J. Guo, and S. Chen, "Joint communications and sensing employing optimized MIMO-OFDM signals," *IEEE Internet of Things Journal*, vol. 11, no. 6, pp. 10 368–10 383, 2024.

[38] B. Liu, J. Liu, and N. Kato, "Optimal beamformer design for millimeter wave dual-functional radar-communication based V2X systems," *IEEE Journal on Selected Areas in Communications*, vol. 40, no. 10, pp. 2980–2993, 2022.

[39] S. Wang, Y. Gong, X. Li, and Q. Li, "Integrated sensing, communication, and computation over the air: Beampattern design for wireless sensor networks," *IEEE Internet of Things Journal*, vol. 11, no. 6, pp. 9681–9692, 2024.

[40] C. Liu, W. Yuan, S. Li, X. Liu, H. Li, D. W. K. Ng, and Y. Li, "Learning-based predictive beamforming for integrated sensing and communication in vehicular networks," *IEEE Journal on Selected Areas in Communications*, vol. 40, no. 8, pp. 2317–2334, 2022.

[41] N. Zhao, Y. Li, S. Zhang, Y. Chen, W. Lu, J. Wang, and X. Wang, "Security enhancement for NOMA-UAV networks," *IEEE Transactions on Vehicular Technology*, vol. 69, no. 4, pp. 3994–4005, 2020.

[42] X. Li, Y. Zheng, M. Zeng, Y. Liu, and O. A. Dobre, "Enhancing secrecy performance for STAR-RIS NOMA networks," *IEEE Transactions on Vehicular Technology*, vol. 72, no. 2, pp. 2684–2688, 2023.

[43] Q. Li, T. Shang, T. Tang, and Z. Xiong, "Adaptive user association scheme for indoor multi-user NOMA-VLC systems," *IEEE Wireless Communications Letters*, vol. 12, no. 5, pp. 873–877, 2023.

[44] Z. Wang, Y. Liu, X. Mu, Z. Ding, and O. A. Dobre, "NOMA empowered integrated sensing and communication," *IEEE Communications Letters*, vol. 26, no. 3, pp. 677–681, 2022.

[45] C. Zhang, W. Yi, Y. Liu, and L. Hanzo, "Semi-integrated-sensing-and-communication (Semi-ISaC): From OMA to NOMA," *IEEE Transactions on Communications*, vol. 71, no. 4, pp. 1878–1893, 2023.

[46] Z. Wang, X. Mu, Y. Liu, X. Xu, and P. Zhang, "NOMA-aided joint communication, sensing, and multi-tier computing systems," *IEEE Journal on Selected Areas in Communications*, vol. 41, no. 3, pp. 574–588, 2023.

[47] Y. Ma, Z. Yuan, S. Xia, G. Yu, and L. Hu, "Highly efficient waveform design and hybrid duplex for joint communication and sensing," *IEEE Internet of Things Journal*, vol. 10, no. 19, pp. 17 369–17 381, 2023.

[48] H. Hua, J. Xu, and T. X. Han, "Optimal transmit beamforming for integrated sensing and communication," *IEEE Transactions on Vehicular Technology*, vol. 72, no. 8, pp. 10 588–10 603, 2023.

[49] Y. Du, Y. Liu, K. Han, J. Jiang, W. Wang, and L. Chen, "Multi-user and multi-target dual-function radar-communication waveform design: Multi-fold performance tradeoffs," *IEEE Transactions on Green Communications and Networking*, vol. 7, no. 1, pp. 483–496, 2023.

[50] N. H. Chu, D. N. Nguyen, D. T. Hoang, Q.-V. Pham, K. T. Phan, W.-J. Hwang, and E. Dutkiewicz, "AI-enabled mm-waveform configuration for autonomous vehicles with integrated communication and sensing," *IEEE Internet of Things Journal*, vol. 10, no. 19, pp. 16 727–16 743, 2023.

[51] X. Chen, Z. Feng, Z. Wei, F. Gao, and X. Yuan, "Performance of joint sensing-communication cooperative sensing UAV network," *IEEE Transactions on Vehicular Technology*, vol. 69, no. 12, pp. 15 545–15 556, 2020.

[52] X. Cheng, D. Duan, S. Gao, and L. Yang, "Integrated sensing and communications (ISAC) for vehicular communication networks (VCN)," *IEEE Internet of Things Journal*, vol. 9, no. 23, pp. 23 441–23 451, 2022.

[53] X. Li and S. Bi, "Optimal AI model splitting and resource allocation for device-edge co-inference in multi-user wireless sensing systems," *IEEE Transactions on Wireless Communications*, vol. 23, no. 9, pp. 11 094–11 108, 2024.

[54] W. Jiang, Z. Wei, F. Liu, Z. Feng, and P. Zhang, "Collaborative precoding design for adjacent integrated sensing and communication base stations," *IEEE Internet of Things Journal*, vol. 11, no. 9, pp. 15 059–15 074, 2024.

[55] K. Gu, Y. Wang, and Y. Shen, "Cooperative detection by multi-agent networks in the presence of position uncertainty," *IEEE Transactions on Signal Processing*, vol. 68, pp. 5411–5426, 2020.

[56] X. Liu, H. Zhang, K. Long, M. Zhou, Y. Li, and H. V. Poor, "Proximal policy optimization-based transmit beamforming and phase-shift design in an IRS-aided isac system for the THz band," *IEEE Journal on Selected Areas in Communications*, vol. 40, no. 7, pp. 2056–2069, 2022.

[57] T. Zhang, K. Zhu, S. Zheng, D. Niyato, and N. C. Luong, "Trajectory design and power control for joint radar and communication enabled multi-UAV cooperative detection systems," *IEEE Transactions on Communications*, vol. 71, no. 1, pp. 158–172, 2023.

[58] P. Liu, G. Zhu, W. Jiang, W. Luo, J. Xu, and S. Cui, "Vertical federated edge learning with distributed integrated sensing and communication," *IEEE Communications Letters*, vol. 26, no. 9, pp. 2091–2095, 2022.

[59] N. Huang, T. Wang, Y. Wu, Q. Wu, and T. Q. Quek, "Integrated sensing and communication assisted mobile edge computing: An energy-efficient design via intelligent reflecting surface," *IEEE Wireless Communications Letters*, vol. 11, no. 10, pp. 2085–2089, 2022.

[60] Y. Gong, Y. Wei, Z. Feng, F. R. Yu, and Y. Zhang, "Resource allocation for integrated sensing and communication in digital twin enabled internet of vehicles," *IEEE Transactions on Vehicular Technology*, vol. 72, no. 4, pp. 4510–4524, 2023.

[61] H. Chen, T. D. Todd, D. Zhao, and G. Karakostas, "Wireless and service allocation for mobile computation offloading with task deadlines," *IEEE Transactions on Mobile Computing*, vol. 23, no. 5, pp. 5054–5068, 2024.

[62] H. He, H. Shan, A. Huang, Q. Ye, and W. Zhuang, "Edge-aided computing and transmission scheduling for LTE-U-enabled IoT," *IEEE Transactions on Wireless Communications*, vol. 19, no. 12, pp. 7881–7896, 2020.

[63] L. Huang, S. Bi, and Y.-J. A. Zhang, "Deep reinforcement learning for online computation offloading in wireless powered mobile-edge computing networks," *IEEE Transactions on Mobile Computing*, vol. 19, no. 11, pp. 2581–2593, 2020.

[64] M. Sheng, Y. Dai, J. Liu, N. Cheng, X. Shen, and Q. Yang, "Delay-aware computation offloading in NOMA MEC under differentiated uploading delay," *IEEE Transactions on Wireless Communications*, vol. 19, no. 4, pp. 2813–2826, 2020.

[65] F. Fang, K. Wang, Z. Ding, and V. C. M. Leung, "Energy-efficient resource allocation for NOMA-MEC networks with imperfect CSI," *IEEE Transactions on Communications*, vol. 69, no. 5, pp. 3436–3449, 2021.

[66] Z. Ding, D. Xu, R. Schober, and H. V. Poor, "Hybrid NOMA offloading in multi-user MEC networks," *IEEE Transactions on Wireless Communications*, vol. 21, no. 7, pp. 5377–5391, 2022.

[67] S. Wang, J. Yang, and S. Bi, "Adaptive video streaming in multi-tier computing networks: Joint edge transcoding and client enhancement," *IEEE Transactions on Mobile Computing*, vol. 23, no. 4, pp. 2657–2670, 2024.

[68] Y. Xu, B. Qian, K. Yu, T. Ma, L. Zhao, and H. Zhou, "Federated learning over fully-decoupled RAN architecture for two-tier computing acceleration," *IEEE Journal on Selected Areas in Communications*, vol. 41, no. 3, pp. 789–801, 2023.

[69] Q. Qi, X. Chen, A. Khalili, C. Zhong, Z. Zhang, and D. W. K. Ng, "Integrating sensing, computing, and communication in 6G wireless networks: Design and optimization," *IEEE Transactions on Communications*, vol. 70, no. 9, pp. 6212–6227, 2022.

[70] L. Zhao, D. Wu, L. Zhou, and Y. Qian, "Radio resource allocation for integrated sensing, communication, and computation networks," *IEEE Transactions on Wireless Communications*, vol. 21, no. 10, pp. 8675–8687, 2022.

[71] D. Wen, P. Liu, G. Zhu, Y. Shi, J. Xu, Y. C. Eldar, and S. Cui, "Task-oriented sensing, computation, and communication integration for multi-device edge AI," *IEEE Transactions on Wireless Communications*, vol. 23, no. 3, pp. 2486–2502, 2024.

[72] N. Huang, H. Dong, C. Dou, Y. Wu, L. Qian, S. Ma, and R. Lu, "Edge intelligence oriented integrated sensing and communication: A multi-cell cooperative approach," *IEEE Transactions on Vehicular Technology*, vol. 73, no. 6, pp. 8810–8824, 2024.

[73] Z. Wei, H. Qu, Y. Wang, X. Yuan, H. Wu, Y. Du, K. Han, N. Zhang, and Z. Feng, "Integrated sensing and communication signals toward 5G-A and 6G: A survey," *IEEE Internet of Things Journal*, vol. 10, no. 13, pp. 11 068–11 092, 2023.

[74] J. Wang, N. Varshney, C. Gentile, S. Blandino, J. Chuang, and N. Golmie, "Integrated sensing and communication: Enabling techniques, applications, tools and data sets, standardization, and future directions," *IEEE Internet of Things Journal*, vol. 9, no. 23, pp. 23 416–23 440, 2022.

[75] H. Zhang, H. Zhang, B. Di, M. D. Renzo, Z. Han, H. V. Poor, and L. Song, "Holographic integrated sensing and communication," *IEEE Journal on Selected Areas in Communications*, vol. 40, no. 7, pp. 2114–2130, 2022.

[76] U. Demirhan and A. Alkhateeb, "Integrated sensing and communication for 6G: Ten key machine learning roles," *IEEE Communications Magazine*, vol. 61, no. 5, pp. 113–119, 2023.

[77] W. Yue, C. Li, G. Mao, N. Cheng, and D. Zhou, "Evolution of road traffic congestion control: A survey from perspective of sensing, communication, and computation," *China Communications*, vol. 18, no. 12, pp. 151–177, 2021.

[78] J. Mu, R. Zhang, Y. Cui, N. Gao, and X. Jing, "UAV meets integrated sensing and communication: Challenges and future directions," *IEEE Communications Magazine*, vol. 61, no. 5, pp. 62–67, 2023.

[79] J. Cong, C. You, J. Li, L. Chen, B. Zheng, Y. Liu, W. Wu, Y. Gong, S. Jin, and R. Zhang, "Near-field integrated sensing and communication: Opportunities and challenges," *IEEE Wireless Communications*, vol. 31, no. 6, pp. 162–169, 2024.

[80] S. Schaible and T. Ibaraki, "Fractional programming," *European Journal of Operational Research*, vol. 12, no. 4, pp. 325–338, 1983.

[81] H. L. Van Trees, *Optimum array processing: Part IV of detection, estimation, and modulation theory*. John Wiley & Sons, 2002.

[82] S. Boyd, S. P. Boyd, and L. Vandenberghe, *Convex optimization*. Cambridge University Press, 2004.

[83] D. Bertsekas, *Convex optimization theory*. Athena Scientific, 2009, vol. 1.

[84] A. E. Roth and M. Sotomayor, "Two-sided matching," *Handbook of Game Theory with Economic Applications*, vol. 1, pp. 485–541, 1992.

[85] E. Bodine-Baron, C. Lee, A. Chong, B. Hassibi, and A. Wierman, "Peer effects and stability in matching markets," in *Algorithmic Game Theory: 4th International Symposium, SAGT 2011, Amalfi, Italy, October 17-19, 2011. Proceedings 4*. Springer, 2011, pp. 117–129.

[86] H. Wu, J. Chen, W. Xu, N. Cheng, W. Shi, L. Wang, and X. Shen, "Delay-minimized edge caching in heterogeneous vehicular networks: A matching-based approach," *IEEE Transactions on Wireless Communications*, vol. 19, no. 10, pp. 6409–6424, 2020.

[87] N. Su, F. Liu, and C. Masouros, "Secure radar-communication systems with malicious targets: Integrating radar, communications and jamming functionalities," *IEEE Transactions on Wireless Communications*, vol. 20, no. 1, pp. 83–95, 2021.

[88] W. Zhao and S. Wang, "Resource sharing scheme for device-to-device communication underlaying cellular networks," *IEEE Transactions on Communications*, vol. 63, no. 12, pp. 4838–4848, 2015.

[89] S. Maghsudi and S. Stańczak, "Hybrid centralized–distributed resource allocation for device-to-device communication underlaying cellular networks," *IEEE Transactions on Vehicular Technology*, vol. 65, no. 4, pp. 2481–2495, 2016.

[90] L. E. Schrage, *Optimization modeling with LINGO*. Lindo System, 2006.

[91] P.-T. De Boer, D. P. Kroese, S. Mannor, and R. Y. Rubinstein, "A tutorial on the cross-entropy method," *Annals of Operations Research*, vol. 134, pp. 19–67, 2005.

[92] D. Feng, L. Lu, Y. Yuan-Wu, G. Y. Li, G. Feng, and S. Li, "Device-to-device communications underlaying cellular networks," *IEEE Transactions on Communications*, vol. 61, no. 8, pp. 3541–3551, 2013.

[93] A. Zhang, M. L. Rahman, X. Huang, Y. J. Guo, S. Chen, and R. W. Heath, "Perceptive mobile networks: Cellular networks with radio vision via joint communication and radar sensing," *IEEE Vehicular Technology Magazine*, vol. 16, no. 2, pp. 20–30, 2021.

[94] J. Zhao, F. Gao, W. Jia, W. Yuan, and W. Jin, "Integrated sensing and communications for UAV communications with jittering effect," *IEEE Wireless Communications Letters*, vol. 12, no. 4, pp. 758–762, 2023.

[95] N. Wu, R. Jiang, X. Wang, L. Yang, K. Zhang, W. Yi, and A. Nallanathan, "AI-enhanced integrated sensing and communications: Advancements, challenges, and prospects," *IEEE Communications Magazine*, vol. 62, no. 9, pp. 144–150, 2024.

[96] H. Luo, T. Zhang, C. Zhao, Y. Wang, B. Lin, Y. Jiang, D. Luo, and F. Gao, "Integrated sensing and communications framework for 6G networks," *IEEE Wireless Communications*, vol. 32, no. 6, pp. 102–109, 2025.

[97] C. Ouyang, Y. Liu, and H. Yang, "Performance of downlink and uplink integrated sensing and communications (ISAC) systems," *IEEE Wireless Communications Letters*, vol. 11, no. 9, pp. 1850–1854, 2022.

[98] Y. Liu, S. Zhang, X. Mu, Z. Ding, R. Schober, N. Al-Dhahir, E. Hossain, and X. Shen, "Evolution of NOMA toward next generation multiple access

(NGMA) for 6G," *IEEE Journal on Selected Areas in Communications*, vol. 40, no. 4, pp. 1037–1071, 2022.

[99] C. Ouyang, Y. Liu, and H. Yang, "Revealing the impact of SIC in NOMA-ISAC," *IEEE Wireless Communications Letters*, vol. 12, no. 10, pp. 1707–1711, 2023.

[100] F. R. Ghadi, K.-K. Wong, F. Javier López-Martínez, H. Shin, and L. Hanzo, "Performance analysis of FAS-aided NOMA-ISAC: A backscattering scenario," *IEEE Internet of Things Journal*, vol. 12, no. 23, pp. 51 326–51 340, 2025.

[101] X. Li, H. Liu, G. Li, Y. Liu, M. Zeng, and Z. Ding, "Effective capacity analysis of AmBC-NOMA communication systems," *IEEE Transactions on Vehicular Technology*, vol. 71, no. 10, pp. 11 257–11 261, 2022.

[102] J. Du, Y. Sun, N. Zhang, Z. Xiong, A. Sun, and Z. Ding, "Cost-effective task offloading in noma-enabled vehicular mobile edge computing," *IEEE Systems Journal*, vol. 17, no. 1, pp. 928–939, 2023.

[103] Y. Wu, Y. Song, T. Wang, L. Qian, and T. Q. S. Quek, "Non-orthogonal multiple access assisted federated learning via wireless power transfer: A cost-efficient approach," *IEEE Transactions on Communications*, vol. 70, no. 4, pp. 2853–2869, 2022.

[104] X. Mu, Y. Liu, L. Guo, J. Lin, and L. Hanzo, "NOMA-aided joint radar and multicast-unicast communication systems," *IEEE Journal on Selected Areas in Communications*, vol. 40, no. 6, pp. 1978–1992, 2022.

[105] L. Suo, H. Li, S. Zhang, and J. Li, "Successive interference cancellation and alignment in K-user MIMO interference channels with partial unidirectional strong interference," *China Communications*, vol. 19, no. 2, pp. 118–130, 2022.

[106] J. Nocedal and S. J. Wright, *Numerical optimization*. Springer, 1999.

[107] P.-T. De Boer, D. P. Kroese, S. Mannor, and R. Y. Rubinstein, "A tutorial on the cross-entropy method," *Annals of operations research*, vol. 134, no. 1, pp. 19–67, 2005.

[108] J.-P. Kermoal, L. Schumacher, K. I. Pedersen, P. E. Mogensen, and F. Frederiksen, "A stochastic MIMO radio channel model with experimental validation," *IEEE Journal on Selected Areas in Communications*, vol. 20, no. 6, pp. 1211–1226, 2002.

[109] Z.-Q. Luo, W.-K. Ma, A. M.-C. So, Y. Ye, and S. Zhang, "Semidefinite relaxation of quadratic optimization problems," *IEEE Signal Processing Magazine*, vol. 27, no. 3, pp. 20–34, 2010.

[110] J. H. Holland, "Genetic algorithms," *Scientific american*, vol. 267, no. 1, pp. 66–73, 1992.

[111] J. Chen, J. Kang, M. Xu, Z. Xiong, D. Niyato, C. Chen, A. Jamalipour, and S. Xie, "Multiagent deep reinforcement learning for dynamic avatar migration in AIoT-enabled vehicular metaverses with trajectory prediction," *IEEE Internet of Things Journal*, vol. 11, no. 1, pp. 70–83, 2024.

[112] J. Zhang, J. Wang, Y. Zhang, Y. Liu, Z. Chai, G. Liu, and T. Jiang, "Integrated sensing and communication channel: Measurements, characteristics, and modeling," *IEEE Communications Magazine*, vol. 62, no. 6, pp. 98–104, 2024.

[113] K. Shi, Y. Fu, and K. Hung, "A diversified recommendation scheme for wireless content caching networks," *IEEE Internet of Things Journal*, vol. 11, no. 9, pp. 15 100–15 112, 2024.

[114] Z. M. Fadlullah and N. Kato, "On smart IoT remote sensing over integrated terrestrial-aerial-space networks: An asynchronous federated learning approach," *IEEE Network*, vol. 35, no. 5, pp. 129–135, 2021.

[115] G. Li, S. Wang, J. Li, R. Wang, F. Liu, X. Peng, T. X. Han, and C. Xu, "Integrated sensing and communication from learning perspective: An SDP3 approach," *IEEE Internet of Things Journal*, vol. 11, no. 4, pp. 5589–5603, 2024.

[116] Y. Huang, Y. Fang, X. Li, and J. Xu, "Coordinated power control for network integrated sensing and communication," *IEEE Transactions on Vehicular Technology*, vol. 71, no. 12, pp. 13 361–13 365, 2022.

[117] Z. Wang, X. Mu, and Y. Liu, "STARS enabled integrated sensing and communications," *IEEE Transactions on Wireless Communications*, vol. 22, no. 10, pp. 6750–6765, 2023.

[118] Y. Xiong, F. Liu, Y. Cui, W. Yuan, T. X. Han, and G. Caire, "On the fundamental tradeoff of integrated sensing and communications under gaussian channels," *IEEE Transactions on Information Theory*, vol. 69, no. 9, pp. 5723–5751, 2023.

[119] M. Hua, Q. Wu, W. Chen, A. Jamalipour, C. Wu, and O. A. Dobre, "Integrated sensing and communication: Joint pilot and transmission design," *IEEE Transactions on Wireless Communications*, vol. 23, no. 11, pp. 16 017–16 032, 2024.

[120] Z. Wang, K. Han, X. Shen, W. Yuan, and F. Liu, "Achieving the performance bounds for sensing and communications in perceptive networks: Optimal bandwidth allocation," *IEEE Wireless Communications Letters*, vol. 11, no. 9, pp. 1835–1839, 2022.

[121] P. Liu, G. Zhu, W. Jiang, W. Luo, J. Xu, and S. Cui, "Vertical federated edge learning with distributed integrated sensing and communication," *IEEE Communications Letters*, vol. 26, no. 9, pp. 2091–2095, 2022.

[122] C. Ding, J.-B. Wang, H. Zhang, M. Lin, and G. Y. Li, "Joint MIMO precoding and computation resource allocation for dual-function radar and communication systems with mobile edge computing," *IEEE Journal on Selected Areas in Communications*, vol. 40, no. 7, pp. 2085–2102, 2022.

[123] Z. Wei, W. Jiang, Z. Feng, H. Wu, N. Zhang, K. Han, R. Xu, and P. Zhang, "Integrated sensing and communication enabled multiple base stations cooperative sensing towards 6G," *IEEE Network*, vol. 38, no. 4, pp. 207–215, 2024.

[124] P. Stoica, J. Li, and Y. Xie, "On probing signal design for MIMO radar," *IEEE Transactions on Signal Processing*, vol. 55, no. 8, pp. 4151–4161, 2007.

[125] K. Shen and W. Yu, "Fractional programming for communication systems—part I: Power control and beamforming," *IEEE Transactions on Signal Processing*, vol. 66, no. 10, pp. 2616–2630, 2018.

[126] N. V. Queipo, R. T. Haftka, W. Shyy, T. Goel, R. Vaidyanathan, and P. K. Tucker, "Surrogate-based analysis and optimization," *Progress in aerospace sciences*, vol. 41, no. 1, pp. 1–28, 2005.

[127] Y. Nesterov and A. Nemirovskii, *Interior-point polynomial algorithms in convex programming*. SIAM, 1994.

[128] M. Temiz, E. Alsusa, and M. W. Baidas, "A dual-function massive mimo uplink OFDM communication and radar architecture," *IEEE Transactions on Cognitive Communications and Networking*, vol. 8, no. 2, pp. 750–762, 2021.

[129] Z.-Q. Luo, W.-K. Ma, A. M.-C. So, Y. Ye, and S. Zhang, "Semidefinite relaxation of quadratic optimization problems," *IEEE Signal Processing Magazine*, vol. 27, no. 3, pp. 20–34, 2010.

[130] B. Radunovic and J.-Y. Le Boudec, "A unified framework for max-min and min-max fairness with applications," *IEEE/ACM Transactions on Networking*, vol. 15, no. 5, pp. 1073–1083, 2007.

[131] Ö. Yeniay, "Penalty function methods for constrained optimization with genetic algorithms," *Mathematical and computational Applications*, vol. 10, no. 1, pp. 45–56, 2005.

[132] P. He, L. Zhao, S. Zhou, and Z. Niu, "Water-filling: A geometric approach and its application to solve generalized radio resource allocation problems," *IEEE Transactions on Wireless Communications*, vol. 12, no. 7, pp. 3637–3647, 2013.

[133] R. Jain, A. Durresi, and G. Babic, "Throughput fairness index: An explanation," in *ATM Forum contribution*, vol. 99, no. 45, 1999, pp. 1–13.

[134] F. Liu, Y. Cui, C. Masouros, J. Xu, T. X. Han, Y. C. Eldar, and S. Buzzi, "Integrated sensing and communications: Toward dual-functional wireless networks for 6G and beyond," *IEEE Journal on Selected Areas in Communications*, vol. 40, no. 6, pp. 1728–1767, 2022.

[135] Y. Mao, C. You, J. Zhang, K. Huang, and K. B. Letaief, "A survey on mobile edge computing: The communication perspective," *IEEE Communications Surveys & Tutorials*, vol. 19, no. 4, pp. 2322–2358, 2017.

[136] N. Abbas, Y. Zhang, A. Taherkordi, and T. Skeie, "Mobile edge computing: A survey," *IEEE Internet of Things Journal*, vol. 5, no. 1, pp. 450–465, 2018.

[137] P. Mach and Z. Becvar, "Mobile edge computing: A survey on architecture and computation offloading," *IEEE Communications Surveys & Tutorials*, vol. 19, no. 3, pp. 1628–1656, 2017.

[138] N. C. Luong, X. Lu, D. T. Hoang, D. Niyato, and D. I. Kim, "Radio resource management in joint radar and communication: A comprehensive survey," *IEEE Communications Surveys & Tutorials*, vol. 23, no. 2, pp. 780–814, 2021.

[139] A. Magbool, V. Kumar, Q. Wu, M. Di Renzo, and M. F. Flanagan, "A survey on integrated sensing and communication with intelligent metasurfaces: Trends, challenges, and opportunities," *IEEE Open Journal of the Communications Society*, vol. 6, pp. 7270–7318, 2025.

[140] H. Hua, T. X. Han, and J. Xu, "MIMO integrated sensing and communication: CRB-rate tradeoff," *IEEE Transactions on Wireless Communications*, vol. 23, no. 4, pp. 2839–2854, 2024.

[141] K. Meng, C. Masouros, K.-K. Wong, A. P. Petropulu, and L. Hanzo, "Integrated sensing and communication meets smart propagation engineering: Opportunities and challenges," *IEEE Network*, vol. 39, no. 2, pp. 278–285, 2025.

[142] W. Wu, F. Zhou, R. Q. Hu, and B. Wang, "Energy-efficient resource allocation for secure NOMA-enabled mobile edge computing networks," *IEEE Transactions on Communications*, vol. 68, no. 1, pp. 493–505, 2020.

[143] B. Wu, F. Fang, and X. Wang, "Joint age-based client selection and resource allocation for communication-efficient federated learning over NOMA networks," *IEEE Transactions on Communications*, vol. 72, no. 1, pp. 179–192, 2024.

[144] R. Li, P. Hong, K. Xue, M. Zhang, and T. Yang, "Resource allocation for uplink NOMA-based D2D communication in energy harvesting scenario: A two-stage game approach," *IEEE Transactions on Wireless Communications*, vol. 21, no. 2, pp. 976–990, 2022.

[145] T. Hou, Y. Liu, Z. Song, X. Sun, Y. Chen, and L. Hanzo, "Reconfigurable intelligent surface aided NOMA networks," *IEEE Journal on Selected Areas in Communications*, vol. 38, no. 11, pp. 2575–2588, 2020.

[146] O. Maraqa, A. S. Rajasekaran, S. Al-Ahmadi, H. Yanikomeroglu, and S. M. Sait, "A survey of rate-optimal power domain NOMA with enabling technologies of future wireless networks," *IEEE Communications Surveys & Tutorials*, vol. 22, no. 4, pp. 2192–2235, 2020.

[147] S. Pakravan, M. Ahmadzadeh, M. Zeng, Z. Yang, G. A. Hodtani, J.-Y. Chouinard, and Q.-V. Pham, "Fluid antenna-assisted uplink NOMA networks under imperfect SIC," *IEEE Transactions on Vehicular Technology*, vol. 75, no. 1, pp. 1689–1694, 2026.

[148] Y. J. A. Zhang, L. Qian, J. Huang *et al.*, "Monotonic optimization in communication and networking systems," *Foundations and Trends in Networking*, vol. 7, no. 1, pp. 1–75, 2013.

[149] H. Tuy, "Monotonic optimization: Problems and solution approaches," *SIAM Journal on Optimization*, vol. 11, no. 2, pp. 464–494, 2000.

[150] P. D. Hough, T. G. Kolda, and V. J. Torczon, "Asynchronous parallel pattern search for nonlinear optimization," *SIAM Journal on Scientific Computing*, vol. 23, no. 1, pp. 134–156, 2001.